UNDERSTANDING THE REGULATORY MECHANISMS OF MICROTUBULE BASED MOLECULAR MOTORS

A Dissertation Submitted to the Sambalpur University in Partial Fulfillment of the Requirements for the Degree of

DOCTOR OF PHILOSOPHY
IN
BIOTECHNOLOGY

By

Pushpanjali Soppina
Regd. No.10408/2019/ Biotechnology

DEPARTMENT OF BIOTECHNOLOGY AND BIOINFORMATICS
SAMBALPUR UNIVERSITY, JYOTIVIHAR,
SAMBALPUR- 768019, ODISHA

February 2023

UNDERSTANDING THE REGULATORY MECHANISMS OF MICROTUBULE BASED MOLECULAR MOTORS

A Dissertation Submitted to the Sambalpur University in Partial Fulfillment of the Requirements for the Degree of

DOCTOR OF PHILOSOPHY
IN
BIOTECHNOLOGY

By

Pushpanjali Soppina
Regd. No.10408/2019/ Biotechnology

Under the Joint Supervision of

Supervisor: *Dr. Pradeep K. Naik, Professor & Head, Department of Biotechnology and Bioinformatics, Sambalpur University*

Co- Supervisor: *Dr. Sivapriya Kirubakaran, Associate Professor, Department of Chemistry, Indian Institute of Technology Gandhinagar*

DEPARTMENT OF BIOTECHNOLOGY AND BIOINFORMATICS
SAMBALPUR UNIVERSITY, JYOTIVIHAR,
SAMBALPUR- 768019, ODISHA

February 2023

DECLARATION

I hereby declare that, the work reported in the Ph.D. thesis entitled ***"Understanding the regulatory mechanisms of microtubule based molecular motors"*** *submitted at Sambalpur University is the original report of my research, under the joint guidance of Dr. Pradeep Kumar Naik, Dept. of Biotechnology & Bioinformatics, Sambalpur University and Dr. Sivapriya Kirubakaran, Department of Chemistry, Indian Institute of Technology Gandhinagar, Gujarat.*

I have not submitted this work previously to any other organization for any degree or professional qualification. I have confirmed the norms and guidelines given in the ethical code of conduct of the university. Whenever I have used materials (data, theoretical analysis and text) from other sources, I have given due credit to them by citing them in the text of the thesis and given their details in the references.

Date: **(Pushpanjali Soppina)**

COURSE WORK AND COMPREHENSIVE EXAMINATION
COMPLETION CERTIFICATE

This is to certify that ***Miss. Pushpanjali Soppina****, bearing Registration* ***No-10408/2019/Biotechnology****, a bonafide Ph.D. scholar of Sambalpur University, Sambalpur, who has successfully completed her course work and comprehensive examination, which is a part of her Ph.D. Programme.*

Date:

(Dr. Pradeep Kumar Naik)
Head of the Department
Dept. of Biotechnology & Bioinformatics
Sambalpur University, Jyotivihar, Burla

Dr. Pradeep K. Naik
Professor and Head
Dept. of Biotechnology & Bioinformatics

SAMBALPUR UNIVERSITY
JYOTI VIHAR – 768019
SAMBALPUR, ODISHA
Mob.: +91-9479268802
Fax: (0663) – 2430158
E-mail: *pknaik1973@gmail.com*

CERTIFICATE

This is to certify that the research work entitled, ***"Understanding the regulatory mechanisms of microtubule based molecular motors"*** *submitted by* ***Miss. Pushpanjali Soppina*** *at* ***Sambalpur University, Odisha, India*** *is a bonafide record of her original work carried out under my supervision and her co-supervisor Dr. Sivapriya Kirubakaran (Indian Institute of Technology Gandhinagar). This work has not been submitted partially or wholly to any other University or Institute for any degree or diploma. I recommend this thesis in fulfillment of the award of the degree of* ***Doctor of Philosophy*** *in* ***Biotechnology.***

Supervisor:
Dr. Pradeep Kumar naik
Professor and Head
Dept. of Biotechnology & Bioinformatics,
Sambalpur University,
Jyotivihar, Burla.
Date:

Co-Supervisor:
Dr. Sivapriya Kirubakaran
Associate Professor
Department of Chemistry
Indian Institute of Technology
Gandhinagar, Gandhinagar
Date:

Acknowledgements

First and foremost, I would like to thank my funding agency DST WOS-A fellowship for providing an opportunity to pursue the doctoral program and continue my career in science. Also, I am very much thankful to OHEPEE, Govt. of Odisha for providing the necessary facilities to conduct my research work in the Centre of Excellence in Natural Products and Therapeutics, Dept. of Biotechnology and Bioinformatics.

A simple thank you would not suffice to Dr. Pradeep Naik, my PhD supervisor for the opportunity he offered me when most of them turned down my applications due to a long gap from academics. I thank him for making my PhD journey very smooth by his solid guidance, unconditional support, confidence and freedom. I really appreciate his humbleness and kind nature towards all his students and holding the team together. I also thank Dr. Amiya Kumar Patel for his support and great help during my visit to the campus.

Furthermore, I would like to extend my sincere gratitude to Dr. Sivapriya Kirubakaran, my co-supervisor and mentor of DST WOS-A grant. I sincerely thank her for agreeing to be my mentor and guide through my entire grant tenure at IITGN, without her constant support this journey would have been very difficult. I thank her for being so patient, kind and a strong support system during stressful time. With her strong leadership qualities she influences women power to a greater extent.

Next, I thank all my lab mates at IITGN- Nisha, Ruchi, Dipeshwari, Aravintha, Surbhi, and Tarushyam for their constant feedback, discussions, support, care, and together contributing for the development of a healthy scientific temper. Be it scientifically or personally these people were a solid support during despondent times. We together have treasured tones of beautiful moments to cherish and also learnt life lessons that gave us strength to dream big and never quit. I also thank the Pindoriya family for being our well-wisher and best friends at IITGN campus. Thank you all for being an intrinsic part of our family. I really appreciate and am thankful to my Sambalpur lab mates and friends,

Shruti, Monica, Sadni, Swaraj and Pratyush for their tremendous help and support not only during my stay in the campus but also for any online academic requirements needed on my behalf. I specially thank Pratyush for his efforts and contribution during the JoVE videography.

I also thank the people who inspired and incentivized me to be in this field, teaching me from scratch, trusting and giving me the responsibilities- Dr. Maithreyi Narsimha, Dr. Roop Mallik, Dr. Krishanu Ray, Dr. Kristen Verhey, Dr. Catherine Collins and Dr. Virupakshi Soppina. Achievements and accolades of these people in science inspire many of us.

I would like to take this opportunity to thank my husband, my pride and my whole world, Dr. Virupakshi and my lovely son Ansh, for giving me that push to soar high. Without their encouragement, sacrifices and loads of understanding, this journey would have been impossible. I apologize to my son for reversing the roles and expecting so much at this tender age. I thank him for being a cheerleader to the entire lab during our tough times; he was really a ray of hope. Today, I proudly dedicate this thesis to both of them and say that it's because of them I could reach this far and dream to achieve more. I also thank my uncle Mr. Vasanth Kumar and family for their moral support and compassion during the crucial stages of my life.

Last but not the least I thank my grandparents, parents and my siblings for their love and affection.

Thank you one and all.

Table of Contents

		Page Number
Abstract		**: 8 – 10**
Chapter 1: Introduction		**: 11 – 23**
1.1	Intracellular transport	: 11 – 12
1.2	Dyneins	: 12 – 13
1.3	Kinesins	: 14 – 17
1.4	Kinesin-3	: 17 – 23
1.5	Organization of the thesis work - Objectives	: 24
Chapter 2: Review of literature		**: 25 – 33**
2.1	Mechanochemical ATPase cycle of kinesin-1 motor.	: 25 – 27
2.2	Mechanochemical ATPase cycle of kinesin-3 motor.	: 27 – 30
2.3	Purification of active kinesin-3 motors.	: 30 – 33
Chapter 3: Materials and methods		**: 34 – 50**
3.1	DH10Bac competent cell preparation.	: 34
3.2	Generation of recombinant bacmid.	: 34 – 35
3.3	Sf9 cell culture, transfection, and recombinant baculovirus production.	: 35 – 38
3.4	Sf9 purification of kinesin-3 motors.	: 38 – 39
3.5	Circular Dichroism (CD) spectroscopy.	: 40
3.6	Bacterial purification of constitutively active kinesin-1.	: 40
3.7	Cell culture, transfection and fluorescence microscopy.	: 40 – 42
3.8	Tubulin purification and labeling.	: 42
3.9	*In vitro* single-molecule motility assay using Sf9-purified kinesin-3 motors.	: 42 – 47
3.10	*In vitro* microtubule gliding assay using Sf9-purified kinesin-3 motors.	: 47 – 48
3.11	ATPase assay using Sf9-purified kinesin-3 motors.	: 48 – 49
3.12	Data analysis.	: 49
3.13	Microtubule bending analysis.	: 49 – 50
Chapter 4: Results and Discussion		**: 53 – 92**
4.1	Generation of bacmids and purification of kinesin-1 and kinesin-3 motors using Sf9 baculovirus system.	: 54 – 57
4.2	Sf9-purified kinesin-3 motors are fast and superprocessive.	: 57 – 63

4.3 Kinesin-3 motors exhibit high ATP turnover rates. : 63 – 70

4.3.1 Full-length kinesin-3 motors exhibit low ATPase activities. : 65
4.3.2 KIF1A dimers exhibit the highest ATP turnover rates. : 65 – 67
4.3.3 KIF13 dimers show higher ATPase activity. : 67 – 68
4.3.4 KIF16B dimers show high ATPase activity. : 68 – 70

4.4 Kinesin-3 motor velocities inversely correlate to their microtubule binding affinity. : 70 – 77
4.5 Kinesin-3 motors influence microtubule bending *in vitro*. : 77 – 79
4.6 Kinesin-3 motors influence microtubule bending *in vivo*. : 79 – 82
4.7 The K-loop influences microtubule bending *in vivo*. : 83 – 87
4.8 The K-loop influences microtubule bending *in vitro*. : 87 – 92

Chapter 5: Conclusions : 93 – 95

Bibliography : 98 - 117

List of Publications : 118 – 119

Index of Figures

Figure Number	Caption	Page Number
Figure 1.1:	Molecular motors and Intracellular transport.	: 12
Figure 1.2:	Cartoon diagram of cytoplasmic dynein.	: 13
Figure 1.3:	Phylogenetic tree of kinesin superfamily.	: 14
Figure 1.4:	Functions and diseases associated with KIF genes.	: 15
Figure 1.5:	Domain organization of kinesin-1 motor.	: 16
Figure 1.6:	Autoinhibited and active state of kinesin-1 motor.	: 17
Figure 1.7:	Domain organization of kinesin-3 family motors.	: 18
Figure 1.8:	Regulation mechanism of kinesin-3 motors.	: 19
Figure 1.9:	K-loop influences high microtubule landing rate in ADP state.	: 20
Figure 2.1:	Mechanochemical ATPase cycle of kinesin-1 motor.	: 26
Figure 2.2:	Bac-to-Bac Baculovirus Expression System.	: 32
Figure 4.1:	Bacterial expression of KHC (1-560) resulted in inactive and degraded protein.	: 53
Figure 4.2:	Generation of recombinant bacmids for kinesin-1 and kinesin-3 motors.	: 55
Figure 4.3:	48 h post-transfection of Sf9 cells with fluorescently tagged kinesin-3 motor.	: 56
Figure 4.4:	72 h post-transfection of Sf9 cells with fluorescently tagged kinesin-3 motor.	: 57
Figure 4.5:	Baculovirus-purified constitutively active kinesin-1 and kinesin-3 motors.	: 58
Figure 4.6:	Sf9-baculovirus purified kinesin-3 motors are robust and superprocessive.	: 60
Figure 4.7:	Kymograph of In vitro microtubule-based single-molecule motility assays of constitutively active kinesin-3 motors.	: 61
Figure 4.8:	Kinesin-3 motors exhibit high ATPase activity and differential microtubule affinity.	: 66
Figure 4.9:	Kinesin-3 motor velocity inversely correlates with microtubule affinity.	: 72
Figure 5.0:	Ribbon diagram of KIF1A motor domain interacting with tubulin subunits.	: 74
Figure 5.1:	Loop8 contributes to the strong microtubule-binding affinity for kinesin-3 motors.	: 75
Figure 5.2:	Kinesin-3 motors glide microtubules faster.	: 80
Figure 5.3:	Multi-motor microtubule gliding analysis of kinesin-3 motors.	: 81

Figure 5.4:	Kinesin-3 motors induce frequent microtubule bending in multi-motor gliding assay.	: 82
Figure 5.5:	Kinesin-3 motors induce microtubule bending in cells.	: 84
Figure 5.6:	Kinesin-3 motors influence microtubule bending in vivo.	: 85
Figure 5.7:	Amino acid sequence alignment of kinesin-3 and kinesin-1 K-loop and their mutants.	: 86
Figure 5.8:	Positively charged lysine resides in the K-loop influence microtubule bending in cells.	: 88
Figure 5.9:	Positively charged lysine resides in the K-loop influence microtubule bending in cells.	: 90
Figure 5.10:	K-loop, a family specific insert in the loop12 of Kinesin-3 motor domain, influence microtubule bending.	: 91

Index of Tables

Table Number	Caption	Page Number
Table 1:	List of selected cargoes of kinesin-3 motors.	: 22
Table 2:	Buffers and Reagent preparation.	: 51 – 52
Table 3:	Biochemical and biophysical properties of Kinesin-3 family motors.	: 62
Table 4:	Summary of ATPase properties of full-length kinesin-1 and kinesin-3 motors.	: 67

Movie legends (Movies are provided as separate file)

Movie Number	Caption	Page Number
Movie 1	Microtubule gliding assay of constitutively active kinesin-1 motor, KHC(1- 560).	
Movie 2	Microtubule gliding assay of constitutively active kinesin-3 motor KIF1A(1-393LZ).	
Movie 3	Microtubule gliding assay of constitutively active kinesin-3 motor, KIF13A(1-411ΔP).	
Movie 4	Microtubule gliding assay of constitutively active kinesin-3 motor, KIF13B(1-412ΔP).	**: 96 – 97**
Movie 5	Microtubule gliding assay of constitutively active kinesin-3 motor, KIF16B(1-400).	
Movie 6	Microtubule gliding assay of KIF1A(1-393LZ) All-alanine mutant.	
Movie 7	Microtubule gliding assay of KIF1A(1-393LZ) Swap mutant.	
Movie 8	Microtubule gliding assay of KHC(1-560) Swap mutant.	

List of Abbreviations

Sf9	*Spodoptera frugiperda* insect cells
ATP	Adenosine triphosphate
ADP	Adenosine diphosphate
GTP	Guanosine triphosphate
GDP	Guanosine diphosphate
mCit	Monomeric citrine (variant of YFP)
GFP	Green Fluorescent Protein
COS	African green monkey kidney cells
CAD	Mouse catecholaminergic cell line
DMEM	Dulbecco's Modified Eagle Medium
FBS	Fetal bovine serum
TIRF	Total internal reflection fluorescence
PTM	Post translational modification
WT	Wild type
KIF	Kinesin superfamily
KHC	Kinesin heavy chain
KLC	Kinesin light chain
LZ	Leucine zipper
MD	Motor domain
NL	Neck linker
NC	Neck coil
CC	Coil-coil
PH	Pleckstrin homology
PX	Phox homology
CAP-Gly	Cytoskeleton associated protein-glycine domain
FHA	Forkhead-associated
FL	Full-length
GAKIN	Guanylate kinase-associated kinesin
ΔP	Constitutively active dimer of KIF13 (ΔP390/P391)
PIP3	Phosphotidylinositol (3,4,5) trisphosphate
BICD2	Bicaudal D2
Dlg	Disc large
BSA	Bovine serum albumin
B-PER™	Bacterial protein extraction reagent
DTT	1,4-Dithiothreitol
EDTA	Ethylenediaminetetraacetic acid

EGTA	Ethylene glycol-bis (β-aminoethyl ether)-N,N,N',N-tetra acetic acid
HEPES	4-(2-hydroxyethyl)-1-piperazineethanesulfonic acid
IGEPAL	Octylphenoxy poly (ethyleneoxy) ethanol
IPTG	Isopropyl β-D-1-thiogalactopyranoside
PBS	Phosphate-buffered saline
PIPES	1,4-Piperazinediethanesulfonic acid, Piperazine-1,4-bis (2-ethanesulfonic acid), Piperazine-N, N-bis (2-ethanesulfonic acid)
PMSF	Phenylmethylsulfonyl fluoride
SDS	Sodium dodecyl sulfate
SDS-PAGE	Sodium dodecyl sulfate polyacrylamide gel electrophoresis
SD	Standard deviation
SEM	Standard error mean
PCR	Polymerase chain reaction
OD	Optical density
NA	Numerical aperture

Abstract

Cytoskeleton and its associated many cytoplasmic proteins determine the cell shape, transport system, cell motility, and cell division. The transport system within the cell plays a key role in regulating these mechanisms. Short-range transport is primarily carried out by actin and its associated motor protein myosin. In contrast, long-range intracellular transport predominantly depends on microtubule and its associated motor proteins, kinesin and dynein. Motor proteins are mechanochemical ATPases that convert chemical energy to drive mechanical work. ATPase cycle is integral to molecular motors' processive motility to drive long-distance intracellular transport. Detailed studies on biochemical and biophysical properties of motor proteins have been done on kinesin-1, first among the kinesin superfamily to be discovered.

Kinesin-3 constitutes one of the large families among the kinesin superfamily that plays critical roles in cellular and physiological functions ranging from intracellular cargo transport to cell division to development. Defective motor functions implicated in many developmental, neurological and cancerous diseases. Kinesin-3 motors are further branched out to five subfamilies (KIF1, KIF13, KIF14, KIF16 and KIF28) endowed with unique features and functions. Kinesin-3 motors are remarkably superprocessive, hence the name 'marathon runners' with high velocity, superprocessive motility and strong microtubule affinity. Previous studies from kinesin-1 and myosin motors shows that adenosine triphosphate (ATP) turnover rate regulates the stepping rate and processivity of the molecular motors. However, the regulating mechanism of this ATP turnover or the chemomechanics of kinesin-3 motors is poorly understood.

To understand the evolutionary modifications that furnished superprocessive nature to kinesin-3 motors and their regulatory mechanisms we employ cellular, biochemical and biophysical approaches. Such studies demand purified proteins on a large scale. Expression and purification of these motors using mammalian cells yield much less protein and these protocols would be expensive and time-consuming. In comparison, expressing these proteins in prokaryotic expression system resulted in significantly inactive and protein aggregation. To overcome the limitations posed by bacterial

purification systems and mammalian cell lysate, we have established a robust Sf9-baculovirus expression system to express and purify full-length and constitutively active kinesin-3 motors.

In the present work, we have established the purification of kinesin-3 motors using Sf9-baculovirus expression system. The full-length and constitutively active kinesin-3 motors are C-terminally tagged with 3-tandem fluorescent proteins that provide enhanced signals and decreased photobleaching, critical for single-molecule motility assays. First, we performed *in vitro* single-molecule and multi-motor gliding assays under Total Internal Reflection Fluorescence (TIRF) illumination using Sf9 purified proteins. We demonstrate that the functional output of motor proteins purified from the Sf9-baculovirus system are comparable to those expressed in mammalian cells. Remarkably, their motility properties are identical to that of motors prepared from mammalian cell lysates.

As the processivity is guided by ATP turnover rate by the motor proteins, we performed microtubule-stimulated ATPase measurements using Sf9 purified kinesin-3 motors. To do this, we adapted a colorimetric ATPase assay based on formation of phosphomolybdate complex formation. We show for the first time that kinesin-3 motors are robust ATPases with high ATP turnover rates, which is 1.3 to 3-fold higher compared to a well-studied kinesin-1 motor. Remarkably, these ATPase rates correlate to kinesin-3 motors stepping rate, suggesting a tight coupling between chemical and mechanical cycles.

Intriguingly, kinesin-3 velocities (KIF1A > KIF13A > KIF13B > KIF16B) show an inverse correlation with their microtubule-binding affinities (KIF1A < KIF13A < KIF13B < KIF16B). Interestingly, our *in silico* analysis using the coupled Brownian motor model also predicted a similar trend (KIF1A > KIF13 > KIF16B) that is observed experimentally. We did mutational studies to demonstrate that the positively charged residues in loop8 of the kinesin-3 motor domain largely contribute this differential microtubule-binding affinity. Most importantly, the presence of arginine residue enables multiple stable electrostatic interactions with negatively charged glutamate residue at the

C-terminal tail region in tubulin. Collectively, we demonstrate that a fine balance between ATP hydrolysis and microtubule-binding affinity rate enables kinesin-3 motors with novel mechanical outputs.

To understand the collective behavior of kinesin-3 motors we performed microtubule-gliding assay with constitutively active kinesin-3 motors. Microtubule gliding with kinesin-3 motors displayed significant microtubule bending without affecting their gliding velocities compared a well-characterized motor, kinesin-1. Furthermore, we did *in vivo* cell culture studies to investigate the underlying mechanism of microtubule bending. Microtubule-bending analysis of cells expressing kinesin-3 motors showed significant bending compared to kinesin-1 motor. Our previous work has suggested the K-loop, a conserved; hallmark insert in loop 12 of kinesin-3 motor domain plays an essential role in motor microtubule interaction in the ADP state. Hence to dissect its role in bending we created K-loop mutations and performed live cell studies and *in vitro* microtubule gliding assay. Analysis from these studies suggests that positively charged lysine residues in the K-loop influence kinesin-3 driven microtubule bending in cells.

Together, we successfully purified full-length and constitutively active kinein-3 motors from Sf9-baculovirus expression system and performed biochemical and biophysical studies. We show that these purified proteins are of high quality and functionally on par with motors from mammalian lysates as demonstrated in single-molecule, gliding and ATPase assays. We also show that Loop8 of kinesin-3 motor domain largely contributes to the differential microtubule-binding affinities. Interestingly, these microtubule-binding affinities inversely correlate to the velocities of kinesin-3 motors. Furthermore, the K-loop, a positively charged insert in the loop12 of the kinesin-3 motor domain promotes microtubule-bending. Hence, we propose that kinesin-3 motors are fine-tuned at the molecular level to endow diverse mechanical outputs critical for myriad of cellular processes.

Keywords: Chemomechanical/ Kinesin-3/ Microtubule-bending/ Baculovirus/ Superprocessive / ATPases

Chapter 1

Introduction

1.1. Intracellular transport

Eukaryotic cell size, shape, motion, division and intracellular transport system is well supported by three main classes of proteins- actin, intermediate filaments and microtubules. Many genetic screening experiments have provided direct evidence of defective intracellular transport as a factor for neuronal pathologies like spastic paraplegia, microcephaly, seizures, intellectual disabilities and many more (Anderson et al., 2013; De Vos et al., 2008; Franker and Hoogenraad, 2013).

Microtubules play a crucial role in maintaining long-distance intracellular transport and organization of cellular components spatially and temporally, especially in axons and dendrites for establishing neuronal polarity (Kapitein and Hoogenraad, 2011). These microtubules get nucleated at the microtubule-organizing center (MTOC) forming minus ends and extending towards the cell periphery as plus ends. Long polymers of microtubules comprise α-β tubulin heterodimers, both binding to guanosine triphosphate, GTP but slowly hydrolyzed by β-tubulin only and leading to highly dynamic microtubules, stochastically switching between growth and shrinkage. These α-β tubulin heterodimers are usually arranged into 13 protofilaments, arranged laterally to form a long hollow tube with 24 nm width (Goodson and Jonasson, 2018; Nogales, 2000; Wickstead and Gull, 2011). Along with heterodimer formation other mechanisms that regulates microtubule system are post-translational modifications (PTMs) (Verhey and Gaertig, 2007; Wloga and Gaertig, 2010). Some common PTMs are phosphorylation, acetylation, sumoylation, tyrosination, detyrosination, polyglutamylation and many others. These PTMs dictate the stability of microtubules, assembly of cilia, basal bodies and centrioles, provide structural cues for severing proteins, plus-end tracking proteins and molecular motors (Hammond et al., 2010). Along with many microtubule-associated proteins (MAPS) like MAP1, MAP2 and tau, kinases like Protein kinase A (PKA), and enzymes like GAPDH, microtubules also supports molecular motors like kinesin and dynein (Mandelkow and Mandelkow, 1995).

Intracellular transport of protein complexes and organelles is mainly directional and it involves molecular motors, myosin along the actin network for short-distance transport and kinesin and dynein along microtubule tracks for long-distance transport mechanism **(Figure.1.1)** (Mallik and Gross, 2004; Vale, 2003). Kinesins display anterograde motion towards the cell periphery; in contrast, dyneins follow retrograde motion towards the nucleus. Basically these molecular motors are interdependent in their mode of functioning to ensure smooth intracellular transport.

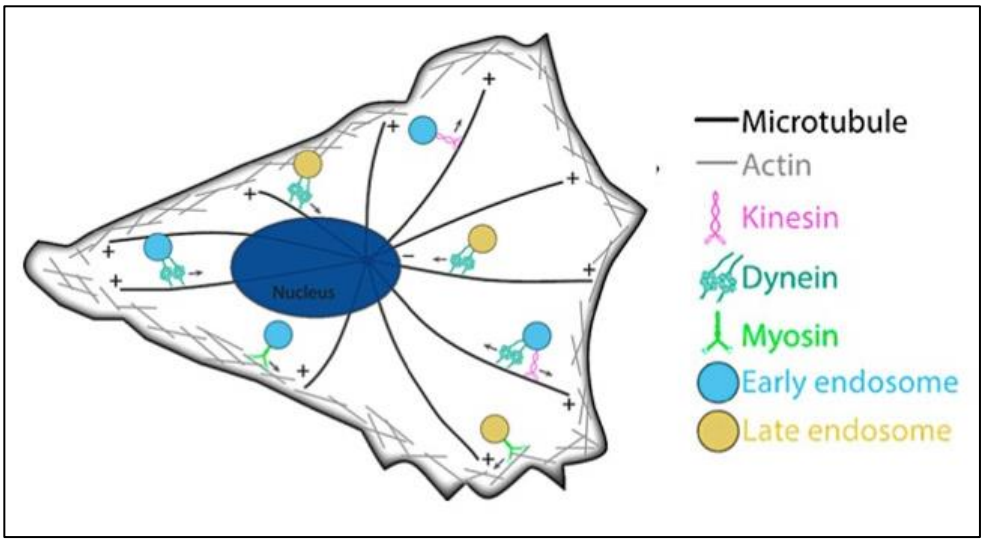

Figure 1.1: Molecular motors and Intracellular transport. Molecular motors kinesin and dynein walks along microtubule tracks (long black lines running from the center of the cell to periphery) whereas myosins along actin (short gray lines at the cell periphery). Kinesin motor walks towards plus-end of the microtubule, while dynein motor towards the minus-end. Endosomes are shown as cargoes for motors. [Adapted from (Tirumala and Ananthanarayanan, 2020)].

1.2. Dyneins

Dyneins are minus end-directed microtubule associated motor proteins. Dyneins comprises two major classes axonemal and cytoplasmic dyneins, categorized based on their structure and function. Axonemal dyneins are involved in ciliary and flagellar beating whereas cytoplasmic dynein is responsible for retrograde cargo trafficking,

mitosis, and cell movement. There are two classes of cytoplasmic dynein, cytoplasmic dynein 1 and cytoplasmic dynein 2. Cytoplasmic dynein 1 is most abundant and responsible for transporting organelles like lysosomes and endosomes and perinuclear positioning of Golgi apparatus. Cytoplasmic dynein 2 is located within and around the base of cilia and flagella, responsible for retrograde intraflagellar transport (Allan, 2011; Hook and Vallee, 2006; Hou and Witman, 2015; Tirumala and Ananthanarayanan, 2020). Dysfunction of cytoplasmic dynein leads to several neurodegenerative and neurodevelopmental diseases (Chen et al., 2014).

Dynein is a huge protein with a molecular mass of about 1.5 megadaltons (MDa). Dynein function is aided by forming a tri-complex with dynactin and cargo adaptors like BicD2, Hook1− 3, Spindly and Rabll-FIP3. p150-Glued assists dynactin by acting as a linker in microtubule attachment. This interaction activates and increases dynein's processivity (**Figure 1.2)**.

Dynein's takes variable step size and is estimated to be 8, 24, or 32nm based on cargo load (Mallik et al., 2004; Reck-Peterson et al., 2006). Also its force generation varies between the organism (~4.3pN for human dynein (Belyy et al., 2016) and ~ 7pN for yeast dynein (Gennerich et al., 2007)).

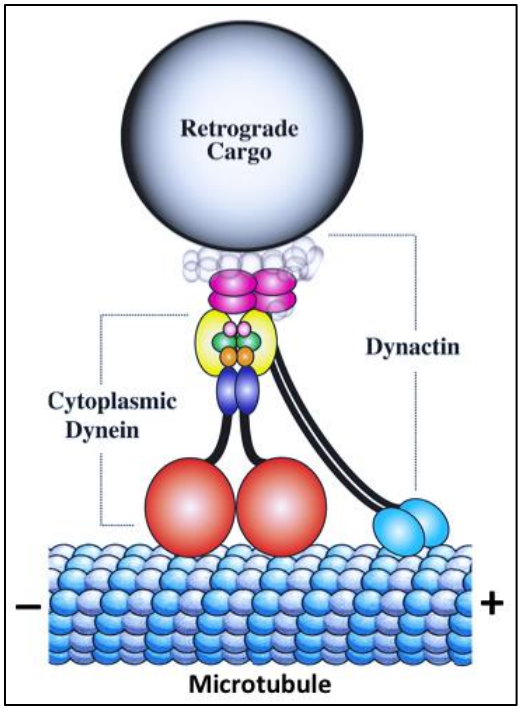

Figure 1.2: Cartoon diagram of cytoplasmic dynein. Cartoon diagram of cytoplasmic dynein forming a complex with dynactin to bind to microtubule and transport the cargo in a retrograde direction towards the nucleus. [Adapted from, (Duncan and Goldstein, 2006)].

1.3. Kinesins

Conventional kinesin, kinesin-1, was first isolated from squid axons while looking for a force-generating protein involved in the intracellular transport system (Vale et al., 1985). Since then, more than 100 kinesins have been identified. Complete sequence alignment from different model systems yielded a detailed phylogenetic tree of kinesin superfamily (KIFs) and accordingly based on their family-specific characteristics they have been grouped into 14 families **(Figure 1.3)** (Hirokawa and Takemura, 2005; Miki et al., 2005; Verhey et al., 2011a).

KIFs have been shown to transport mRNAs, synaptic vesicles, organelles and during cell division, they segregate chromosomes (Miki et al., 2005; Schnitzer and Block, 1997). Defects in the functioning of these motors leads to wide range of pathological diseases like polycystic kidney disease, left-right asymmetry defects, cancer, Charcot-Marie-Tooth disease, and hereditary spastic paraplegia **(Figure 1.4)** (Hirokawa et al., 2010; Kalantari and Filges, 2020; Vale, 2003).

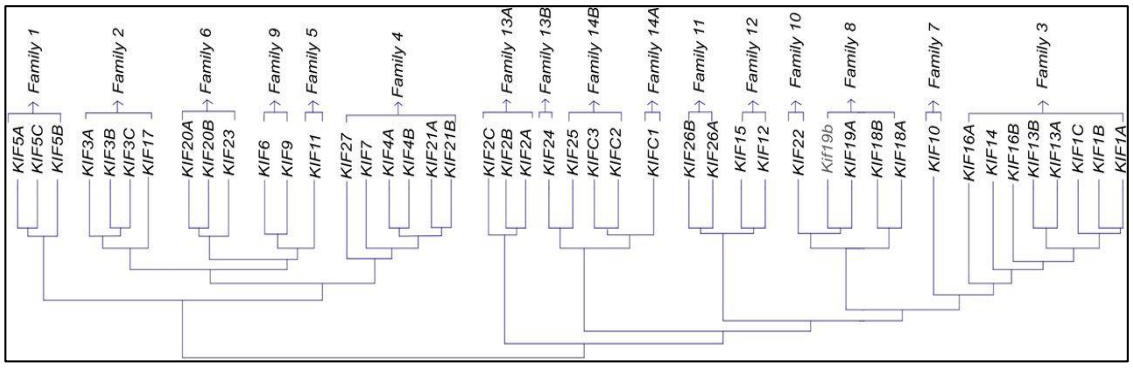

Figure 1.3: Phylogenetic tree of kinesin superfamily. Kinesin superfamily genes identified in humans and mouse grouped into 14 families (kinesin1 to kinesin14). [Adapted from (Hirokawa and Tanaka, 2015)].

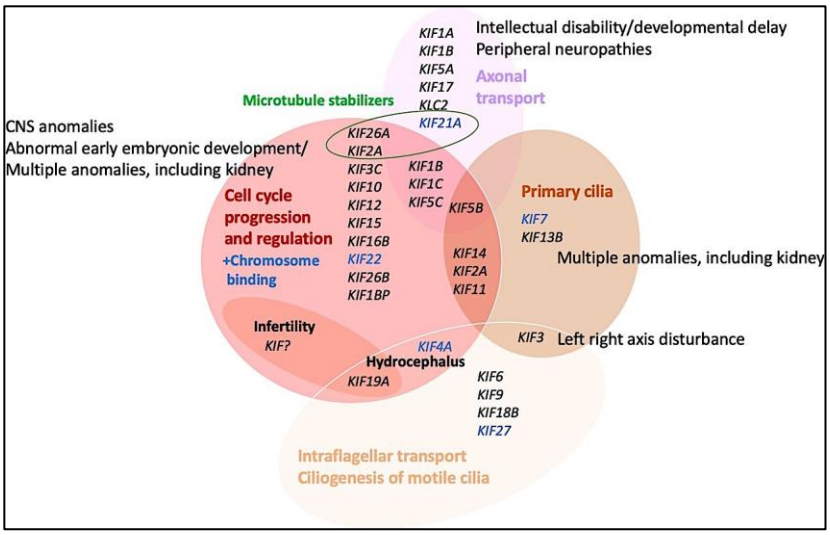

Figure 1.4: Functions and diseases associated with KIF genes. Some of the functions and diseases related to KIF genes. [Adapted from (Kalantari and Filges, 2020)].

Since its discovery much progress has been made in understanding the structural details of kinesin motors using high-resolution cryo-electron microscopy and X-ray crystallography. Kinesin motors form a superfamily with more than 45 members that are grouped into 3 families based on signature sequence conservation in their core catalytic motor domain. N-type; motor domain situated at N-terminus walks directionally towards plus end of the microtubule. M-type; motor domain situated in the central region destabilizes the microtubule and C-type; motor domain at the C-terminus walks in the opposite direction towards the microtubule minus-end (Marx et al., 2009; Miki et al., 2005; Verhey and Hammond, 2009; Wang et al., 2015). Along with the catalytic motor domain, regions outside this domain contribute significantly to the differences observed in motor functions and motility properties.

Much of the current understanding of kinesin motors structure, function and mechanics comes from studies done on kinesin-1. Towards amino terminus, kinesin motors consists of core catalytic motor domain that consists of ATP and microtubule binding sites. Followed by a neck linker and neck coil, that is critical for motor dimerization and generating processive motility. Extended towards the carboxyl-terminal are coiled-coil stalk regions primarily involved in regulatory functions and cargo binding **(Figure 1.5)**

(Coy et al., 1999; Verhey et al., 2011b; Woehlke and Schliwa, 2000; Yildiz et al., 2004).

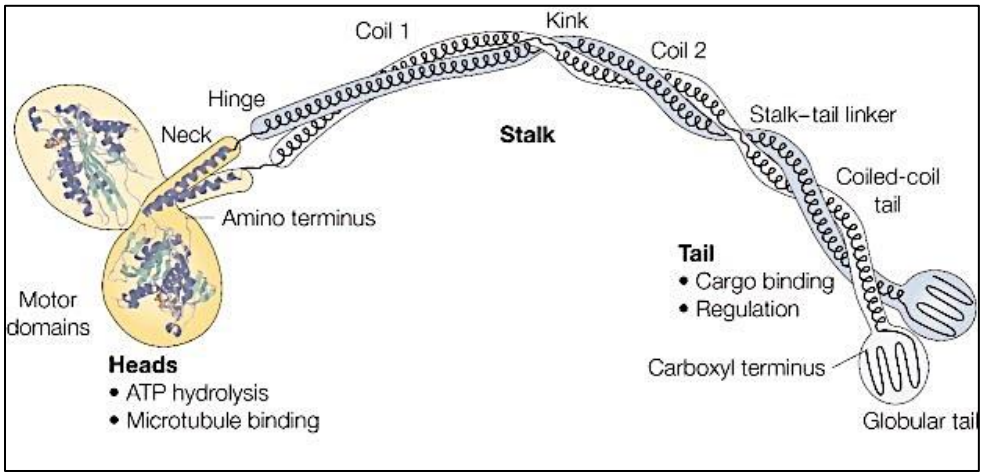

Figure 1.5: Domain organization of kinesin-1 motor. Structure of dimerized kinesin-1 motor derived from cryo-electron microscopy and coil-coil programme. Head region constitutes ATP and microtubule binding region, stalk includes hinge and coil-coil regions for dimerization and tail region supports cargo binding and regulation of motor. [Adapted from (Woehlke and Schliwa, 2000)]

In general, kinesin motors harness energy derived from the kinetics of ATP turnover and generates mechanical force to walk processively along microtubule tracks. Kinesin-1 motor walks in a hand-over-hand manner (Yildiz et al., 2004). Binding of kinesin motor to the microtubule in ADP bound state triggers ADP release resulting in empty state (apo) of motor. Subsequently, ATP will bind and fill the pocket; binding of ATP changes the conformation of neck linker, forcing the rear domain to forward position. ATP from the rear head is hydrolyzed and subsequently releases the phosphate, leading to detachment of the motor head from the microtubule and cycle continues after reattachment.

Studies using advanced microscopy techniques have shown that kinesin-1 motor is ATP dependent, highly processive (ability to take multiple steps before detaching from microtubule) and robust motor. Motor takes about 100 steps with an 8 nm step size hydrolyzing one ATP per step and it can exert maximum force of 6-8 pN (Cross, 1997; Mallik and Gross, 2004; Rice et al., 1999; Schnitzer and Block, 1997). DdUnc-104, a

dimeric kinesin-3 motor that exerts maximum force of 6-8 pN has been shown to win a tough tug-of-war against four to eight dyneins that exert a maximum force of 1 pN during endosome motion (Soppina et al., 2009).

Structural studies have shown that kinesin-1 motor when not bound to cargo folds its tail region onto the motor domain and inhibits ATPase activity, which significantly reduces motors stepping rate **(Figure 1.6)**. This inhibited motor state is commonly referred to as autoinhibition, a mechanism that helps minimize ATP turnover rate, unnecessary crowding of microtubule and mislocalization of motor (Coy et al., 1999; Mallik et al., 2004; Verhey and Hammond, 2009; Verhey et al., 2011b). Autoinhibition can be relieved by cargo binding, phosphorylation or binding of small GTPases like Rabs.

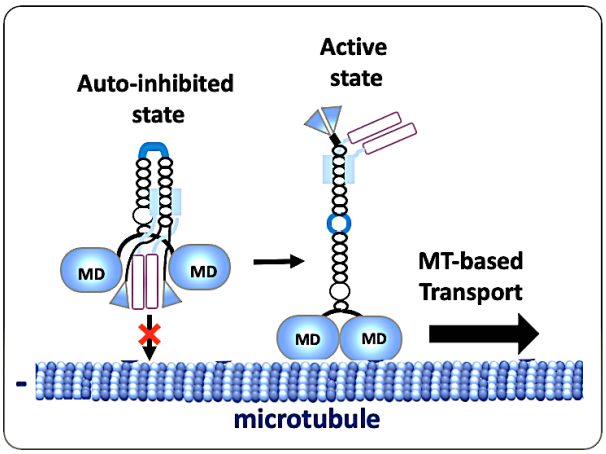

Figure 1.6: Autoinhibited and active state of kinesin-1 motor. Schematic of autoinhibited/inactive and active states of kinesin-1 motor. (https://www.i2bc.paris-saclay.fr/structural-biochemistry-of-microtubules-kinesins-and-their-cargos-gigant-menetrey/topics-gigant-menetrey)

1.4. Kinesin-3

Kinesin-3 motors are the largest among 14 kinesin families in the mammalian system, consisting of five subfamilies (KIF1, KIF13, KIF14, KIF16, and KIF28**) (Figure 1.7)**. These kinesin-3 motors were first identified during a forward genetic screen experiment in Caenorhabditis elegans (*C.elegans*), *Ce*UNC-104, showing severe uncoordinated and slow movement phenotype. Later electron microscopic analysis of these mutant

C.elegans worms displayed transport defect phenotype of synaptic vesicles in axons (Bloom, 2001; Hall and Hedgecock, 1991). Similar to *Ce*UNC-104, knockout studies in mice identified mammalian homologue, KIF1A with a similar presynaptic vesicle transport defect (Okada et al., 1995). Since its discovery, kinesin-3 motors have been shown to play key role in cell division, development, transport of synaptic vesicle, lysosomes, mitochondria, endosomes, signaling molecules, viral particles etc. Defects in functional output of these kinesin-3 motors results in many developmental, cancerous, and neurological diseases (Franker and Hoogenraad, 2013; Hirokawa et al., 2010; Lee et al., 2015; Zhao et al., 2001).

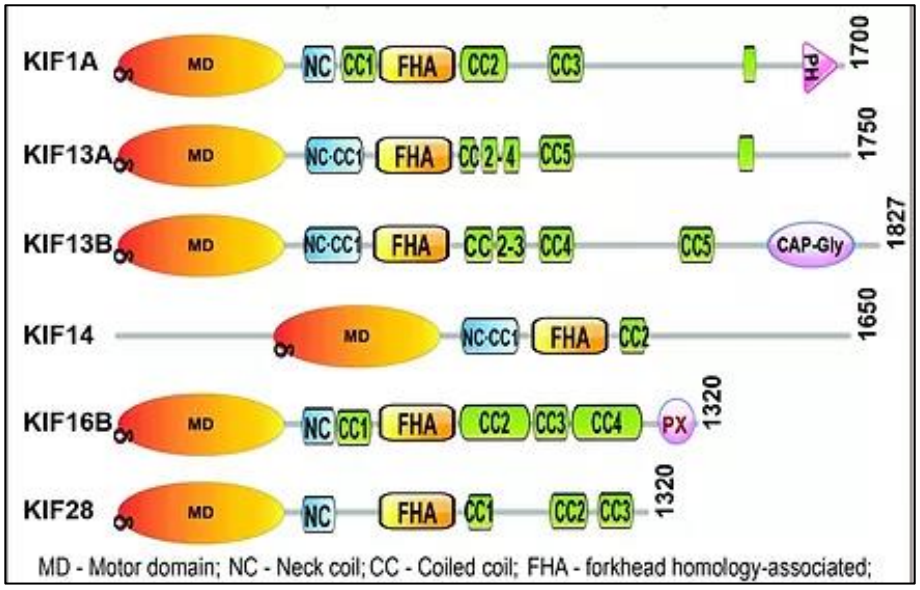

Figure 1.7: Domain organization of kinesin-3 family motors. Kinesin-3 consists five subfamilies, KIF1, KIF13, KIF 14, KIF16, and KIF28. [Adapted from (Soppina et al., 2014)].

Earlier studies on KIF1A motor in mammals demonstrated that these motors exist in a monomeric state and undergo biased diffusional motion along microtubules due to the weak neck-coil dimerization domain and velocity of these monomeric motors was ~10-fold slower than kinesin-3 cargoes transported in cells. Interestingly, recent studies have suggested that, members of kinesin-3 motors are autoinhibited in a monomeric state due to intramolecular interaction, when not bound to cargo and gets activated or dimerized

upon binding to cargo due to intermolecular interaction. Basically, kinesin-3 motors undergo cargo-induced homodimerization **(Figure 1.8).** Kinesin-3 motors employ a unique mechanism of regulation to ensure that cargo binding and processive motility are tightly linked.

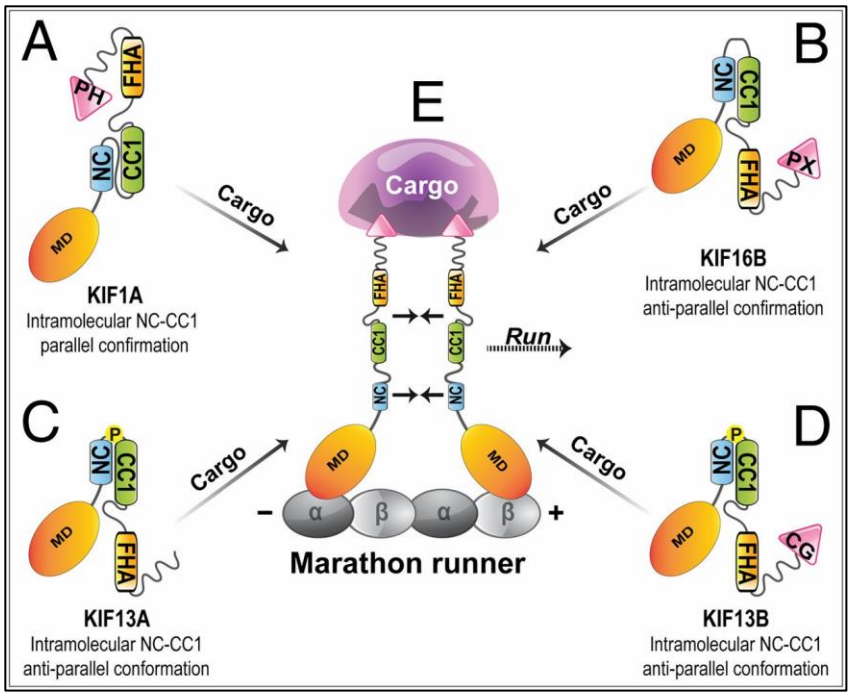

Figure 1.8: Regulation mechanism of kinesin-3 motors. Intramolecular interaction within kinesin-3 motors mediated by the neck coil-coil coiled (NC-CC1) region is relieved upon cargo binding and motors get dimerized through intermolecular interaction. Dimerized motors are fast and superprocessive. [Adapted from (Soppina et al., 2014)].

Corresponding to other plus end directed kinesin motors, motor domain of kinesin-3 motors also locates towards N-terminus, encompassing microtubule-binding region and ATP binding region. Interestingly, kinesin-3 motors possess a stretch of lysine residues in its loop 12 region of the motor domain, termed as K-loop. This positively charged K-loop region interacts with negatively charged glutamate residues in the E-hook region located towards the C-terminus tail of microtubule (Okada and Hirokawa, 1999). K-loop assists kinesin-3 motor high landing rate on microtubules in its ADP-bound state compared to kinesin-1 motors that shows weak binding to microtubules in ADP-bound

state. This interesting observation hints at kinesin-3 motors evolutionary modifications to carryout long-distance transport in neurons (Soppina and Verhey, 2014) **(Figure 1.9)**.

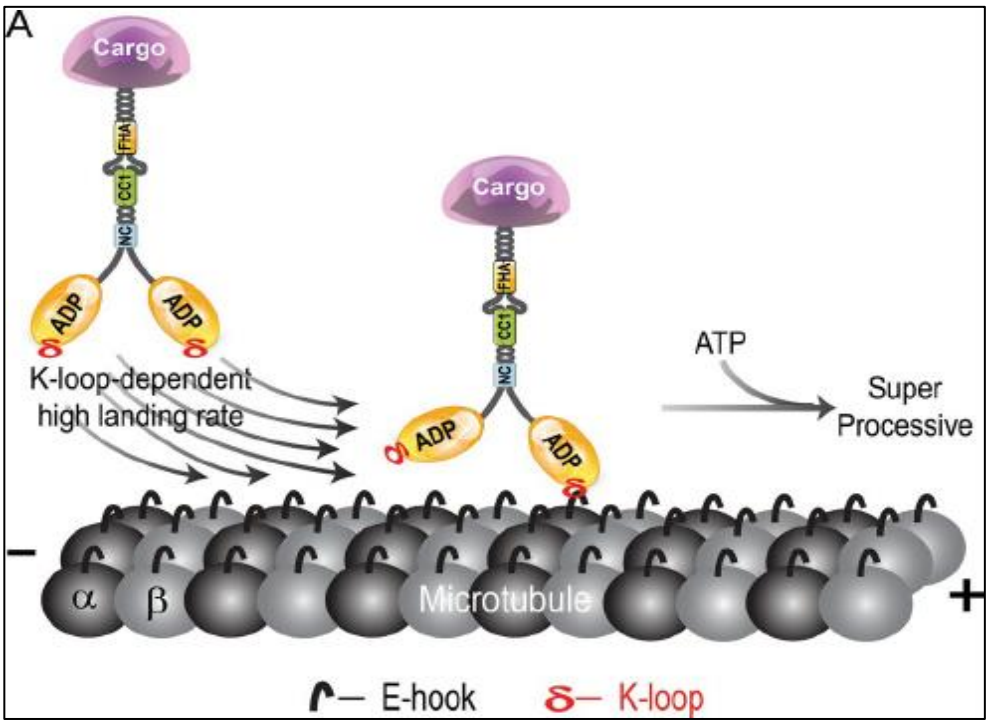

Figure 1.9: K-loop influences high microtubule landing rate in ADP state. Positively charged K-loop binds to negatively charged E-hook region on microtubule and increased binding efficiency in ADP-bound state. [Adapted from (Soppina and Verhey, 2014)].

Following the motor domain, kinesin-3 motors share a conserved α-helical neck coil (NC) region that shows weak coiled-coil propensity. This neck-coil domain engages in intermolecular interaction, resulting in motor dimerization. Succeeding NC region are the coiled-coil 1 and 2 (CC1 and CC2) regions that orchestrates higher folding ability and are believed to assist in regulation and dimerization mechanism (Ren et al., 2018). Between these two regions is a well-conserved globular forkhead-associated (FHA) domain. FHA domain is believed to mediate protein–protein interactions in a phosphorylation-dependent manner, it recognizes and binds to phospho-Thr/Ser proteins (Al-Bassam and Nithianantham, 2018; Li et al., 2000; Siddiqui and Straube, 2017; Westerholm-Parvinen et al., 2000). Recent studies have shown that FHA domain play a

key role in motor regulation (Al-Bassam et al., 2003; Lee et al., 2004). C-terminal tail region of kinesin -3 motors consists of unique membrane binding regions, Plekstrin homology (PH) domain in KIF1A, Phox homology (PX) domain in KIF16B, and Cytoskeleton associated protein Gly-rich (Cap-Gly) domain in KIF13B that binds end-binding homology domains, zinc-finger motifs and proline-rich sequences (Siddiqui and Straube, 2017; Soppina et al., 2014; Steinmetz and Akhmanova, 2008) (**Table 1**).

KIF1A/UNC-104 was the first long distance neuronal specific kinesin-3 motor identified in *Caenorhabditis elegans*, responsible for the transport of synaptic vesicles. Similar to kinesin-1, KIF1A motor is believed to undergo an autoinhibition state when not bound to cargo (Al-Bassam et al., 2003; Hammond et al., 2009; Lee et al., 2004). Globular lipid binding pleckstrin homology (PH) domain towards the C-terminus of KIF1A binds to phosphatidylinositol (4,5) bisphosphate (PIP2)-containing vesicles (Klopfenstein et al., 2002). KIF1A motor has been shown to be the fastest motor among kinesin family (Soppina et al., 2014). Several clinical studies have linked mutations in KIF1A gene to neurological pathologies (Cheon et al., 2017; Esmaeeli Nieh et al., 2015; Hirokawa et al., 2010; Langlois et al., 2016; Okamoto et al., 2014; Zhao et al., 2001).

KIF13A is a member of kinesin-3 family motor, involved in transport of proteins like mannose-6-phosphate and serotonin receptors and control the anxiety levels. Recent *in vivo* studies have shown that KIF13A motors function as weak dimers and regulate recycling endosome (RE) tubulation and cargo recycling. Authors have shown that proline-induced autoinhibition of KIF13A motors is relieved *in vivo* by binding of Rab22a, a GTPase and regulates motor dimerization, processivity and force production during RE tubule formation and sorting (Patel et al., 2021).

KIF13B/ GAKIN (guanylate kinase-associated kinesin), a homolog of KIF13A binds to phosphatidylinositol- (3,4,5)-trisphosphate (PIP3)-interacting protein, PIP3 BP and forms a complex to transport PIP3 vesicles to the neurite ends and regulates axon-dendrite polarity determination. Autoinhibited KIF13B motor is activated by human discs large (hDlg) protein (Yamada et al., 2007). Though KIF13A/13B are structurally similar, KIF13B motor has a globular CAP-Gly domain that binds to microtubule.

Table 1: List of selected cargoes of kinesin-3 motors

Cargoes transported by kinesin-3 motors.

[Adapted by (Siddiqui and Straube, 2017)].

Kinesin-3 motors	Cargoes	References
KIF1A	Tyrosine kinase A receptor (TrkA)	(Tanaka et al., 2016)
	Beta secretase_1 (BACE_1)	(Hung and Coleman, 2016)
	AMPA receptors	(Shin et al., 2003)
	Synaptotagmin and Synaptophysin	(Okada et al., 1995)
	Dense core vesicles (DCVs)	(Lo et al., 2011)
KIF1B	Mitochondria	(Nangaku et al., 1994)
	Lysosomes	(Matsushita et al., 2004)
	SCG10 / Stathmin_2	(Drerup et al., 2016)
KIF1C	α5β1_integrin	(Theisen et al., 2012)
KIF13A	Serotonin type 1A receptor	(Zhou et al., 2013)
	Mannose-6-phosphate receptors	(Nakagawa et al., 2000)
	(MPRs)	(Sagona et al., 2010)
	FYVE_CENT	(Fehling et al., 2013)
	Viral matrix proteins	
KIF13B	Human discs large (hDlg) tumor suppressor	(Yamada et al., 2007)
	PtdIns(3,4,5)P3_containing vesicles	(Horiguchi et al., 2006)
	Transient receptor potential vanilloid 1 (TRPV1)	(Xing et al., 2012)
	Vascular endothelial growth factor receptor 2 (VEGFR2)	(Yamada et al., 2014)
KIF16B	Fibroblast growth factor receptor (FGFR)	(Ueno et al., 2011)

However, a detailed functional role of CAP-Gly domain and its physiological significance still needs to be established.

Furthermore, KIF16B motor regulates early endosome trafficking towards plasma membrane by binding to small GTPase Rab5 via its C-terminal PhoX (PX) homology domain (Hoepfner et al., 2005). KIF14 motor plays major role in later stages of cytokinesis by localizing to midbody region and it is overexpressed in many cancerous conditions (Arora et al., 2014).

Recent single molecule studies have shown that kinesin-3 motors are fast and superprocessive, ability to take steps without detaching from microtubule (Soppina et al., 2014). Since the measured run lengths and speed matches with that of cargo transported *in vivo* in long axons, these kinesin-3 motors are believed to be evolutionarily adapted to drive long distance transport. Hence these kinesin-3 motors are considered as marathon runners of the cellular world (Soppina et al., 2014). Biochemical and biophysical studies done on KIF1A/UNC-104 motor demonstrates that processivity is intrinsic to its core motor domain (Tomishige et al., 2002).

Extensive studies from kinesin-1 motor have demonstrated that ATP binding and hydrolysis in each motor head coordinates conformation change and influences microtubule binding that enables processivity of the motor. Though the motor domain region is highly conserved among kinesin family, a unique superprocessive function of kinesin-3 motors has intrigued the entire molecular motor field. How kinesin-3 motors are evolutionarily modified to gain family-specific motility properties is an interesting question to address. In an attempt to address these questions, in this dissertation I have tried to understand molecular basis of kinesin-3 family specific superprocessivity, high velocity and high landing rate ability compared to well characterized motor, kinesin-1.

1.5. Organization of the thesis work

To summarize briefly**,** during this thesis I have thoroughly investigated biochemical and biophysical properties of kinesin-3 motors. Kinesin-3 is one of the largest among kinesin superfamily, consisting of five subfamilies (KIF1, KIF13, KIF14, KIF16 and KIF28). Kinesin-3 motors are fast and superprocessive with high microtubule affinity. Here I have purified kinesin-3 motors using the Sf9-baculovirus expression system and demonstrated that they exhibit high ATP turnover rates. Kinesin-3 velocities (KIF1A > KIF13A > KIF13B > KIF16B) show an inverse correlation with microtubule affinities (KIF1A < KIF13A < KIF13B < KIF16B). Furthermore, *in vitro* and *in vivo* studies displayed significant microtubule-bending. To conclude, for the first time, we have shown that a fine balance between the rate of ATP hydrolysis and microtubule affinity endows kinesin-3 motors with distinct mechanical outputs.

Thesis includes five chapters:

Chapter 1 – Introduction about intracellular transport, kinesin motors, kinesin-3 motor and objectives of the thesis. Chapter 2 – Detailed literature review about biochemical and biophysical properties of kinesin motors. Chapter 3 – Materials required and methods employed to address the objectives proposed in chapter 1. Chapter 4 – Results obtained during the entire study and significance of these results. Chapter 5 – Discussion of conclusions of the whole thesis work.

Objectives:

1. **To standardize Sf9-baculovirus expression system to purify kinesin-3 motors.**
2. **To study biophysical properties of Sf9- purified kinesin-3 motors using *in vitro* single molecule studies.**
3. **To study biochemical properties of Sf9- purified kinesin-3 motors by ATPase measurement studies.**
4. **To study collective behavior of Sf9- purified kinesin-3 motors using *in vitro* microtubule gliding assay.**
5. ***In vitro* and *in vivo* studies to understand the molecular basis of microtubule binding and bending properties of kinesin-3 motors.**

Chapter 2

Review of literature

2.1. Mechanochemical ATPase cycle of kinesin-1 motor

The fundamental behavior of a crowded cell is packaging, distributing and delivering molecules and organelles to their precise location spatially and temporally. Remarkable advances in microscopy techniques have identified unique proteins that drive directed trafficking inside the cell. These proteins transport cargoes along cytoskeletal tracks following a defined motion and were grouped as myosins, which walk along actin filaments and kinesin and dynein, which walk along microtubules. Several studies have reported that the cycle of ATP turnover is a traditional integral mechanism that these motors adapt to be processive. Kinesin superfamily motor proteins are ATPases that utilizes energy from ATP hydrolysis to generate processive motility along the microtubule tracks. The chemical and mechanical cycles are coupled together to drive motor binding and processivity along microtubules. This nucleotide-binding and hydrolysis pocket is located in the conserved motor domain region of kinesin motors. Though the motor domain is highly conserved among kinesin superfamily, variation in the functional output signifies diversity in the kinetic and structural properties.

Conventional kinesin-1 is a well-characterized motor and much of the knowledge we have about the biophysical and biochemical properties of motors come from kinesin-1. Typical dimeric kinesin takes a step size of 8nm (Svoboda et al., 1993), which corresponds to the space between β-tubulin units along the microtubule filament. The landing of motor on the microtubule track initiates the mechanochemical ATPase cycle in the motor domain. Generally, all processive kinesin motors consume usually one ATP molecule per 8nm step (Schnitzer and Block, 1997). Critical steps involved during ATPase cycle are- nucleotide free (apo, (Ø), ATP-bound, ADP–Pi-bound, and ADP-bound states (Friel and Howard, 2012; Hackney, 1994; Vale and Milligan, 2000). In the cytosol, kinesin motors exist in a autoinhibited weak ADP bound state. Upon binding to microtubules ADP is released and renders the motor in a nucleotide free (apo, (Ø) state,

which shows strong microtubule binding. Until this, the neck linker region following the motor domain is free swinging. However, binding of MgATP to the empty pocket induces partial docking of the neck linker on the motor head with its C-terminal facing microtubule plus end, which creates a strain biasing the tethered head forward. Subsequently ATP in the trailing head gets hydrolyzed into ADP–Pi state which leads to complete docking of neck linker, binding of tethered head tightly, the release of ADP and finally resulting in a single step. Phosphate release from the trailing head results in a weak ADP state, which shows a greater tendency to detach and the cycle of attachment and detachment, continues by hydrolysis of one ATP/step (Cross, 2016) **(Figure 2.1)**.

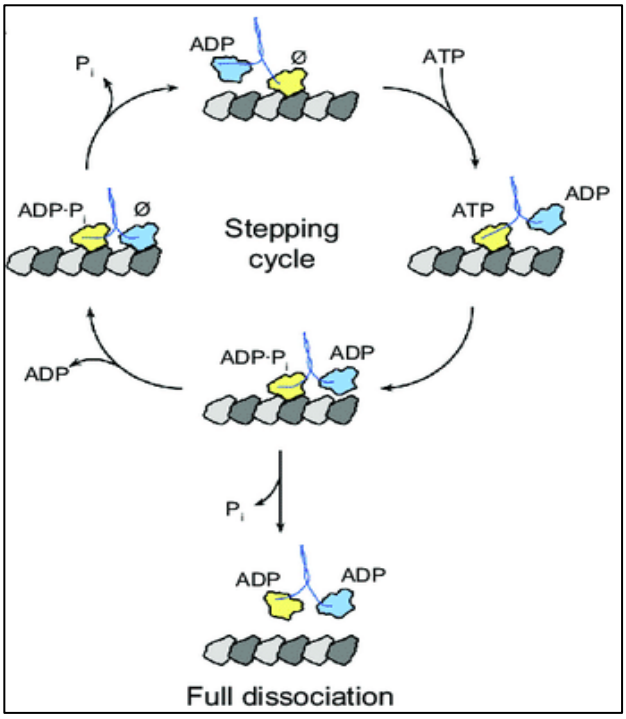

Figure 2.1: Mechanochemical ATPase cycle of kinesin-1 motor. Binding of kinesin motor to microtubule triggers ADP release from the leading head and is in apo or empty state (strongly bound state). Next binding of ATP creates strain in the neck linker and throws the trailing head forward. Subsequently ATP gets hydrolyzed in the trailing head into ADP–Pi state (strongly bound state) followed by the release of phosphate rendering the motor in a weak ADP bound state. [Adapted from (Olmsted et al., 2015)].

Previous studies have suggested a direct link between ATPase activity and speed of muscle contraction by myosin (Barany, 1967) and processivity of kinesin-1 motors (Friel and Howard, 2012). ATPase activity of kinesin-1 is strongly stimulated by binding to microtubules (Kuznetsov and Gelfand, 1986) and they hydrolyze more than 100 ATP molecules before detaching (Hackney, 1994). At near-zero load, kinesin molecules hydrolyze a single ATP molecule per 8-nm advance (Schnitzer and Block, 1997). Single molecule studies revealed, kinesin-1 walks with a maximum velocity of ~800-900 nm s^{-1} with a mean run length of ~1 μm, considering kinesin-1 motor advances by 8nm step the motility properties indicate that it takes more than 100 steps before release (Seitz and Surrey, 2006; Soppina et al., 2014). Biochemical studies to understand ATP hydrolysis rate of kinesin-1 motor determined k_{cat} of 94 s^{-1} (maximal ATPase rate) and K_m of 11 μM (tubulin concentration at which half-maximal hydrolysis rate occur) (Coy et al., 1999). The ratio of the speed of kinesin-1 to its microtubule stimulated ATP hydrolysis rate yields a step size of ~8.54 nm and stoichiometry of 1.07 steps/ATP hydrolyzed, indicating a tight coupling between their chemical and mechanical cycles. These studies done on kinesin-1 leads the way in understanding other kinesin motor family members that are gifted with a unique crucial role to play at every stage of development.

2.2. Mechanochemical ATPase cycle of kinesin-3 motor

The mammalian kinesin-3 family is one of the largest among kinesin superfamily and consists of five subfamilies (KIF1, KIF13, KIF14, KIF16 and KIF28) (Miki et al., 2005). CeUNC104, a *Caenorhabditis elegans* homolog of mammalian KIF1A, was first identified during genetic screening where its mutation severely affected the transport of synaptic vesicles to axonal terminal (Hall and Hedgecock, 1991). Since then, kinesin-3 motors have been found to be associated with diverse cellular and physiological functions including vesicle transport, signaling, mitosis, nuclear migration and development (Ahmed et al., 2012; Arora et al., 2014; Barkus et al., 2008; Sagona et al., 2010). Defects in kinesin-3 transport have been implicated in a wide variety of neurodegenerative, developmental and cancer diseases (De Vos et al., 2008; Gunawardena et al., 2014; Hirokawa et al., 2010).

Kinesin motors are grouped based on core motor domain sequence alignment. It is hypothesized that catalytic functions may also correlate with well-characterized kinesin-1 motor. Surprisingly, recent work has demonstrated that kinesin-3 motors are unique in their microtubule on-rate (Soppina and Verhey, 2014), high velocity, superprocessivity and they employ cargo-induced dimerization mechanism to transport cellular cargoes (Soppina et al., 2014). These motility properties are reflected in the motion of known kinesin-3 cargoes in neurons (Barkus et al., 2008; Hung and Coleman, 2016; Lee et al., 2003; Zhou et al., 2001). We therefore, hypothesize that family-specific evolutionary adaptations in the kinesin-3 motor domain endowed these motors with distinct mechanical outputs critical for their neuronal transport and functions. The ATP turnover cycle is fundamental to the action of motor proteins along the microtubules. Its alteration in the ATP turnover cycle provides one way the characteristic motor domain can be tuned to diversity in the function observed for kinesin-3 motors.

Therefore, understanding the kinesin-3 chemomechanical cycle is critical for interpreting the motor's diverse cargo transport properties and cellular functions. Most importantly, how kinesin-3 motors have evolutionarily adapted to accomplish functional diversity is of particular biological significance. Therefore, dissection of the cycle of ATP turnover of kinesin-3, both in the presence and absence of microtubules, can help interpret the observed behavior. ATP turnover cycle of these highly processive kinesin-3 motors is poorly studied. Some of the studies are explained below-

Pioneering work from Hirokawa lab has measured the kinetic parameters of truncated monomeric KIF1A motor (C351) containing only motor domain followed by 23-aminoacid linker of kinesin-1, which is not sufficient for dimerization. The measured k_{cat} value was found to be $110 \pm 5\ s^{-1}$, which is very close to k_{cat} value of kinesin-1 motor. The possible reason could be that these motors are monomeric and diffusive along negatively charged microtubule surface through an electrostatic interaction with family-specific positively charged insert the K-loop in the loop12. Interestingly, KIF1A motor (C351) took more than 600 steps before releasing from microtubule making it five times more processive than the dimeric conventional kinesin-1 construct (Okada and

Hirokawa, 1999, 2000). One difficulty with the monomeric motor was the 10-fold slower than that of multiple KIF1A motors or kinesin-3 cargoes transported in cells.

To test the possibility that Unc104/KIF1A might function as a dimer, constitutively active green fluorescent protein (GFP) tagged Unc104 dimer was engineered by fusing the GCN4 leucine zipper (LZ) after the neck coiled-coil or by joining the kinesin-1 neck coiled-coil and stalk to Unc104 motor domain. Single-molecule studies from these constructs yielded an average velocity of 2 μm s^{-1} and measured ATPase rate, k_{cat} value of 30-100 s^{-1} per head instead of 125 s^{-1} per head. The observed discrepancy could be due to portion of bacterially purified inactive proteins possibly due to improper folding (Tomishige et al., 2002).

More recently and a detailed chemomechanical analysis of KIF1A established that it follows the same chemomechanical cycle as demonstrated for kinesin-1 and -2. The authors utilized KIF1A chimera (KIF1A-406), which includes 61 residues from the kinesin-1 neck coil added after the native KIF1A head and neck linker. Interestingly, KIF1A showed increased rear-head detachment rate and strong microtubule binding state post ATP hydrolysis step, hence majority of KIF1A chemomechanical cycle is spent in a one-head-bound state. The biochemical assay measured k_{cat} value of 115 ± 16 s^{-1} and k_m of 1.2 ± 0.5 mM per dimer. The measured ATPase value barely matches its stepping rate, which should be around 200-250 s^{-1}. Hence possible slow ATPase rate might be due to bacterial expression and purification of KIF1A protein and also may be due to weak dimerization status of KIF1A-406 construct (Zaniewski et al., 2020).

Very few reports are available on ATPase measurement for other members of the kinesin-3 family and are poorly studied. Asaba et al., measure the microtubule stimulated ATP turnover rates for truncated KIF13B/GAKIN motor and revealed a k_{cat} value of 45 s^{-1} and k_m of 0.1 μM. The measured k_{cat} values are significantly lower than a well-characterized moderately processive kinesin-1. There might be two possibilities for such a low activity; first, the use of a bacterial expression system to purify motor proteins, which yields a large fraction of misfolded proteins. Second, the construct GAKIN 1–368

(G368) lacks the neck-coil domain, critical for motor dimerization and processive motility (Asaba et al., 2003). Similar, ATPase measurements of truncated KIF13B/GAKIN motor purified from bacterial expression systems also showed lower activities than the well-studied kinesin-1 motor (Ren et al., 2018).

In summary, the current biochemical understanding of kinesin-3 family motors is limited. However, the measured kinesin-3 motor ATPase rates didn't correlate with the stepping rate deduced from in vitro single-molecule and the speed of known kinesin-3 cargoes transported in vivo. Such analysis requires purified, active and robust motor proteins. Hence in this dissertation, I first established Sf9-baculovirus expression stem and purified members of superprocessive kinesin-3 motors of high purity. These purified motors were used to characterize their biochemical properties and demonstrated for the first time that members of kinesin-3 family motors are robust ATPases with significantly higher ATP turnover rates compared to a well-established kinesin-1 motor. Additionally, the measured ATPase rates of kinesin-3 motors inversely correlate with their microtubule binding affinity, a unique mechanism to regulate the speed of cargo transport. We also established a detailed mechanism that kinesin 3 motors utilize to generate microtubule bending *in vitro* and *in vivo*.

2.3. Purification of active kinesin-3 motors

Understanding regulatory mechanisms of superprocessive kinesin-3 motors using cellular, biochemical and biophysical approaches demand purified proteins at a large scale. Recently, kinesin-3 motors have been demonstrated as marathon runners of the cellular world using motor lysates prepared from mammalian cells. The single-molecule motility analysis of these motors showed higher microtubule affinity, inherently fast and remarkably superprocessive motility (Soppina et al., 2014). However, large-scale expression and purification of these motors using mammalian cells would be expensive and time-consuming when we aim for large culture. An alternate approach that immediately crosses the mind would be prokaryotic expression system, a primary choice of protein purification at a large scale. Unfortunately, expression of kinesin proteins in bacteria resulted in a large population of inactive or aggregated motors, presumably due

to incompatible protein synthesis, lack of protein folding and modification machinery or premature translation termination, (Korten et al., 2016; Schmidt, 2004; Tao and Scholey, 2010). Hence some studies have adapted an extra step of microtubule affinity purification in their protocol to remove inactive motor proteins (Case et al., 1997; Tomishige and Vale, 2000).

The baculovirus expression system has proven its excellence in high-throughput eukaryotic recombinant protein expression (Felberbaum, 2015; Kost et al., 2005). Due to its cost-effectiveness, safe handling and high amount of active protein expression with proper folding and post-translational modifications comparable to native systems both structurally and functionally, it has become a powerful tool (Kumar et al., 2017). Baculovirus possesses a strong polyhedrin promoter that assists in heterologous gene expression and the production of soluble recombinant proteins (Kurland and Gallant, 1996).

Baculoviruses are grouped under large double-stranded DNA viruses that prefer insect species as their host system for survival (Matthews, 1982). Autographa californica nuclear polyhedrosis virus (AcNPV) is the commonly used baculovirus that has a strong polyhedrin promoter. Polyhedrin protein is required at later stages in formation of occlusion bodies. Since deletion of this gene is not detrimental, it can be replaced with a gene of interest in recombinant baculoviruses. During recombinant baculovirus generation, a transfer vector containing the gene of interest is co-transfected with AcNPV DNA into insect cells and due to homologous recombination the foreign gene is inserted into the baculovirus. Later based on plaque phenotype and color selection, positive recombinant baculoviruses are selected. However, due to the lack of expression efficiency and time-consuming part of this traditional homologous recombination method it has been substituted with a highly improved method, ‘‘Bac-to-Bac Baculovirus Expression System” (Invitrogen).

Bac-to-Bac baculovirus expression system employs site-specific transposition of a foreign gene into bacmid DNA in *E.coli* containing a helper plasmid. To begin with, a

gene of interest is cloned into pFastBac vector containing AcNPV polyhedrin promoter for high-level expression in insect cells and left and right arms of Tn7 transposon for efficient transposition. pFastBac vector is transformed into DH10Bac *E.coli* cells that contain baculovirus shuttle vector(bacmid) containing Tn7 target site and helper plasmid. Transposition happens between Tn7 target site of pFastBac vector and bacmid with the help of transposition proteins supplied by the helper plasmid. Transformed colonies are selected based on blue/white screening. Since recombinant bacmid is really huge (>135kb), PCR analysis is employed to detect the insert. Positive recombinant bacmid is isolated using standard DNA isolation kits and transfected into insect cells (*Spodoptera frugiperda* (Sf9)). Recombinant baculoviruses are generally secreted ~72hr post transfection and this virus stock is further amplified for expression and purification of recombinant proteins in large-scale Sf9 cell culture **(Figure 2.2)**.

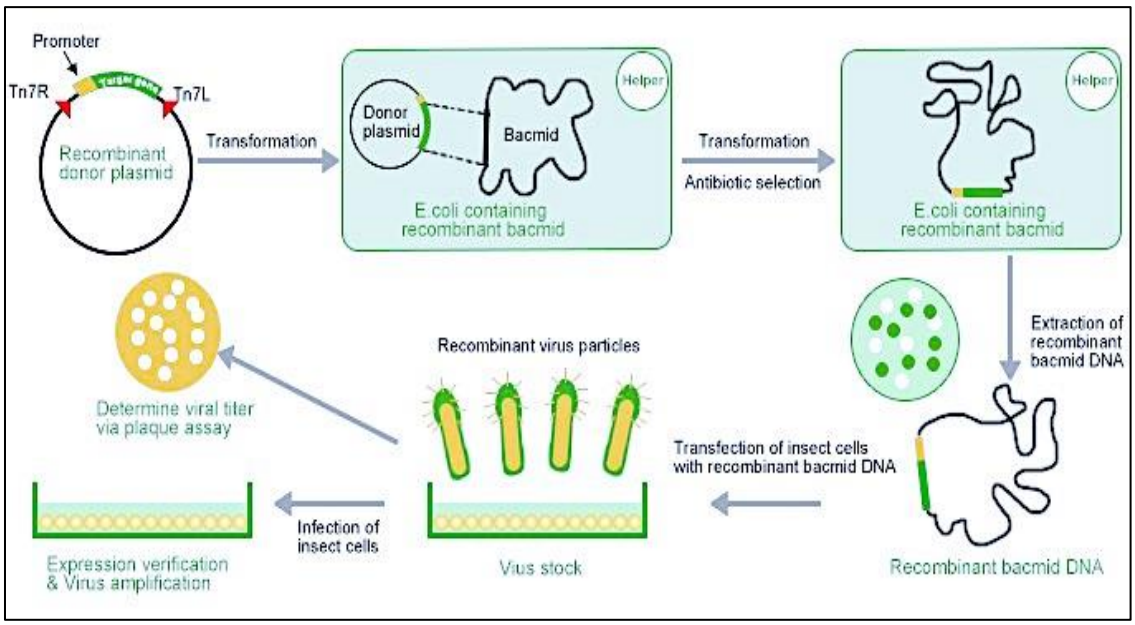

Figure 2.2. Bac-to-Bac Baculovirus Expression System. Gene of interest is cloned into pFastBac vector and transformed into DH10Bac *E.coli* cells for recombination. Recombinant bacmid is isolated and transfected into Sf9 cells for viral production and amplification. Adapted from https://www.geneuniversal.com.

To overcome the limitations posed by bacterial purification systems and mammalian cell lysate and to increase the yield here we have established a robust Sf9-baculovirus expression system to express and purify superprocessive kinesin-3 motors. Since the commercially available bacmid generating kits are expensive and we will be working with more samples, we developed an in-house protocol for both large and small inserts of kinesin-3 motors into bacmids. Sf9-purified kinesin-3 motors were used to characterize *in vitro* single-molecule and multi-motor microtubule gliding properties using total internal reflection fluorescence (TIRF) microscopy.

Chapter 3

Materials and Methods

3.1. DH10Bac competent cell preparation: Luria Bertani (LB) broth supplemented with kanamycin and tetracycline was inoculated with overnight grown DH10Bac primary culture and incubated at 37°C until OD reached 0.4-0.6. The cells were harvested by spinning at 8000 rpm for 10 min at 4°C and resuspended in 100 ml competency buffer (60 mM $CaCl_2$, 10 mM PIPES, 15% glycerol, pH 7.0). After 30 min of incubation on ice, cells were collected by centrifuging at 4000 rpm for 10 min, 4°C. This final pellet was resuspended in competency buffer and snap-frozen into small aliquots in liquid nitrogen before storing at -80°C.

3.2. Generation of recombinant bacmid: Recombinant expression of a specific protein in Sf9 cells requires the generation of a recombinant bacmid. A key step in generating recombinant bacmid is the transposition of gene-of-interest into the bacmid (Zhai et al., 2019). Though the generation of recombinant bacmid using commercially available bac-to-bac kits (ThermoScientific) is simple and works well for small inserts, recombination is difficult for large-size inserts. Members of the kinesin-3 superfamily are large proteins with a molecular weight ranging from 140 kDa – 200 kDa. Moreover, it would be costly, especially when working with multiple samples. Thus, we generated recombinant bacmids containing full-length and constitutively active kinesin-1 and kinesin-3 motors by employing bac-to-bac methodology in-house. The coding sequence for kinesin-1 [full-length, KHC-mCit-Flag and constitutively active, KHC(1-560)-mCit-Flag] and kinesin-3, [full-length, KIF1A-mCit-Flag, KIF13A-mCit-Flag, KIF13B-mCit-Flag and KIF16B-mCit-Flag and constitutively active, KIF1A(1-393LZ)-mCit-Flag, KIF13A(1-411ΔP390)-mCit-Flag, KIF13B(1-412ΔP391)-mCit-Flag and KIF16B (1-400)-mCit-Flag] were sub-cloned into pFastBac backbone plasmid using PCR amplification.

The above plasmids were transformed into DH10Bac competent *E. coli* carrying bacmid genome and helper plasmid and incubated at 37 ^{0}C for site-specific homologous

recombination to generate recombinant bacmids with gene-of-interest. For full-length motors, 12–16 hours of incubation time was required for successful homologous recombination between pFastBac [containing C-terminal mCitrine-Flag (mCit-Flag)-tagged full-length versions of kinesin-1 and kinesin-3 motors] and bacmid in DH10Bac cells due to their large insert size. For constitutively active versions of kinesin-1 and kinesin-3 motors, incubation for approximately 6–8 hours was sufficient.

In general, blue-white screening for recombinant bacmid often gives false positive colonies, and contamination of empty bacmid will result in low-to-no expression. Also, selection of recombinant bacmids usually requires screening a large number of white colonies (>10) by isolating bacmid DNA using expensive bacmid isolation kits. Therefore, we performed colony-PCR using bacmid-specific primer pair and screened more than 40 and 20 colonies each for full-length and constitutively active motors, respectively. Subsequently, we purified only the colony-PCR positive recombinant bacmids using PureLink plasmid isolation kit (Invitrogen) and confirmed the transposition using bacmid-specific primers. Additionally, we performed PCR with a combination of bacmid-specific and gene-specific primers. These purified recombinant bacmids were used for transfection and recombinant protein production in Sf9 insect cells. Together, these results suggest that transposition of large inserts can be achieved in-house just by incubating for a longer time in DH10Bac competent cells. This can be applied for recombination of other large proteins in bacmid. Moreover, a simple and economical colony-PCR with bacmid-specific primers can be used for the initial blue/white screening of recombinant bacmids.

3.3. Sf9 cell culture, transfection, and recombinant baculovirus production:

Sf9 cells were a kind gift from Dr. Thomas Pucadyil (Indian Institute of Science Education and Research, Pune, India). Sf9 cells were maintained in 30 mL of Sf-900/SFM medium (Invitrogen) in 100 mL disposable conical flask without any antibiotic/antimycotic at 28 $^{\circ}$C. Keep the suspension culture in an orbital shaker at 90 rpm. Supply of CO_2 and humidity maintenance is not required. Cells are usually

subcultured every fourth day by inoculating 0.5 x 10^6 cells/mL to reach 2.0 x 10^6 cells/mL density on the fourth day.

1. P0 virus stock generation

1.1 For transfection, seed cells into a 35 mm dish with 4.5 x 10^5 cells/mL confluency and maintain at 28 °C without shaking.

1.2 After 24 h, once cells are attached and look healthy, proceed for transfection as described below.

1.3 **Tube A**: Mix 1 µg of bacmid DNA encoding for constitutively active KIF1A(1-393LZ)-mCit-FLAG specific kinesin-3 motor with 100 µL of unsupplemented Grace's media.

1.4 **Tube B**: Mix 6 µL of transfection reagent with 100 µL of unsupplemented Grace's media.

1.5 Carefully transfer the content of **Tube A** into **Tube B** and mix thoroughly by pipetting up and down (approximately 20 times).

1.6 Incubate the mixture for ~45 min at room temperature.

1.7 After completing the incubation, add 0.8 mL of unsupplemented Grace's media to the above mixture and mix slowly by pipetting.

1.8 Gently aspirate the Sf-900/SFM media from cells (to remove any traces of serum that may affect transfection efficiency).

1.9 Add the transfection mixture from step 1.5 dropwise on the top of the cells and incubate the plate for 6 h at 28 °C.

2.0 After the incubation, carefully remove the transfection mixture, add 2 mL of Sf-900/SFM media and incubate further for 48 h at 28 °C.

2.1 Check for the motor protein expression under an inverted fluorescence microscope. The motor protein is tagged with a fluorescent protein, mCitrine, a variant of yellow fluorescent protein.

NOTE: Transfected cells were visualized under an inverted microscope equipped with differential interference contrast (DIC) and epifluorescence illumination with a 20x objective (200 times magnification), mercury lamp and an EM-CCD camera. Check the efficiency of virus generation and infection by monitoring the expression of mCitrine-tagged motors in cells through mCitrine excitation and emission filter cube. In addition, check for morphological changes of infected cells, such as enlarged cells/nuclei.

2.2 Again, check the cells 72 h post-infection. Usually, cells start detaching from the surface.

2.3 If >5% of cells detached from the surface, harvest the media with infected cells in 1.5 mL sterile microcentrifuge tubes and spin for 5 min at 500 x *g*.

2.4 Collect the supernatant and snap freeze aliquots of 1 mL in liquid nitrogen and store as P0 stock at -80 °C or use it to generate P1 virus stock.

2. P1 virus stock generation

2.1 To further amplify the P0 baculovirus stock and confirm protein expression, grow Sf9 cells in liquid suspension culture.

2.2 In a sterile 100 mL conical flask, add 10 mL of Sf-900/SFM media with a cell density of 2 x 10^6 cells/mL and 1 mL of P0 virus stock.

Incubate at 28 °C with constant shaking at 90 rpm.

2.3 After 72 h of infection, check for the protein expression as described earlier. If the protein expression is good (>90% of cells show a bright mCitrine fluorescence signal) and shows significant cell death (approximately 10%–15%), spin down the cells in a 15 mL sterile conical tube at 500x *g* for 5 min.

2.4 Collect the supernatant, snap freeze aliquots of 1 mL (P1 stock) in liquid nitrogen and store at -80°C or proceed for large-scale infection and protein purification.

3. Large-scale infection

3.1 For large-scale protein expression, infect 30 mL of the suspension culture at 2 x 10^6 cells/mL density with 1 mL of P1 virus stock and incubate at 28 °C with constant shaking at 90 rpm.

3.2 After ~72 h post-infection, check for the protein expression (in general, maximum protein expression is achieved between 65–75h post-infection).

3.3 If >90% of cells show a bright fluorescent signal with minimal cell death (<5%), collect the cells in a sterile 50 mL conical tube and spin down at 500 x g at 4 °C for 15 min.

NOTE: There should be minimal cell death (<5%), because dead cells release the cellular contents into the media, which leads to loss of expressed protein.

3.4 Discard the supernatant, collect the cell pellet, and proceed with protein purification.

3.4. Sf9 purification of kinesin-3 motors:

1.1 To the above cell pellet, add 3 mL of ice-cold lysis buffer (Table 2) freshly supplemented with 5 mM DTT, 5 µg/mL of aprotinin, 5 µg/mL of leupeptin, and 5 µg/mL of PMSF and lyse the cells by pipetting 20–25 times without generating any air bubbles.

1.2 Spin the cell lysate at 150,000 x g for 30 min at 4 °C.

1.3 Collect the supernatant into a fresh, sterile tube and mix with ~40 µL of 50% anti-FLAG M2 affinity resin. Incubate the mixture for 3 h at 4 °C with end-to-end tumbling.

1.4 After incubation, pellet the FLAG resin by spinning at 500 x g for 1 min at 4 °C. Gently aspirate the supernatant without disturbing the pellet with a 26 G needle and discard.

1.5 Wash the FLAG resin pellet three times with ice-cold wash buffer (Table 2) freshly supplemented with 2 mM DTT, 5 µg/mL of aprotinin, 5 µg/mL of leupeptin, and 5 µg/mL of PMSF. Pellet the beads by spinning at 500 x g for 1 min at 4 °C in each wash.

1.6 After the third wash, carefully drain the wash buffer as much as possible without disturbing the pellet. For protein elution, add ~70 µL of wash buffer containing 100 µg/mL FLAG peptide to the resin pellet and incubate overnight at 4 °C with end-to-end tumbling.

1.7 On the subsequent day, spin down the resin at 500 x g for 1 min at 4 °C. Collect the supernatant containing purified protein into a fresh tube and supplement with 10% glycerol. Snap freeze aliquots of 5 µL in liquid nitrogen and store at -80 °C until further use.

1.8 Run the SDS-PAGE gel to determine the protein concentration and yield. Along with purified protein of interest, a standard protein control, BSA of known concentrations ranging from 0.2 µg, 0.4 µg, 0.6 µg, 0.8 µg, and 1 µg are loaded to generate a standard curve. Stain the gel with Coomassie Brilliant blue.

1.9 Analyze the gel using a built-in gel quantification tool in ImageJ software. First, measure the band intensity of known concentrations of BSA and generate the standard curve. Then, measure the intensity of the purified protein band and determine the protein concentration.

The purified protein was found to be stable at 4°C for more than a week, with no significant loss of activity. The protocol yielded a recombinant protein of high purity and sufficient quantity for further analysis. The typical yield of purified proteins ranged from 15-20 mg per liter of Sf9 culture with no visible impurities. All the characterization assays were performed using freshly prepared protein samples unless otherwise stated. The homogeneity of the purified protein was further confirmed by size exclusion-high-performance liquid chromatography (SEC-HPLC) using Phenomenex SEC-3000 column with 1xPBS as mobile phase.

3.5. Circular Dichroism (CD) spectroscopy: For CD measurements, the purified protein sample was analyzed at 200 nM concentrations in 10 mM sodium phosphate, pH 7.0. The spectrum was recorded from 190–250 nm at 0.1 nm intervals and 50 nm min^{-1} using spectropolarimeter (Jasco-815). The average of three scans were used to determine the mean residue molar ellipticity [θ] (deg × cm2 × $dmol^{-1}$) was calculated according to the formula:

$$[\theta]= \theta/(NA\times d \times CM\times 10)$$

Where θ, measured ellipticity in degrees; NA, is the number of amino acids per protein; d, is the path length in centimeters; CM, is the molar protein concentration. The factor 10 originates from the conversion of molar concentration to the dmol cm^{-3}concentration unit. The secondary structures estimation and folding status was performed on BeStSel program (Micsonai et al., 2018; Micsonai et al., 2015).

3.6. Bacterial purification of constitutively active kinesin-1: Constitutively active kinesin-1, KHC (1-560)-GFP-His plasmid was transformed into BL21 pLyS cells. The overnight grown primary culture was inoculated into 200 ml LB media along with antibiotics and incubated at 37^{o}C for 2 hrs. Once O.D reaches 0.4-0.6, culture was induced with 0.5 mM Isopropyl β-d-1-thiogalactopyranoside (IPTG), and cells were grown at 22^{o}C overnight. After pelleting, the cells were lysed using B-PER™ reagent (Thermo Fisher Scientific) in the presence of protease inhibitors and processed further for purification using a standardized protocol.

3.7. Cell culture, transfection and fluorescence microscopy: COS-7 (monkey kidney fibroblast; American Type Culture Collection, Manassas, VA) cells were grown in DMEM supplemented with 10% (vol/vol) FBS (ThermoFisher Scientific, USA) at 37°C with 5.0 % CO2. Cells were transfected/cotransfected with plasmid DNA of interest using Turbofect (ThermoFisher Scientific, USA). Subsequent day, cells were lysed to prepare cell lysates or fixed for fluorescence microscopy. The mouse catecholaminergic cell line CAD (Qi et al., 1997) was grown in DMEM F12 with 10% (vol/vol) FBS (ThermoFisher Scientific, USA) at 37°C with 5.0 % (vol/vol) CO2. Cells were prompted

to differentiate by replacing with serum-free media and then transfected with plasmid DNA of interest using Lipofectamine 3000 (ThermoFisher Scientific, USA). After 48 hrs, the cells were prepared for fluorescence microscopy.

For cell lysates, 24 hrs of post-transfection COS-7 cells were washed, trypsinized and lysed in ice-cold lysis buffer (LB; 25 mM 4-(2-hydroxyethyl)-1-piperazineethanesulfonic acid/KOH, 115 mM potassium acetate, 5 mM sodium acetate, 5 mM MgCl2, 0.5 mM ethylene glycol tetraacetic acid [EGTA], 1% [vol/vol] Triton X-100, pH 7.4) freshly supplemented with 1 mM phenylmethylsulfonyl fluoride and protease inhibitors (10 μg/ml leupeptin, 5 μg/ml chymostatin, 3 μg/ml elastatinal, 1 mg/ml pepstatin). The lysates were clarified by centrifugation at 16,000 × g at 4°C and either it was immediately used for single-molecule assays or snap-freeze aliquots were frozen in liquid nitrogen and stored at −80°C until further use.

For fluorescence microscopy, 48hrs of post transfection cells were washed once with warm phosphate buffer saline (PBS), fixed in 4% (vol/vol) paraformaldehyde (PFA) in PBS for 10 mins and then mounted in Prolong Gold (ThermoFisher Scientific, USA). Images were acquired on Nikon Eclipse Ti2-E, motorized automated inverted microscope, attached with Perfect Focus System, oil-immersion 60X 1.49 NA objective, Andor iXon Ultra 897 EMCCD camera, and analyzed using NIS-Elements Advanced Research image acquisition software. To quantify motor accumulation, the average fluorescence intensity of the cell body and its neurite tip were measured using ImageJ software (National Institutes of Health, Bethesda, MD). The mean ± SEM for wild type and mutant motors were plotted as the ratio of average fluorescence intensity in the neurite tip to that in the cell body using Prism 6 software (GraphPad Software, La Jolla, CA).

For landing rate measurements, the amount of wild-type or mutant motors in the COS-7 lysates were first normalized by a dot-blot in which increasing volumes of COS-7 lysates were spotted onto nitrocellulose membrane. The membrane was air-dried and processed for immunoblotting for mCit-tag using anti-GFP antibody (A6455, ThermoFisher Scientific, USA). The spots were quantified to normalize the motor concentration. Equal

amounts of motors were added to flow cells and imaged at 20 fps. The number of motors landing on a microtubule was counted and then divided by the total length of the microtubules and the recording time in order to obtain a landing rate with the units of events/micrometer/minute.

3.8. Tubulin purification and labeling: Tubulin was purified from goat brain using the facility generously provided by Prof. Roop Mallik, TIFR, Mumbai, India, as described previously (Castoldi and Popov, 2003) and stored in liquid nitrogen until further use. Fluorescent labeling of tubulin was performed using protocol described previously with modifications (Hyman et al., 1991). Above purified tubulin was incubated with 20 molar excess NHS-Rhodamine (ThermoScientific) at 37°C for 10 min. The reaction was terminated by adding an equal volume of potassium glutamate, and the mixture was loaded onto a Sephadex G50 column kept at 4°C. The labeled tubulin was collected and cycled through a polymerization and depolymerization before snap freezing into small aliquots.

3.9. *In vitro* single-molecule motility assay using Sf9-purified kinesin-3 motors:

NOTE: The Sf9-purified kinesin-3 motors can be used to study biochemical and biophysical properties such as ATP turnover rate, microtubule affinity, velocity, run length, step size, and force generation. Here, a detailed protocol for *in vitro* single-molecule motility analysis of KIF1A (1-393LZ) using Total Internal Reflection Fluorescence (TIRF) microscopy is described.

1. Microtubule polymerization

1.1 In a pre-chilled 0.5 mL microcentrifuge tube, prepare a polymerization mix by pipetting in the following order: 12.0 µL of BRB80 buffer, pH 6.9; 0.45 µL of 100 mM MgCl2, 1 µL of 25 mM GTP.

1.2 Take out a 10µL aliquot of 10 mg/mL tubulin stored in liquid nitrogen, thaw immediately, and add into the above polymerization mixture. Mix gently by pipetting 2–3 times without creating any air bubbles.

NOTE: Perform the above steps quickly and strictly on ice.

1.3 Let the above mixture sit on ice for 5 min.

NOTE: This is a critical step to prevent denaturing of tubulin or to avoid the formation of short microtubule seeds.

1.4 Transfer the tube into a pre-warmed 37 °C heat block/water bath and incubate for 30 min for polymerization of microtubules.

1.5 While microtubules are polymerizing, thaw an aliquot of P12 buffer and bring it to room temperature.

1.6 Before completing 30 min of incubation, start preparing microtubule stabilization buffer by pipetting 100 µL of P12 buffer into a fresh microcentrifuge tube. To this, add 1 µL of 1 mM taxol and immediately vortex the mixture.

NOTE: Start preparing the microtubule stabilization buffer approximately 5 min before completing the incubation in step 1.4. Taxol stabilizes the polymerized microtubules by binding to β-tubulin.

1.7 Warm the microtubule stabilization buffer for 2–3 min at 37 °C and gently add it to the polymerized microtubules without disturbing the polymerization mixture at the bottom.

NOTE: Warming the stabilization buffer will bring it to the same temperature as the polymerization mixture.

1.8 Do not tap or pipette the mixture and incubate further at 37 °C for 5 min.

1.9 Gently tap the mixture and mix it with a beveled cut tip (200 µL capacity) slowly using the pipette.

NOTE: From this point onward, always handle microtubules with a beveled cut tip to avoid microtubule shearing.

2.0 Take 10–15 µL of polymerized microtubules in a flow cell to check for proper microtubule polymerization.

NOTE: One can visualize the unlabeled microtubules using a DIC microscopy setup.

2.1 If microtubules are concentrated, dilute them with P12 buffer supplemented with 10µM taxol.

2. Preparation of motility flow cell chamber

2.1 Prepare a motility chamber using a glass slide, double-sided tape and glass coverslip (22 mm x 30 mm).

2.2 Take a glass slide, place a drop (~70 µL) of deionized distilled water in the middle and wipe it with a lint-free tissue paper.

2.3 Cut two strips of double-sided tape (~35 x 3 mm) and firmly stick them to the glass slide parallelly, leaving an ~4–5 mm gap between two strips to create a narrow passage.

2.4 Next, take a coverslip and add a drop (~20 µL) of deionized distilled water in the middle. Place a strip of lint-free lens cleaning tissue paper on the water drop until it absorbs the water. Then, slide it slowly toward one end of the coverslip.

NOTE: The coverslip should be completely dry. No water should be visible on the coverslip.

2.5 Place the coverslip on the double-sided strips stuck on the slide and press the coverslip evenly along the strips to stick firmly.

NOTE: Please make sure that the cleaned side of the coverslip faces the glass slide.

2.6 Ensure that together this creates a narrow chamber of 10–15 µL capacity for performing motility assay.

3. *In vitro* single-molecule motility assay:

NOTE: To study the microtubule-based single-molecule motility properties of motors, microtubules need to be adsorbed onto the coverslip surface in the motility chamber.

1.1 Dilute the polymerized taxol-stabilized microtubules in P12 buffer supplemented with 10 µM taxol at 1:5 ratios and mix by pipetting slowly with a beveled tip.

1.2 Keep the flow chamber in a slant position (~15–20°). Flow 30 µL of diluted microtubule solution through the flow chamber from the upper end while keeping a lint-free tissue paper at the lower end to absorb the liquid. This creates a shear force to align the microtubule in the flow direction and helps to adsorb the microtubules straight and align parallel.

1.3 Leave a small drop of liquid on both ends of the chamber and keep the flow cell in an inverted position (coverslip facing the bottom) in a closed, moist chamber to prevent drying of the motility chamber.

1.4 Let it sit for ~30 min so that microtubules adsorb to the surface of the coverslip inside the motility chamber.

1.5 In the meantime, prepare a blocking buffer by mixing 500 µL P12-BSA buffer with 5 µL of 1 mM taxol.

1.6 Flow 40–50 µL of blocking buffer and incubate the slide in an inverted position for 10 min in a moist chamber.

1.7 Prepare a motility mixture by pipetting the following components into a 500 µL capacity sterile microcentrifuge tube in the following order: 25 µL of P12 buffer with taxol, 0.5 µL of 100 mM $MgCl_2$, 0.5 µL of 100 mM DTT, 0.5 µL of 20 mg/mL Glucose oxidase, 0.5 µL of 8 mg/mL Catalase, 0.5 µL of 2.25 M Glucose, and 1.0 µL of 100 mM ATP.

NOTE: Fluorescence imaging has been widely used for biological applications. Photoexcitation of fluorescent proteins generates reactive oxygen species (ROS), which can cause photobleaching of the fluorescent proteins and damage to the biological samples (Wojtovich and Foster, 2014; Zheng et al., 2014). Oxygen scavengers such as glucose oxidase and catalase are routinely used in motility assays to limit photodamage and prolong the bleaching time of fluorescent proteins.

1.8 Finally, add 1 µL of the purified motor to the above motility mix and mix well before flowing into the motility chamber.

1.9 Seal both the ends of the motility chamber with liquid paraffin wax and immediately image under TIRF illumination using 100X TIRF objective of 1.49 NA with 1.5x magnification.

2.0 In order to focus the coverslip surface, first, focus on one of the inner edges of double-sided tape in the motility chamber under differential interference contrast (DIC) illumination.

NOTE: The bright and uneven surface will be visible.

2.1 Then, move the focus into the motility chamber. Using fine adjustment, focus the coverslip surface and look for the microtubules adsorbed on the coverslip surface.

2.2 Once the microtubules are focused, switch to TIRF illumination with a 488 nm excitation laser and adjust the illumination depth by changing the excitation beam angle to get the best and uniform TIRF illumination.

2.3 Focus the individual mCitrine-tagged motors moving processively along the microtubule surface with 100 ms exposure and record the motion using an EM-CCD camera.

NOTE: Although the motility assays were performed on unlabeled microtubules, the maximum intensity z-projection function can be used to reveal the outline of the microtubule track. Preferentially, events on long microtubule tracks were considered for tracking analysis.

2.4 Manually track the position of the fluorescently tagged individual motors walking on long microtubule tracks frame-by-frame using a custom-written plugin in ImageJ (nih.gov) software.

2.5 Generate the histograms of velocity and run length for the motor population by plotting the number of events in each bin. Fit these histograms to a single Gaussian peak function to obtain average velocity and run length (Soppina et al., 2014).

3.10. *In vitro* microtubule gliding assay using Sf9-purified kinesin-3 motors:

NOTE: To understand the collective behavior of kinesin-3 motors, in vitro microtubule gliding assay was performed. Where motors are immobilized onto the coverslip in an inverted position and upon adding microtubules into the chamber, microtubules land on motors and glide along as the motors try to walk on them.

1.1 **Fluorescent microtubule polymerization:** Polymerize the microtubules following the protocol described previously except for mixing rhodamine labeled tubulin (3 mg/mL) with unlabeled tubulin (10 mg/mL) in a ratio 1:10.

1.2 After 30 min of polymerization, gently add 30 µL of pre-warmed microtubule stabilization buffer and incubate further for 5 min at 37 °C.

1.3 Next, shear the microtubules by pipetting with the capillary-loading tip (~25–30 times).

1.4 Prepare the motility flow chamber as described previously, flow 50 µL of Sf9-purified GFP nanobodies (2.5 µL of 100 nM diluted in 50 µL of P12 buffer) and incubate for 30 min at room temperature with the coverslip facing downward in a moist chamber.

NOTE: The motors are C-terminally tagged with mCitrine. GFP nanobodies are used to immobilize the motors due to their low dissociation constant (Muyldermans, 2013).

1.5 Block the coverslip surface by flowing 50 µL of block buffer into the flow chamber to prevent nonspecific protein adsorption and incubate further for 5 min.

1.6 Prepare the motor mix by pipetting 50 µL of block buffer, 1 µL of 100mM ATP, and 5 µL of 100 nM Sf9-purified kinesin-3 motors. Mix gently before flowing into the chamber and incubate for 30 min at room temperature in a moist chamber.

1.7 Wash the chamber twice with 50 µL of P12 casein.

1.8 In a sterile microcentrifuge tube, prepare the gliding assay mixture in the following order, 45 µL of P12-casein with 10 µM taxol, 1 µL of 100 mM ATP, 0.5 µL of 8 mg/mL catalase, 0.5 µL of 20 mg/mL glucose oxidase, 0.5 µL of 2.25 M glucose and 1 µL of sheared fluorescent microtubules. Gently mix the content before flowing into the motility chamber and seal the ends of the chamber with liquid paraffin wax.

1.9 Image microtubule gliding under TIRF illumination at 100 ms exposure and capture the images with attached EM-CCD camera.

NOTE: The average microtubule gliding velocity was determined by manually tracking approximately 100 individual microtubules frame-by-frame using a custom-written plugin in ImageJ29. Determine the average microtubule gliding velocity by generating a histogram and fitting to a Gaussian function.

3.11 ATPase assay using Sf9-purified kinesin-3 motors:

All ATPase assays were performed at room temperature as described previously for smooth muscle myosin (Trybus, 2000). Briefly, an assay mixture containing 10 nM purified kinesin motor, 1-80 µM polymerized microtubule, 1 mM DTT and 20 mM ATP was set up in BRB80 and incubated for 2 hours. At every 30 min time interval, a sample of 25 µl was collected and mixed with 25 µl of stop solution (500 mM EDTA, 10% SDS) to cease the reaction. After completion of all time points, 100 µl of developing solution (0.5% ammonium molybdate, 5 mg/ml ferrous sulfate) was added and absorbance was recorded at 655 nm within 15 min. For generating the standard curve, KH_2PO_4 solution was used.

To determine the ATPase activity, the slope of phosphate release as a function of time was plotted.

To convert nmol/min x µg to sec^{-1},

$$\text{Activity (nmol/min x µg)} = \frac{\text{Slope (OD/min) x Slope of standard curve (nmol/OD)}}{\text{µg in 25 µl}}$$

We divide with a constant, which depends on the molecular weight of the motor protein that is used. To determine the Vmax and *Km*, ATPase activity as a function of substrate concentration is used and fitted to a Michaelis-Menten equation. To determine ATP turnover rate (K_{cat}) following equation is used.

$$K_{cat} = \frac{V_{max}}{Et}$$

Where Et = total enzyme concentration and V_{max} = maximum enzyme activity. All the ATPase assays were performed in duplicates from three independent protein preparations.

3.12. Data analysis:

For single-molecule motility and gliding assays, data analysis was performed using a custom-written ImageJ plug-in (nih.gov). For single-molecule motility assays, fluorescently labeled individual motors were tracked manually frame-by-frame. Similarly, for gliding assays, translocation of fluorescently labeled microtubules was tracked manually frame-by-frame. The number of events for each sample was plotted for velocity and run length as a histogram and fit to a Gaussian distribution. All the statistical analyses were performed using GraphPad Prism (8.0).

3.13. Microtubule bending analysis:

For detailed quantification of microtubule-bending, we have set the following criteria and divided the microtubule bending into four categories based on their degree of bending: Straight (135^o – 180^o), Bent (90^o – 135^o), Moderately Bent (45^o – 90^o) and Highly Bent (0^o – 45^o). To measure microtubule bending angle *in vitro* and *in vivo*, we used built in angle tool in ImageJ software (nih.gov), which measures the angle between

the first and second segment of a segmented line selection. Quantified results are presented as percent bar graphs.

Table 2: Buffers and Reagent preparation

Sl. No	Buffer/ Reagent	Description	Note/ Remark
1.	**Lysis buffer**	20 mM HEPES, pH 7.5, 200 mM NaCl, 4 mM $MgCl_2$, 0.5% IGEPAL 7% Sucrose.	
2.	**Wash buffer**	20 mM HEPES, pH 7.5, 300 mM KCl, 2 mM $MgCl_2$	
3.	**1M K-PIPES (100 mL)**	Take 50 mL of deionized distilled water in a glass beaker and add 30.2 g of PIPES. The solution looks milky white because PIPES is insoluble at acidic pH, but solubility greatly increases when the free acid is converted to sodium or potassium salt. Therefore, slowly add approximately 6.4 g of solid KOH pellets while constantly stirring and roughly monitoring the pH. Once PIPES dissolved completely, allow the solution to cool for 20 min and then adjust pH to 6.8 using 3M KOH with constant stirring. Adjust the final volume to 100 mL, make 10 mL aliquots and store at -20oC.	Please do not overshoot the pH
4.	**200mM NaEGTA (200 mL)**	In a glass beaker, add 180 mL of deionized distilled water and 15.2 g of EGTA. The solution looks cloudy because EGTA is slightly soluble in water and requires an alkaline environment to dissolve completely. Therefore, slowly adjust the pH to 8.0 using 2M NaOH while stirring constantly. Once completely dissolved, make up the volume to 200 mL and store at 4^{o}C.	
5.	**100mM NaGTP (10 mL):**	Solutions of GTP/ATP rapidly hydrolyses to GDP/ADP and phosphate at extreme pH, so when preparing the stock solutions, precautions should be taken to minimize the hydrolysis and maintain pH. Dissolve 524 mg of NaGTP in 7 mL of ice-cold 10mM Na-PIPES pH 6.9 and immediately adjust pH to 7.0 with 5M NaOH while constantly mixing. Finally, adjust the volume up to 10 mL, aliquots of 2-100 µL were stored in a -20^{o}C freezer.	
6.	**10mM Taxol**	Pipette 586 µL anhydrous DMSO into 5 mg bottle of taxol (semisynthetic) and vortex. Prepare 10 µL aliquots and store at -80 ^{o}C freezer. A working stock of 1mM taxol is prepared by diluting a 10 µL aliquot of 10mM Taxol in 90 µL of anhydrous DMSO. Aliquots of 10 µL were stored at -20^{o}C.	***Taxol is stable in DMSO but unstable in water***.
7.	**1M $MgCl_2$ (100 mL)**	Dissolve 20.33g $MgCl_2.6H_2O$ in 70 mL of deionized distilled water and make up the volume of 100 mL. Filter through 0.22 µ filter and store at room temperature.	

8.	**BRB80 (100 mL)**	Take approximately 80 mL of deionized distilled water in a glass beaker and pipette 8 mL 1M K-PIPES pH 6.9, 100 µL of 1M $MgCl_2$ and 500 µL of 200 mM EGTA. Adjust the final volume to 100 mL with water and store 0.1-10 mL aliquots at -20°C freezer.
9.	**P12 buffer (100 mL)**	Take approximately 80 mL of deionized distilled water in a glass beaker and pipette 1.2 ml 1M K-PIPES pH 6.9, 100 µL of 1M $MgCl_2$ and 500 µl of 200 mM EGTA. Bring the volume to 100 mL with water and store aliquots of 500 µL at -20°C freezer.
10.	**P12-BSA (50 ml)**	Dissolve 750 mg BSA in 50 ml of P12 buffer and filter through 0.22 µm filter. Aliquots of 1 mL stored at -20°C freezer.
11.	**1M DTT (1 ml)**	Dissolve 154.3 mg of DTT in deionized distilled water and store at -20°C in 10 µL aliquots.
12.	**Glucose oxidase (20 mg/mL)**	Dissolve 20 mg Glucose Oxidase in 1 mL of P12 buffer, snap freeze 10 µL aliquots in liquid nitrogen and store at -80°C deep-freezer.
13.	**Catalase (8 mg/mL)**	Dissolve 8 mg Catalase in 1 mL of P12 buffer, snap freeze 10 µL aliquots in liquid nitrogen and store at -80°C deep-freezer.
14.	**2.25M Glucose (1 mL)**	Dissolve 450 mg Glucose in 1 mL of P12 buffer, snap freeze 10 µL aliquots in liquid nitrogen and store at -80°C deep-freezer.
15.	**Blocking buffer (10 mL)**	In a conical tube, dissolve 150 mg casein in 10 mL of P12 buffer by incubating at 50°C for 5 h in a water bath with intermittent mixing and filter through 0.22 µm filter. Make 500 µL aliquots and store frozen at -20°C.
16.	**1M HEPES pH 7.5 (50 mL):**	Dissolve 11.915 g of HEPES in 30 mL of deionized distilled water, adjust pH with KOH and make up the final volume to 50ml. Filter with 0.22 µ filter and store at 4°C
17.	**3M NaCl (100 mL)**	Dissolve 17.5 g of NaCl in 70 mL of deionized distilled water and make up the final volume to 100 mL. Filter and store at room temperature.
18.	**Lysis buffer (100 ML):**	20 mM HEPES, pH 7.5, 200 mM NaCl, 4 mM $MgCl_2$, 0.5% IGEPAL 7% Sucrose.

Note: All the single-molecule solutions and reagents should be stored in small aliquots at -20°C. Discard the aliquots once thawed.

Chapter 4

Results and Discussions

Kinesin-3 motors are built with unique mechanical outputs, such as high velocity, superprocessivity and a strong microtubule binding affinity compared to other kinesin family motors (Guo et al., 2019; Scarabelli et al., 2015; Soppina et al., 2014; Soppina and Verhey, 2014). A single kinesin-3 motor can take thousands of steps before detaching from the microtubule and is fueled by ATP hydrolysis (Soppina et al., 2014). Despite rigorous motility analysis over the last few years (Hammond et al., 2009; Huckaba et al., 2011; Okada et al., 2003; Okada and Hirokawa, 1999, 2000; Pierce et al., 1999; Tomishige et al., 2002), the basic chemomechanical properties of these motors remain poorly studied. Often such analysis requires purified, soluble, active motor proteins. The prokaryotic expression system is used widely for recombinant protein expression. As a control, we used a constitutively active version of kinesin-1, KHC (1-560), the founding member of the kinesin superfamily, whose motility properties are well characterized. However, expression and purification of KHC (1-560) in bacteria resulted in multiple low molecular bands **(Figure 4.1)** and protein degradation. Additionally, single-molecule motility analysis resulted in rare motility events and majority of them were bound non-specifically to the glass surface. Studies have shown that expression and purification of motor proteins using a bacterial expression system result in a large population of dead motors due to improper protein folding and/or limited capacity of the host system (Korten et al., 2016; Kurland and Gallant, 1996; Schmidt, 2004; Tao and Scholey, 2010). Thus, an additional step of microtubule affinity purification is critical to eliminate dead and inactive motor fractions to some extent (Case et al., 1997; Tomishige and Vale, 2000).

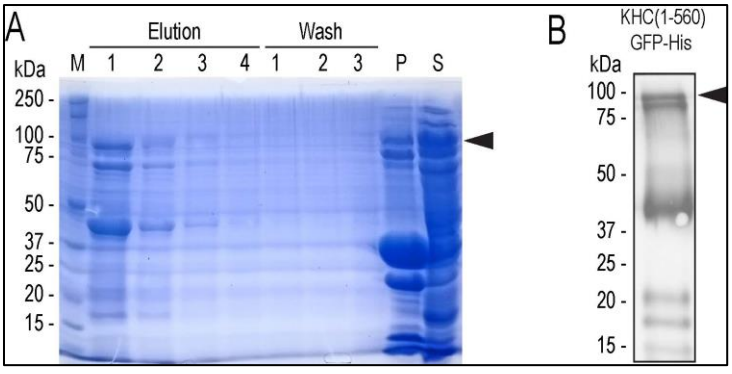

Figure 4.1. Bacterial expression of KHC (1-560) resulted in inactive and degraded protein. (A-B) Coomassie gel and Western blot images showing purified KHC (1-560) GFP-His protein from bacterial expression system. (A) Coomassie gel representing purified protein fractions, protein standard (M), elution fractions (lane 2-5), washed fractions (lane 6-8), pellet (P), and supernatant (S) after bacterial lysis and high-speed centrifugation. Though expected band size is ~80kDa, multiple bands can be seen in purified sample also. (B) For confirmation, elution fraction 1 was blotted with anti-His primary antibody. Again, multiple bands can be seen in Western blot, could be due to premature translation termination or degradation.

4.1. Generation of bacmids and purification of kinesin-1 and kinesin-3 motors using Sf9 baculovirus system.

To overcome these setbacks, we used baculovirus expression, one of the most powerful and versatile eukaryotic expression systems. Baculovirus has a strong polyhedrin promoter to drive the high-level expression of heterologous genes. In addition, this system employs the ability of cultured Sf9 cells to perform post-translational modification of expressed proteins, similar to those that occur in the natural host cell. Thus, we generated bacmids to purify full-length and constitutively active versions of kinesin 3 and kinesin-1 motors **(Figure 4.2).**

Generated bacmids were transfected into Sf9 cells and checked for the efficiency of virus generation and infection by monitoring the expression of mCitrine-tagged motors in cells under an inverted microscope equipped with differential interference contrast (DIC) and epifluorescence illumination after 48h. In addition, check for morphological changes of infected cells, such as enlarged cells/nuclei **(Figure 4.3)**. Maximum expression happens around 72 h post-infection. Usually, cells start detaching from the surface **(Figure 4.4)**. Infected cells were collected and subjected to a one-step purification approach **(Figure 4.5 A-C)**. Size-exclusion-high performance liquid chromatography (SEC-HPLC) and circular dichroism (CD) analysis of these purified motor proteins showed a homogeneous protein population with regular secondary structures and protein folding, respectively. For representation, HPLC elution profile and CD spectra of KIF1A (1-393LZ)-mCit-

FLAG is shown in **(Figure 4.5 D and E)**. These Sf9-purified motors were used for detailed biochemical and biophysical characterizations.

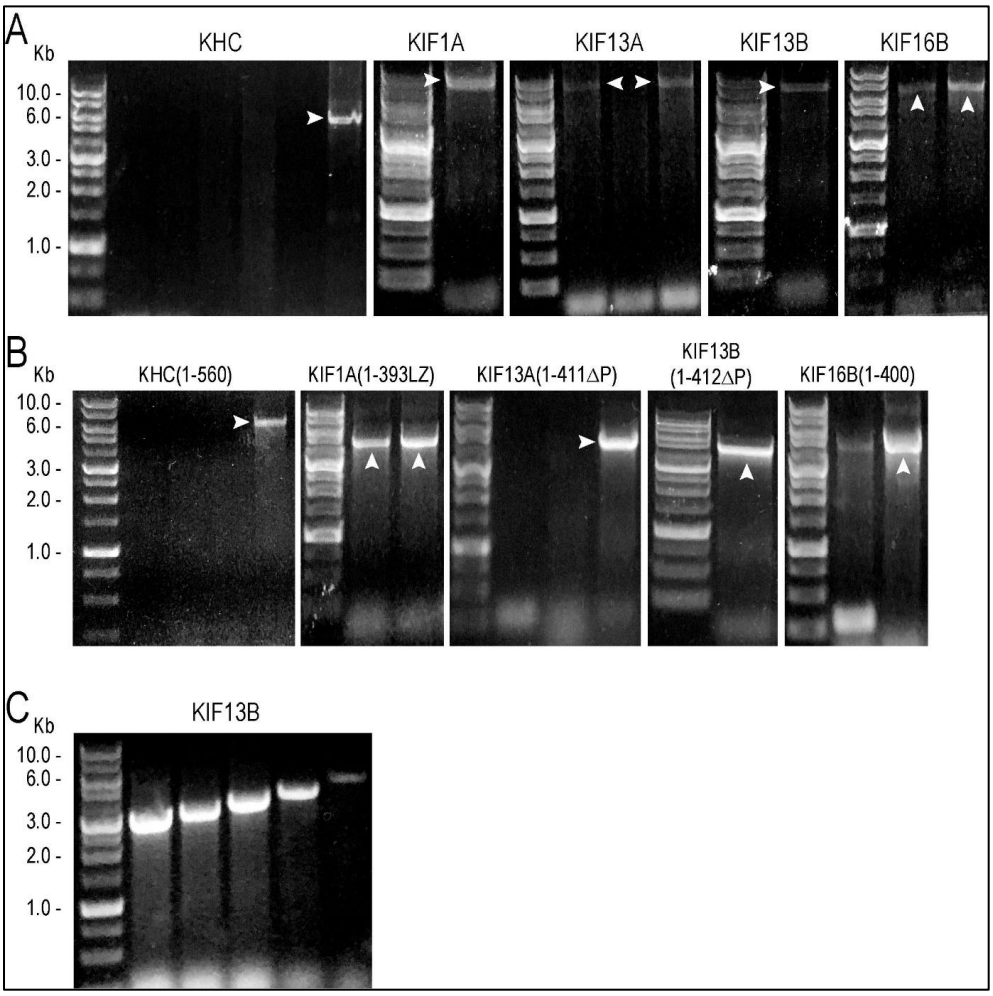

Figure 4.2. **Generation of recombinant bacmids for kinesin-1 and kinesin-3 motors.** Recombinant bacmids were generated for full-length and truncated constitutively active kinesin-1 and kinesin-3 motors using bac-to-bac system. (A-B) Screening for positive recombinant bacmid for full-length (A) and constitutively active (B) motors via colony-PCR. Expected band for recombinant bacmid for each kinesin motor is indicated with white arrowhead. (C) Representative gels for screening of bacmid with gene-specific (KIF13B) primers binding at different positions throughout the gene.

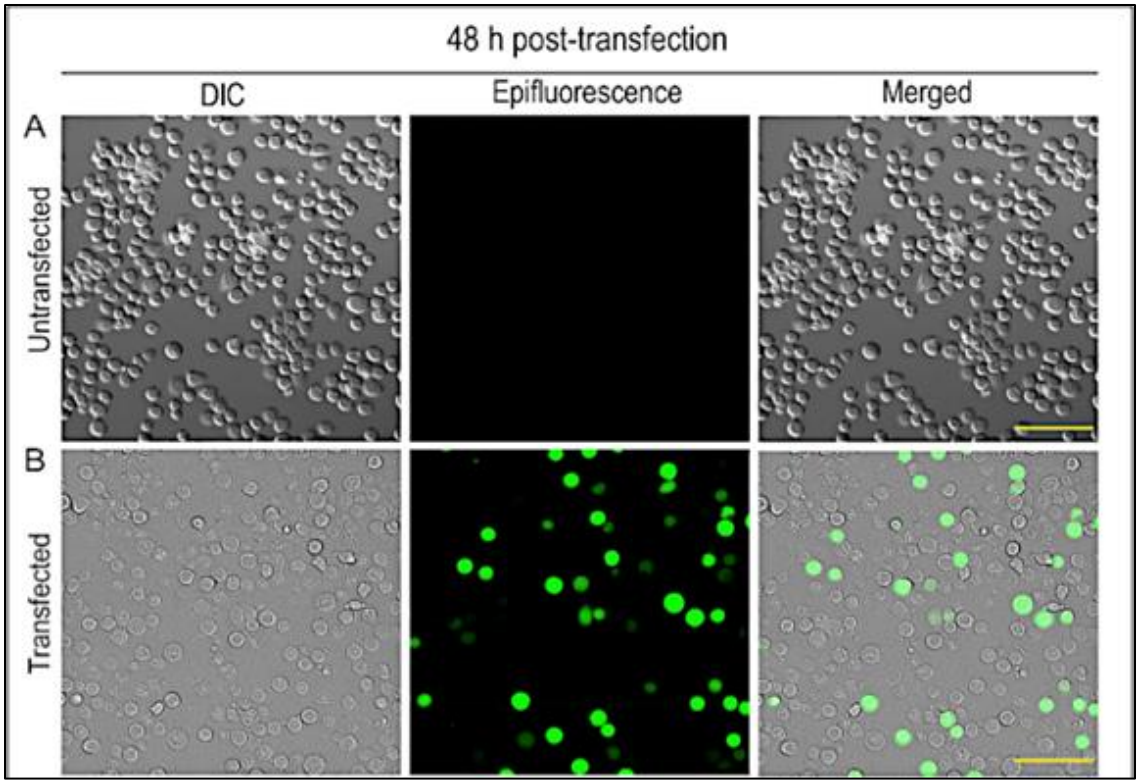

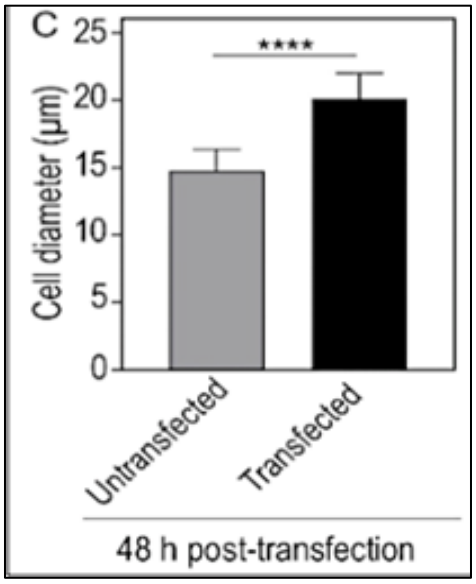

Figure 4.3. 48 h post-transfection of Sf9 cells with fluorescently tagged kinesin-3 motor. Sf9 cells were plated on a 35 mm dish at a density of 4.5 x 10^5 cells/mL. After 24 h, cells were transfected with recombinant bacmid DNA encoding specific kinesin-3 motor, KIF1A(1-393LZ)-mCit-FLAG using transfection reagent. After 48 h of transfection, images were captured under differential interference and contrast (DIC) and Epifluorescence illumination. (A) Untransfected cells, small, round, and firmly attached. (B) Transfected cells expressing KIF1A(1-393LZ)-mCit-FLAG tagged protein showing enlarged cell diameter and loosely attached to the surface. Scale bar, 100 µm. (C) Bar graph indicating average cell diameter of untransfected and transfected cells. Error bars represent mean ± SD. N = 50 cells. Student's t-test is used to find the significance value (****$p < 0.0001$).

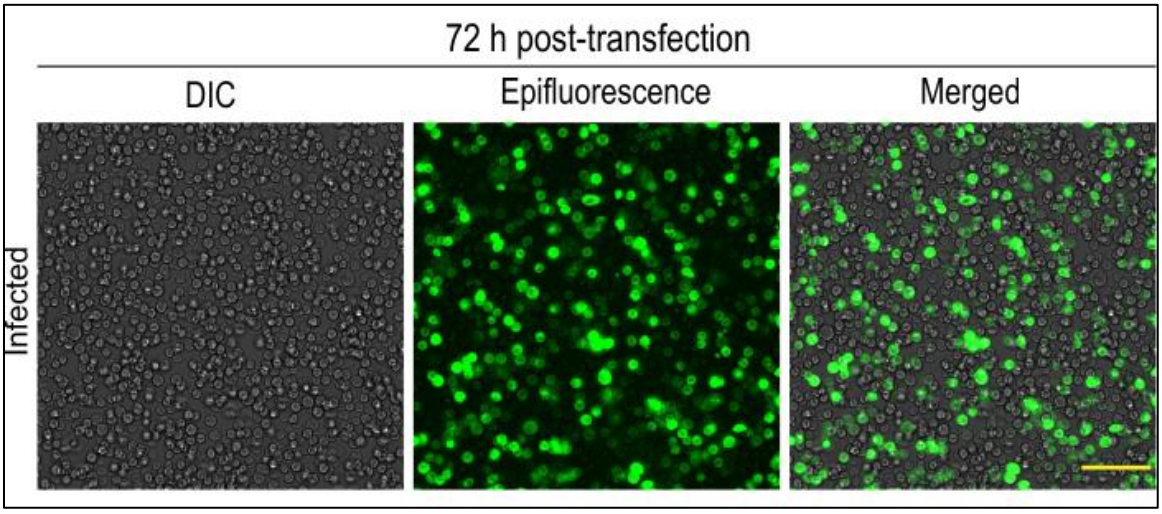

Figure 4.4. 72 h post-transfection of Sf9 cells with fluorescently tagged kinesin-3 motor. Images showing more than 90% of Sf9 cells expressing fluorescently tagged kinesin-3 motor, KIF1A(1-393LZ). Cells are loosely bound to the surface.

4.2. Sf9-purified kinesin-3 motors are fast and superprocessive.

First, we wanted to establish whether Sf9-purified kinesin-3 motors could support microtubule based superprocessive motility. We performed *in vitro* single-molecule motility assays of dimeric active kinesin-3 motors as described previously (Soppina et al., 2014; Soppina and Verhey, 2014). The control constitutively active kinesin-1, KHC (1-560) motor, showed processive motion along the microtubule tracks with an average velocity of 0.82 µm s^{-1} and 1.14±0.04 µm run length **(Figure 4.6, Figure 4.7A and Table 3)** (Clancy et al., 2011; Coy et al., 1999; Schnitzer and Block, 1997; Soppina et al., 2014). As kinesin-1 motor takes 8 nm steps (Coy et al., 1999; Sudhakar et al., 2021; Yildiz et al., 2004), the measured velocity renders a stepping rate (average number of steps taken in one second) of 102.15 s^{-1} and a mean run time (average time spent on the microtubule) of 1.39±0.3 s with a motor off-rate (frequency of motor detachment from the microtubule in one second) 0.72±0.05 s^{-1}.

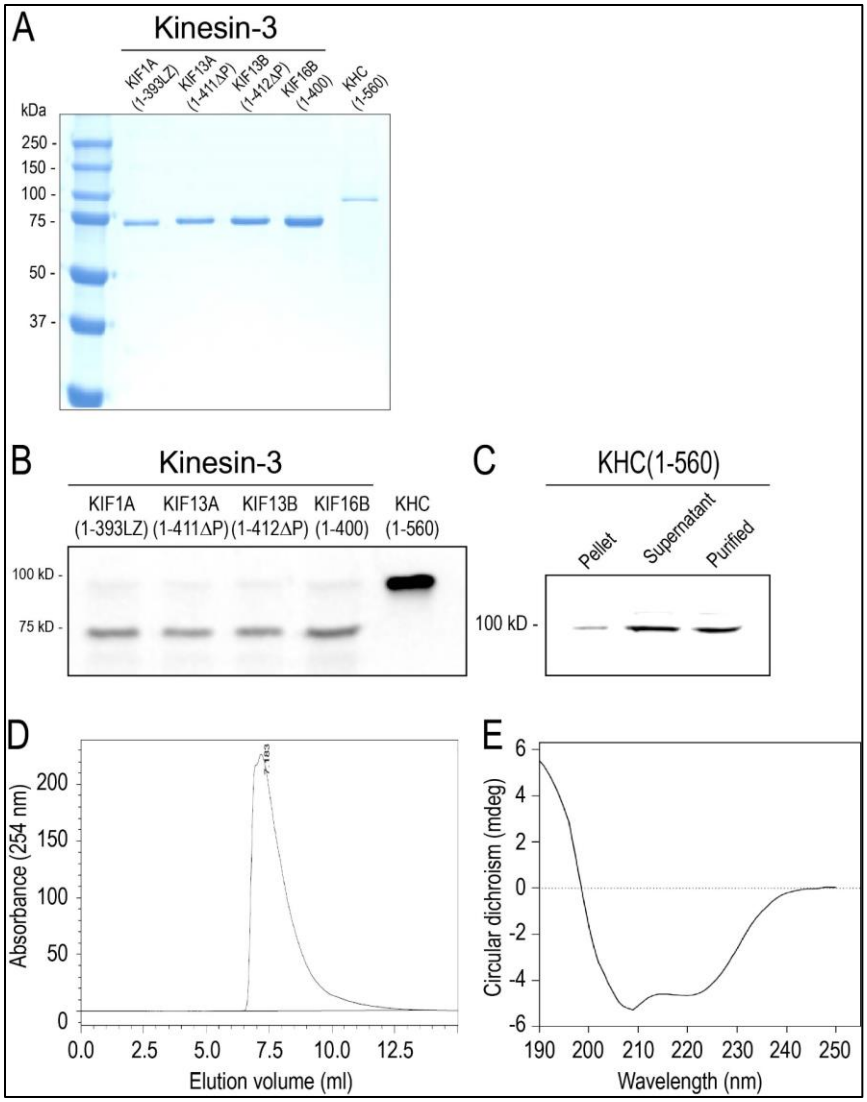

Figure 4.5. **Baculovirus purified constitutively active kinesin-1 and kinesin-3 motors.** (A) Coomassie-stained SDS-PAGE showing Sf9-baculovirus-purified truncated constitutively active kinesin-1 and kinesin-3 motors, as indicated on top. (B) Recombinant bacmids for constitutively active kinesin motors tagged with mCitrine-Flag were expressed in Sf9 cells. After 72 hrs of transfection, Sf9 cells were lysed and blotted for Flag using anti-Flag antibody to check their expression. (C) Pellet, supernatant and final purified product for KHC (1-560)-mCit-Flag were blotted with anti-Flag antibody, showing that motors expressed in Sf9 cells are largely cytoplasmic and soluble. (D) HPLC analysis of purified KIF1A (1-393LZ)-mCit-FLAG protein shows elution as a single peak. (E) Circular dichroism (CD) spectroscopy shows the helical propensities of the purified KIF1A (1-393LZ)-mCit-FLAG. The estimated secondary structures showed 48% of α-helix, 32% of β-structure and 19% others.

Next, single-molecule motility analysis of Sf9-purified active dimeric kinesin-3 motors displayed robust superprocessive motion with high velocities along the microtubule **(Figure 4.6B-E, Figure 4.7B-E and Table 3)** when compared to kinesin-1. It has been shown that the wild-type KIF1A (1-393) motors exhibit diffusive motion and short processive motion *in vitro* owing to weak neck-coil dimerization potential (Soppina et al., 2014; Tomishige et al., 2002). Therefore, we used its stable version, KIF1A (1-393LZ), in which a leucine zipper (LZ) segment of GCN4 was fused to the C-terminus of KIF1A (1-393) (Soppina et al., 2014). The KIF1A (1-393LZ) motor traveled with an average speed of 2.41±0.02 µm s^{-1} and a distance of 10.56±0.26 µm **(Figure 4.6B, Figure 4.7B and Table 3)**, akin to our previous measurements using mammalian cell lysates (Soppina et al., 2014; Soppina and Verhey, 2014). As KIF1A motors takes 8 nm step/ATP hydrolysis (Budaitis et al., 2021; Okada et al., 2003; Tomishige et al., 2002), the determined velocity corresponds to a stepping rate of 301.29 s^{-1}, which is approximately 3-fold faster than kinesin-1. Furthermore, considering the determined average run length and the velocity over the total track, we computed a motor average run time of 4.38±1.3 s, which corresponds to an off-rate of 0.23±0.05 s^{-1}.

The wild type KIF13A (1-411) and KIF13B (1-412) motors exist as inactive monomers due to proline-mediated intramolecular neck coil-coiled coil1 (NC-CC1) interaction (Soppina et al., 2014). We therefore, used proline-deleted dimeric versions, KIF13A (1-411ΔP390) and KIF13B (1-412ΔP391), respectively. The motility analysis of KIF13A (1-411ΔP390) [from now on referred to as KIF13A (1-411ΔP)] and KIF13B (1-412ΔP391) [from now on referred to as KIF13B (1-412ΔP)], exhibited average velocities of 1.55±0.02 µm s^{-1} and 1.36±0.01 µm s^{-1} and run lengths of 10.24±0.22 µm and 10.96±0.22 µm, respectively **(Figure 4.6C-D, Figure 4.7C-D and Table 3)**. Assuming these motors take 8 nm steps, their velocities reveal stepping rates of 194.19 s^{-1} and 170.16 s^{-1}, respectively. Furthermore, based on the measured average run lengths and the velocities over the total track, we computed an average run time of 6.61±2.6 s and 8.06±2.4 s, which corresponds to motor detachment rates of 0.15±0.07 s^{-1} and 0.12±0.09 s^{-1}, respectively.

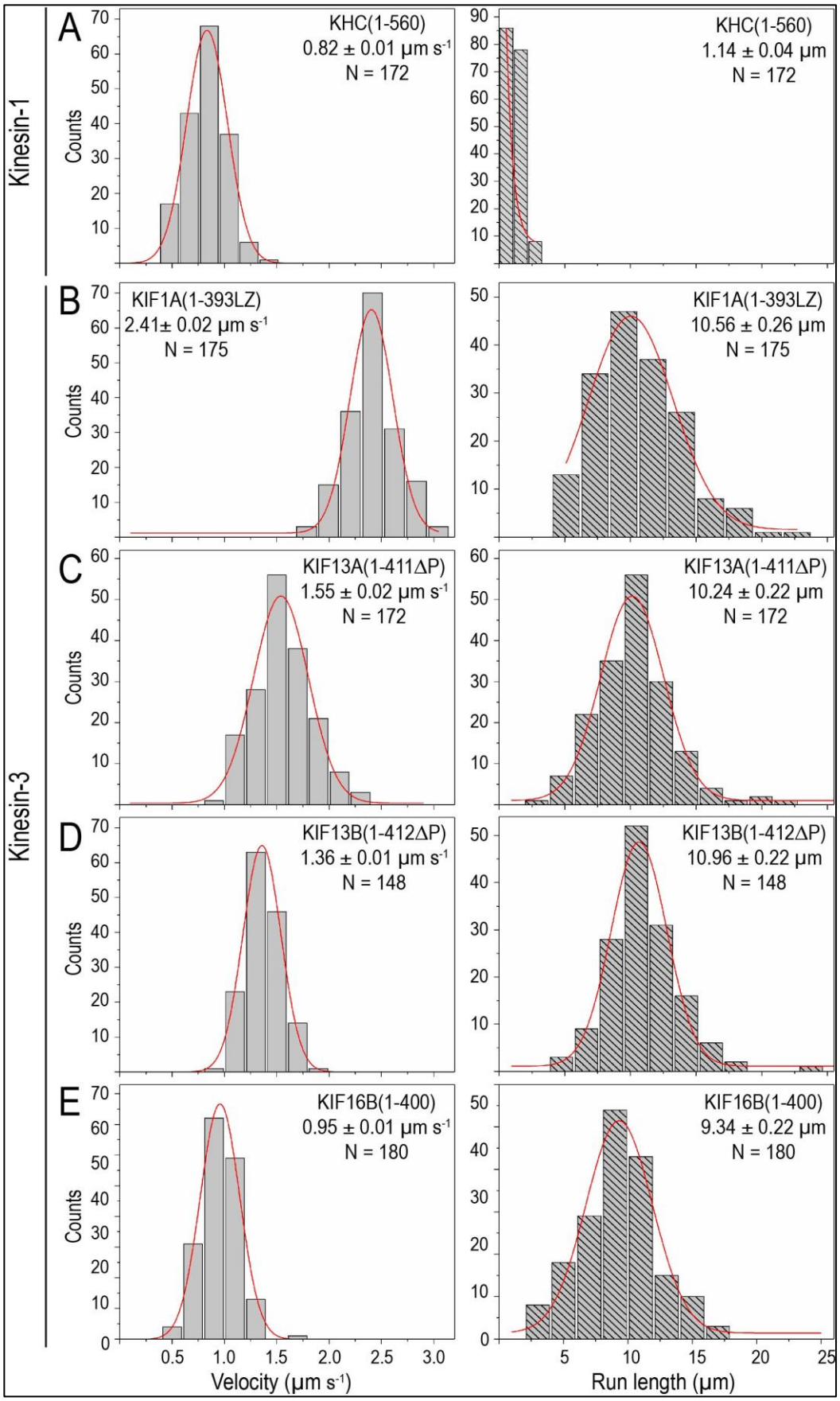
Kinesin-1
Kinesin-3
A
KHC(1-560)
0.82 ± 0.01 μm s-1
N = 172
KHC(1-560)
1.14 ± 0.04 μm
N = 172
B
KIF1A(1-393LZ)
2.41± 0.02 μm s-1
N = 175
KIF1A(1-393LZ)
10.56 ± 0.26 μm
N = 175
C
KIF13A(1-411ΔP)
1.55 ± 0.02 μm s-1
N = 172
KIF13A(1-411ΔP)
10.24 ± 0.22 μm
N = 172
D
KIF13B(1-412ΔP)
1.36 ± 0.01 μm s-1
N = 148
KIF13B(1-412ΔP)
10.96 ± 0.22 μm
N = 148
E
KIF16B(1-400)
0.95 ± 0.01 μm s-1
N = 180
KIF16B(1-400)
9.34 ± 0.22 μm
N = 180
Counts
Velocity (μm s-1)
Run length (μm)

Figure 4.6. Sf9-baculovirus purified kinesin-3 motors are robust and superprocessive. (A-E) Fluorescently tagged truncated constitutively active motors were purified using Sf9-baculovirus expression system. *In vitro* single-molecule motility assays of Sf9-purified (A) kinesin-1, KHC (1-560) and (B-E) kinesin-3 motor (B) KIF1A(1-393LZ), (C) KIF13A(1-411ΔP), (D) KIF13B(1-412ΔP) and (E) KIF16B(1-400) motors. For each population of motors, histograms of velocities (left panel) and run lengths (right panel) were plotted and fit to a single Gaussian. Average velocity and run length of the corresponding population of motors (N) are indicated on top-right or left-corner as mean ± SEM. Data presented from three independent experiments.

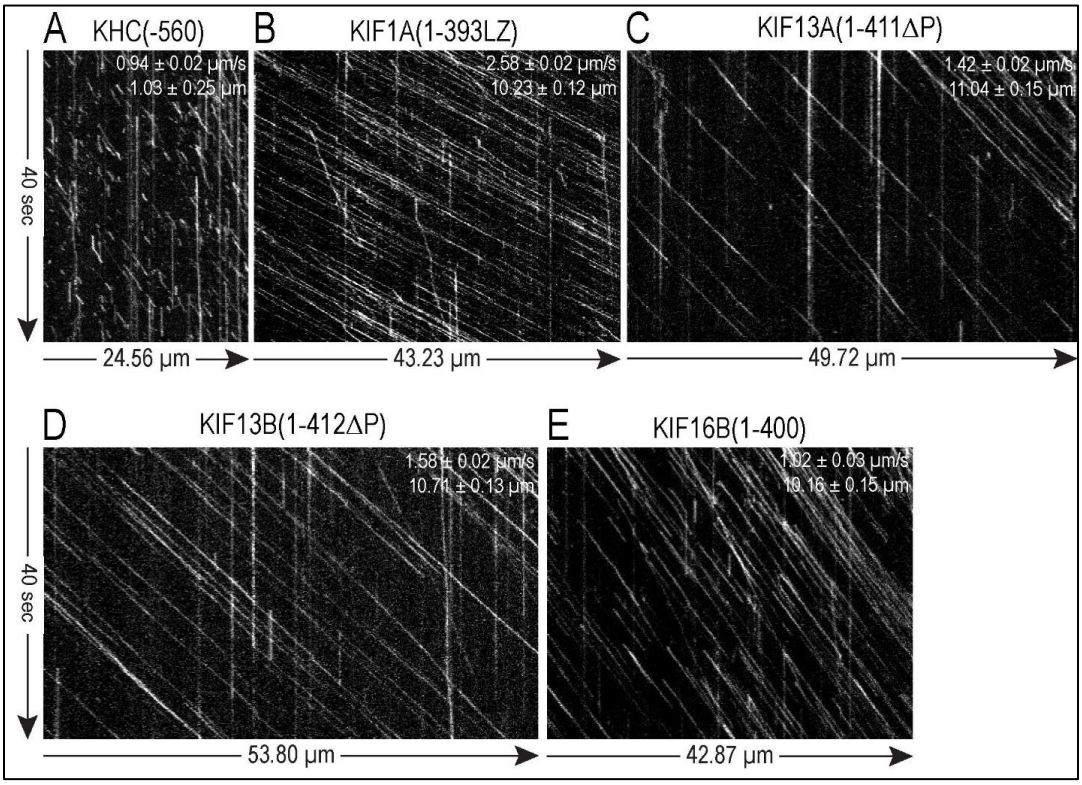

Figure 4.7. **Kymograph of *In vitro* microtubule-based single-molecule motility assays of constitutively active kinesin-3 motors.** Single-molecule motility properties were analysed using fluorescently tagged constitutively active kinesin motors purified from Sf9-baculovirus expression system. (A-E) Representative kymographs of individual kinesin motors walking processively (white lines) along the MT surface for (A) KHC(1-560), (B) KIF1A(1-393LZ), (C) KIF13A(1-411ΔP) (D) KIF13B(1-412ΔP) and (E) KIF16B(1-400).Time on y-axis (vertical arrow) and distance on x-axis (horizontal arrow).

Table 3: Biochemical and biophysical properties of Kinesin-3 family motors:

Single-Molecule Motility Assay

Motor	Velocity ($\mu m\ s^{-1}$)	Run length (μm)	Estimated Stepping rate (s^{-1})	Mean run time (s)	Detachment rate (s^{-1})
KIF1A(1-393LZ)	2.41 ± 0.02	10.56 ± 0.26	301.29	4.38 ±1.3	0.23 ± 0.05
KIF13A(1-411ΔP)	1.55 ± 0.02	10.24 ± 0.22	194.19	6.61 ± 2.6	0.15 ± 0.07
KIF13B(1-412ΔP)	1.36 ± 0.01	10.96 ± 0.22	170.16	8.06 ± 2.4	0.12 ± 0.09
KIF16B(1-400)	0.95 ± 0.01	9.34 ± 0.22	118.75	9.83 ± 1.2	0.10 ± 0.02
KHC(1-560)	0.82 ± 0.01	1.14 ± 0.04	102.15	1.39 ± 0.3	0.72 ± 0.05

ATPase Assay

Motor	k_{cat} (s^{-1})	K_m (μM)	Basal activity (s^{-1})	Step size (nm)
KIF1A(1-393LZ)	290.9 ± 8.69	7.03 ± 0.79	0.08	8.28
KIF13A(1-411ΔP)	181.7 ± 8.31	5.16 ± 0.84	0.014	8.53
KIF13B(1-412ΔP)	171.8 ± 7.82	4.23 ± 0.74	0.08	7.91
KIF16B(1-400)	124.7 ± 6.94	2.43 ± 0.58	0.32	7.61
KHC(1-560)	95.44 ± 15.5	10.23 ± 3.63	0.044	8.54

Microtubule Gliding Assay

Motor	Gliding Velocity ($\mu m\ s^{-1}$)
KIF1A(1-393LZ)	1.16 ± 0.14
KIF13A(1-411ΔP)	0.58 ± 0.05
KIF13B(1-412ΔP)	0.60 ± 0.06
KIF16B(1-400)	0.48 ± 0.08
KHC(1-560)	0.46 ± 0.06

Furthermore, motility analysis with active KIF16B (1-400) also exhibited long uniform motion along the microtubule with an average velocity of 0.95±0.01μm s^{-1} and run-length 9.34±0.22 μm **(Figure 4.6E, Figure 4.7E and Table 3)**. These motility properties showed remarkable consensus with previously measured kinesin-3 motility properties

using mammalian cell lysate (Budaitis et al., 2021; Lessard et al., 2019; Scarabelli et al., 2015; Soppina et al., 2014; Soppina and Verhey, 2014). Considering KIF16B takes 8 nm steps, the determined velocity translates to a stepping rate of 118.75 s^{-1}. Furthermore, based on the measured run length and the velocity over the entire track, we found that the motor run time of 9.83±1.2 s corresponds to a motor off-rate of 0.10±0.02 s^{-1}.

Together, these results demonstrate that the functional output of motor proteins purified from the Sf9-baculovirus system are comparable to those expressed in mammalian cells. Their motility properties are on par with those measured previously using motor proteins prepared from mammalian cells. The results also suggest that the high velocity and superprocessivity of kinesin-3 motors is inherent to their motor domains. Notably, this one-step motor purification protocol can be adapted to purify any other protein of interest.

4.3. Kinesin-3 motors exhibit high ATP turnover rates.

The ability of kinesin motors to take processive steps along the microtubule is tightly coupled to the ATP hydrolysis cycle because binding of ATP causes conformational changes in the motor domain before hydrolysis. Studies on kinesin-1 and myosin have directly correlated their velocity and ATP turnover rate (Barany, 1967; Friel and Howard, 2012). However, previous chemomechanical studies of kinesin-3 motors have reported significantly lower ATP turnover rates (Okada and Hirokawa, 1999, 2000; Tomishige et al., 2002; Zaniewski et al., 2020). which do not correlate with the measured high velocity and superprocessive motility (Soppina et al., 2014; Soppina and Verhey, 2014). Thus, understanding the microtubule stimulated chemomechanical behavior of kinesin-3 motors can help to elucidate the observed unique kinesin-3 motility properties. Therefore, we decided to do microtubule stimulated ATPase measurements of full-length and constitutively active kinesin-3 motors. To do this, we adapted an ATPase assay based on phosphomolybdate complex formation, as described for smooth muscle myosin (Trybus, 2000).

As a control, we used a dimeric KHC (1-560), constitutively active kinesin-1 motor whose catalytic rate constants have been well characterized, to optimize assay conditions. First, we determined the optimal motor concentration required to measure the ATPase

activity by assaying a range of KHC (1-560) motor concentrations (1 nM to 100 nM) with a constant microtubule concentration. We found that a motor concentration of 10 nM is optimal for reliable and consistent measurement of ATPase activity across the preparations (Atherton et al., 2014). Next, we determined the range of microtubule concentrations desired to accurately measure ATPase activity for the individual motor type, depending on when the ATPase activity attains its steady-state maxima. For reliable ATPase measurements, an assay mixture containing purified motor protein, ATP, and varying microtubules concentrations was incubated at room temperature for two hours. Samples were collected every 30 min and inorganic phosphate release was measured (Trybus, 2000).

The assay with full-length KHC showed low basal ATPase activity even after adding microtubules **(Figure 4.8A and Table 4)** (Hackney and Stock, 2008; Kuznetsov and Gelfand, 1986). Consistent with the fact that kinesin-1 predominantly exists in a compact autoinhibited conformation, the tail domain folds back to interact with the motor domain directly (Cai et al., 2007; Coy et al., 1999; Friedman and Vale, 1999). This folded tail-to-head intramolecular interaction precludes the motor microtubule association and subsequent ATP hydrolysis and holds the motor in an inactive folded conformation (Aoki et al., 2013; Hackney and Stock, 2000; Kaan et al., 2011; Verhey et al., 2011a). In contrast, constitutively active dimer, KHC (1-560), displayed approximately 10-fold higher activity following the addition of microtubules **(Figure 4.8B and Table 3)**. The determined *kcat* and *Km* were 95.44 ± 15.5 s^{-1} and 10.23 ± 3.63 µM, respectively, which agrees with previous reports (Coy et al., 1999; Friel et al., 2011; Woehlke et al., 1997; Zaniewski et al., 2020). The ratio of the speed of kinesin-1 to its rate of microtubule stimulated ATP hydrolysis yields a step size of ~8.54 nm and stoichiometry of 1.07 step/ATP hydrolyzed, suggesting a tight coupling between their chemical and mechanical cycles (Coy et al., 1999; Schnitzer and Block, 1997).

A similar analysis using bacterially purified KHC (1-560) **(Figure 4.1)** exhibited deficient activity, indicating that majority of the motors were inactive. This finding again lends support to the importance of purifying kinesin motors from the eukaryotic expression system rather than from the prokaryotic system. Together, these results

support the general autoinhibition mechanism in the field proposed for kinesin-1 and that the stepping rate of kinesin-1 is directly proportional to the speed of ATP hydrolysis.

4.3.1. Full-length kinesin-3 motors exhibit low ATPase activities.

Next, we measured the ATPase activity of kinesin-3 family motors with and without microtubules. Analogous to kinesin-1, the addition of microtubules to full-length kinesin-3 motors did not stimulate their ATP hydrolysis **(Figure 4.8A and Table 4)**. This observation is consistent with non-cargo-bound full-length kinesin-3 motors that exist in an autoinhibited state. Autoinhibition of motors prevents unnecessary hydrolysis of cellular ATP and interference with cargo trafficking on the microtubule. For kinesin-3, studies have shown that intramolecular interaction between the NC and CC1 domains keeps the motor in a monomeric, autoinhibited state (Al-Bassam et al., 2003; Al-Bassam and Nithianantham, 2018; Huo et al., 2012; Nakagawa et al., 2000; Patel et al., 2021; Ren et al., 2016; Ren et al., 2018; Soppina et al., 2014; Yamada et al., 2007). However, the detailed mechanism of kinesin-3 autoinhibition is still poorly understood.

4.3.2. KIF1A dimers exhibit the highest ATP turnover rates.

Unlike full-length motors, the addition of microtubules to constitutively active, dimeric kinesin-3 motors remarkably stimulated their ATPase activity, which is 1.3 to 3-fold higher than kinesin 1 **(Figure 4.8C-F)**. The rate of ATP hydrolysis for dimeric active KIF1A (1-393LZ) motor (Soppina et al., 2014; Soppina and Verhey, 2014) was found to be *kcat* 290±9 s^{-1}, which is 3 times faster than the activity of KHC (1-560) **(Figure 4.8C and Table 3)**. The determined high *kcat* is in close agreement with the estimated stepping rate (~301.29 s^{-1}) with a step size of ~ 8.28 nm and stoichiometry of 1.0 step/ATP, suggesting a tight coupling between chemical and mechanical cycles. A similar step size of ~ 8 nm has been reported recently for KIF1A and UNC-104 motors (Budaitis et al., 2021). Together, these results explain the fast velocity reported for this motor (Soppina et al., 2014; Soppina and Verhey, 2014; Tomishige et al., 2002).

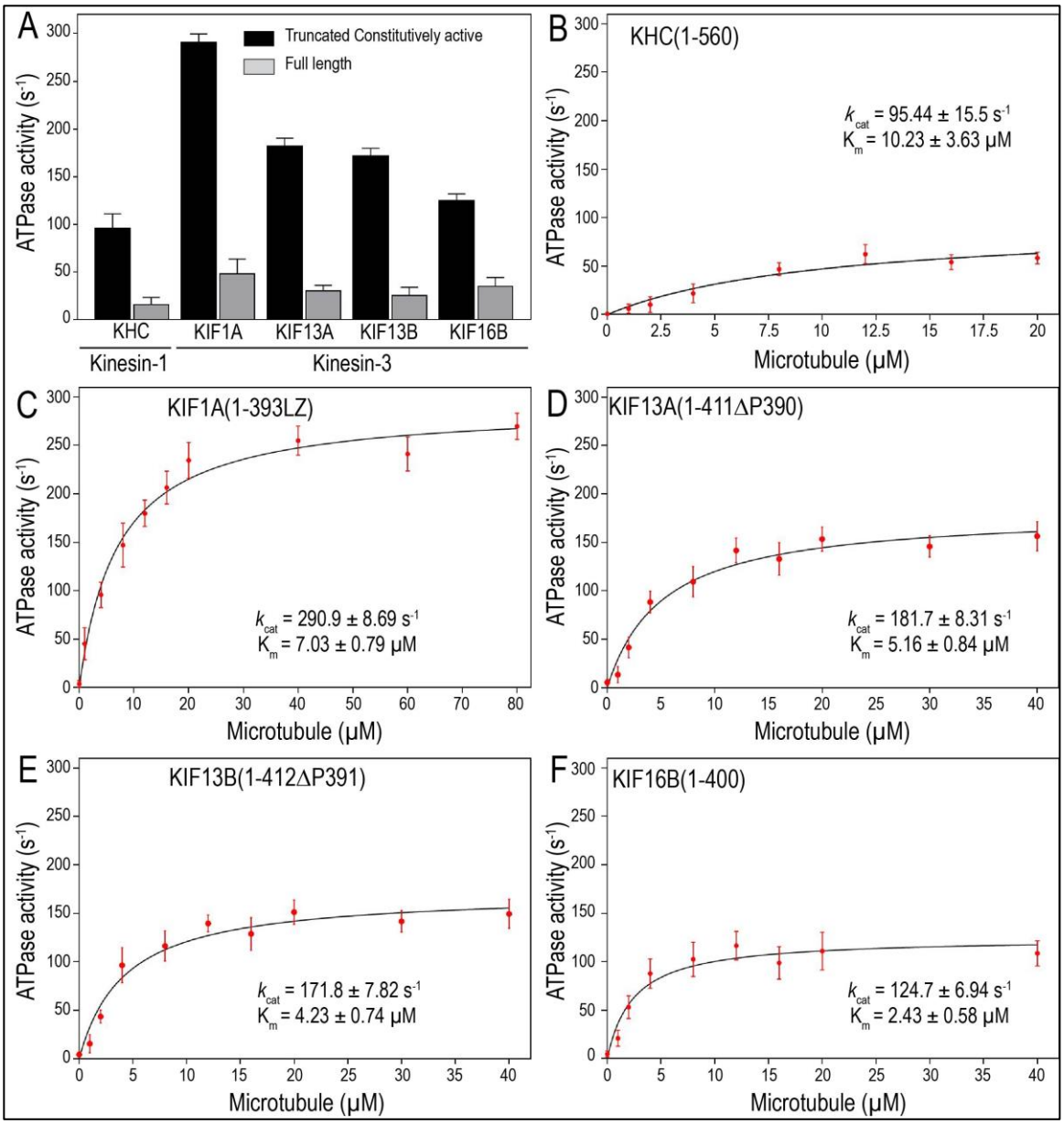

Figure 4.8. Kinesin-3 motors exhibit high ATPase activity and differential microtubule affinity. Microtubule stimulated ATPase activity of full-length and truncated constitutively active motors were measured using Sf9-purified proteins (A) Comparison of ATPase activity between full-length and constitutively active kinesin motors. ATPase activities for full-length motors were measured at microtubule concentration that had highest ATPase activity for the respective constitutively active motor. (B-F) Plots showing ATPase activity against varied concentrations of microtubules for (B) constitutively active kinesin-1 motor, KHC (1-560) and kinesin-3 motors (C) KIF1A(1-393LZ), (D) KIF13A(1-411ΔP), (E) KIF13B(1-412ΔP) and (F)

KIF16B(1-400) and fit to Michaelis-Menten equation. Maximal turnover (*kcat*) and microtubule affinity (*Km*) parameters were determined using GraphPad Prism. Error bars represent mean ± SD. Data presented from three independent experiments.

Table 4: Summary of ATPase properties of full-length kinesin-1 and kinesin-3 motors.

Motor	ATPase activity (s^{-1})	Microtubule concentration (µM)
KHC	15.98	5.0
KIF1A	48.02	20.0
KIF13A	30.05	8.0
KIF13B	25.00	8.0
KIF16B	35.00	8.0

The measured ATPase activity is considerably higher than pioneering work from Hirokawa lab that demonstrated an ATP turnover rate of 110±5 s^{-1} for a monomeric KIF1A (Okada and Hirokawa, 1999, 2000). Similarly, an elegant and detailed experimental analysis of active UNC104 dimers showed a lower ATP turnover rate of 100 s^{-1}/head (Tomishige et al., 2002). Recent work from Zaniewski et al. also reported a significantly lower *kcat* 115 s^{-1} for a stable KIF1A (1-406) dimers, suggesting a significant fraction of the molecules may be inactive, presumably due to motors purified from bacterial expression system (Zaniewski et al., 2020). The determined higher microtubule affinity of KIF1A (1-393LZ) (*Km* 7.03 µM) compared to KHC (1-560) (*Km* = 10.23 µM) agrees with previous studies on KIF1A/CeUnc104 (Okada and Hirokawa, 2000; Soppina et al., 2014; Tomishige et al., 2002).

4.3.3. KIF13 dimers show higher ATPase activity.

Contrary to full-length KIF13 motors, the addition of microtubules to the dimeric active KIF13A (1-411ΔP) and KIF13B (1-412ΔP) motors strongly stimulated their ATPase rates with *kcat* of 181.7 s^{-1} and 171.8 s^{-1}, respectively **(Figure 4.8D-E and Table 3)**.

These rates match their measured *in vitro* velocities (1.55 µm/s and 1.36 µm/s) and estimated stepping rates of 194.19 s^{-1} and 170.16 s^{-1}, respectively (Soppina et al., 2014; Soppina and Verhey, 2014; Verhey et al., 2011a). Similar to KIF1A, the ratio of KIF13A and KIF13B motor velocities with their rates of ATP hydrolysis generates a step size of 8.53 nm and 7.91 nm, respectively, yielding a stoichiometry of ~1, suggesting a tight relation between ATP hydrolysis and motor stepping. Additionally, the measured ATPase rate constants of KIF13 motors were twice the rate of kinesin 1, corresponding to the observed difference in their velocities (Hammond et al., 2009; Soppina et al., 2014; Verhey et al., 2011b). However, earlier studies using the truncated KIF13B (1-368) motor containing a catalytic motor domain and neck linker exhibited microtubule stimulated ATP turnover rate 45 s^{-1} and Km of 0.1 µM (Asaba et al., 2003). The observed low catalytic activity was presumably due to motor truncation lacking the dimerization domain (NC) and purified from bacterial expression system.

Similarly, previous microtubule stimulated ATPase measurements for KIF13B full-length and motor truncation after FHA domain showed low ATP turnover rates (*kcat* = 0.3 s^{-1} and *kcat* = 4.6 s^{-1}, respectively) (Yamada et al., 2007), suggesting motors were probably in the autoinhibited state. Similarly, recent ATPase measurements of KIF13B truncations (including ΔP391) purified from bacterial expression system, showed lower activities compared to kinesin-1 (Ren et al., 2018). Together, these results suggest that KIF13A and KIF13B motors have higher (~1.9 and 1.8 -fold higher, respectively) ATPase activity than kinesin-1 motor and complement their measured velocities *in vitro*.

4.3.4. KIF16B dimers show high ATPase activity.

The addition of MTs to KIF16B (1-400) triggered the ATP turnover rate *kcat* (124.7±6.94 s^{-1}), which is approximately 1.3 fold higher than kinesin-1 but lower than KIF13 (1.4-fold) and KIF1A (2.3-fold) motors **(Figure 4.8F and Table 3)**. The ratio between the measured motor velocity and rate of ATP turnover resulted in an average step size of 7.61 nm/ATP, which implies a tight coupling between ATP hydrolysis and mechanical stepping. Additionally, KIF16B motor showed strongest microtubule affinity (*Km* = 2.43

μM) compared to KIF13A (*Km* = 5.16 μM), KIF13B (*Km* = 4.23) KIF1A (*Km* = 7.03 μM) and KHC (*Km* = 10.23 μM) motors. These binding affinities correlate with their measured difference in landing rates (Soppina et al., 2014; Soppina and Verhey, 2014). The binding affinity of kinesin-3 motors is influenced mainly by the positively charged lysine residues in the K-loop, a family-specific insert in the loop12 of the kinesin-3 motor domain **(Figure 5.6A and Figure 5.0)**. Crystal structure studies of KIF1A motor bound to microtubules revealed that the motor utilizes microtubule-binding loops, loop11 and loop12, in an alternative manner to switch its interaction with microtubule during ATPase cycle. In which conformational changes due to ATP hydrolysis withdraw loop11 from the microtubule and then engage loop12 with the microtubule (Nitta et al., 2004). Further detailed analysis using K-loop mutants with a varying number of lysine residues showed that the positively charged lysine residues in the K-loop dramatically increased the affinity to microtubules (Okada and Hirokawa, 1999, 2000). Though KIF16B motor contains only three lysine residues in the K-loop compared to six in KIF1A, the motor showed significantly higher microtubule affinity is interesting and requires future investigation. Together, our data suggest that despite kinesin-3 motors sharing a highly conserved motor domain, it's fine-tuning at the molecular level yields diverse motility outputs.

Our results provide the first comprehensive chemomechanical basis for high velocity and superprocessive motility of kinesin-3 family motors (Soppina et al., 2014; Soppina and Verhey, 2014). We also show for the first time that the rate of ATP hydrolysis for kinesin-3 motors remarkably agrees with their stepping rate, suggesting a tight coupling between chemical and mechanical cycles. A characteristic feature of a processive motor is its ATPase cycle, which is gated by its ADP release and very slow in the absence of microtubules. This ADP release is greatly accelerated by microtubules, which consequently accelerates ATP turnover ~ 50 times as reported for kinesin-1 (Hackney, 1988; Hackney and Stock, 2000; Kuznetsov and Gelfand, 1986). Based on these chemomechanical properties and structural similarities, we propose that kinesin-3 motors follow a similar transition state sequence, as demonstrated for kinesin-1. The truncated motors used in the ATPase assays consist of only the core catalytic motor domain and

NC domain, critical for motor dimerization. Regions beyond the NC domain are known to regulate motor activity by inhibiting ATPase activity or preventing microtubule binding or motor dimerization (Asaba et al., 2003; Kurland and Gallant, 1996; Siddiqui and Straube, 2017; Soppina et al., 2014; Verhey et al., 2011b; Yamada et al., 2007). Therefore, kinesin-3 motors' ability to hydrolyze ATP at higher rates is intrinsic to their motor domains.

One possibility that can impact kinesin-3 motility is having a different sequence of chemomechanical states altogether than kinesin-1. However, this seems unlikely to explain kinesin 3 superprocessivity because kinesin motors share a highly conserved motor domain with > 65% sequence similarity. An alternative possibility is differences in specific rate constants in the ATP turnover cycle to influence motor speed and superprocessivity. Indeed, a recent chemomechanical analysis of KIF1A motor suggested that the rates of rear-head detachment, leading head attachment, and a strong microtubule interaction in the weakly bound state contribute to high velocity and superprocessivity of kinesin-3 motors (Zaniewski et al., 2020). The fact that all kinesin-3 motors have an average run-length of 10 µm **(Figure 4.7 and Table 3)** with varying velocities suggests that faster motors will take a short time to travel 10 µm and so will have a higher *koff* and thus higher *Km*. Based on these findings, we propose that differential microtubule binding affinities with consequent robust ATPase activities are evolutionarily designed to render kinesin-3 family motors with unique mechanical outputs. To the best of our knowledge, this is the first comprehensive analysis of kinesin-3 motors and provides direct biochemical demonstration paralleling their observed high velocities, longer run-lengths, and strong microtubule affinity. These findings open up many interesting questions of great biological significance across the field.

4.4. Kinesin-3 motor velocities inversely correlate to their microtubule-binding affinity.

The velocities of kinesin-3 motors are tightly coupled with the rate of ATP hydrolysis and interestingly, these velocities (KIF1A > KIF13A > KIF13B > KIF16B) showed an inverse correlation with their microtubule binding affinities (KIF16B > KIF13B >

KIF13A > KIF1A) **(Figure 4.9)**. As shown in Figure 4.6, all kinesin-3 motors have a similar mean run-length of ~ 10 µm, but their measured velocities inversely correlate with their microtubule binding affinities **(Table 3)**. For instance, KIF1A motors with faster velocity (2.41 µm s^{-1}) and lower microtubule binding affinity (*Km*=7.03 µM) takes a shorter time of 4.38 s to run a distance of 10 µm, so they have a high microtubule detachment rate (*koff* = 0.23 s^{-1}).

By contrast, KIF16B motors with slow velocity (0.95 µms^{-1}) and high microtubule binding affinity (*Km*=2.43 µM) take a longer time of 9.83s to cover the same 10 µm distance, hence have a low *koff* (0.10 s^{-1}). Similarly, KIF13 family motors, KIF13A and KIF13B with intermediate velocities (1.55±0.02 µm s^{-1} and 1.36±0.01 µm s^{-1}, respectively) and moderate microtubule binding affinities (*Km*=5.16 µM and *Km*=4.23 µM, respectively) take modest time scale of 6.61±2.6 s and 8.06±2.4 s, respectively to cover a distance of 10 µm, so the intermediate *koff* (0.15s^{-1} and 0.12 s^{-1}, respectively). Interestingly, our recent *in silico* analysis using the coupled Brownian motor model also predicted a similar trend (KIF1A > KIF13 > KIF16B) that is observed experimentally (Mukherjee et al., 2022).

One hypothesis is that electrostatic interactions between the positively charged K-loop and the negatively charged microtubule surface contribute to the motor's affinity for the microtubule, landing rate and diffusion (Cooper and Wordeman, 2009; Kikkawa et al., 2000; Okada and Hirokawa, 1999, 2000; Soppina and Verhey, 2014). However, the K-loop of KIF1A contains six lysine residues, and the motor showed the lowest affinity for the microtubule than KIF13A, KIF13B and KIF16B motors that have only three lysine residues **(Figure 5.6 and Table 3)**. Alternatively, the loop8, a third microtubule-binding region that does not change its conformation or position relative to the microtubule during ATPase turnover, interacts with the microtubule independent of its nucleotide state **(Figure 5.0)** (Kikkawa et al., 2000; Kikkawa et al., 2001).

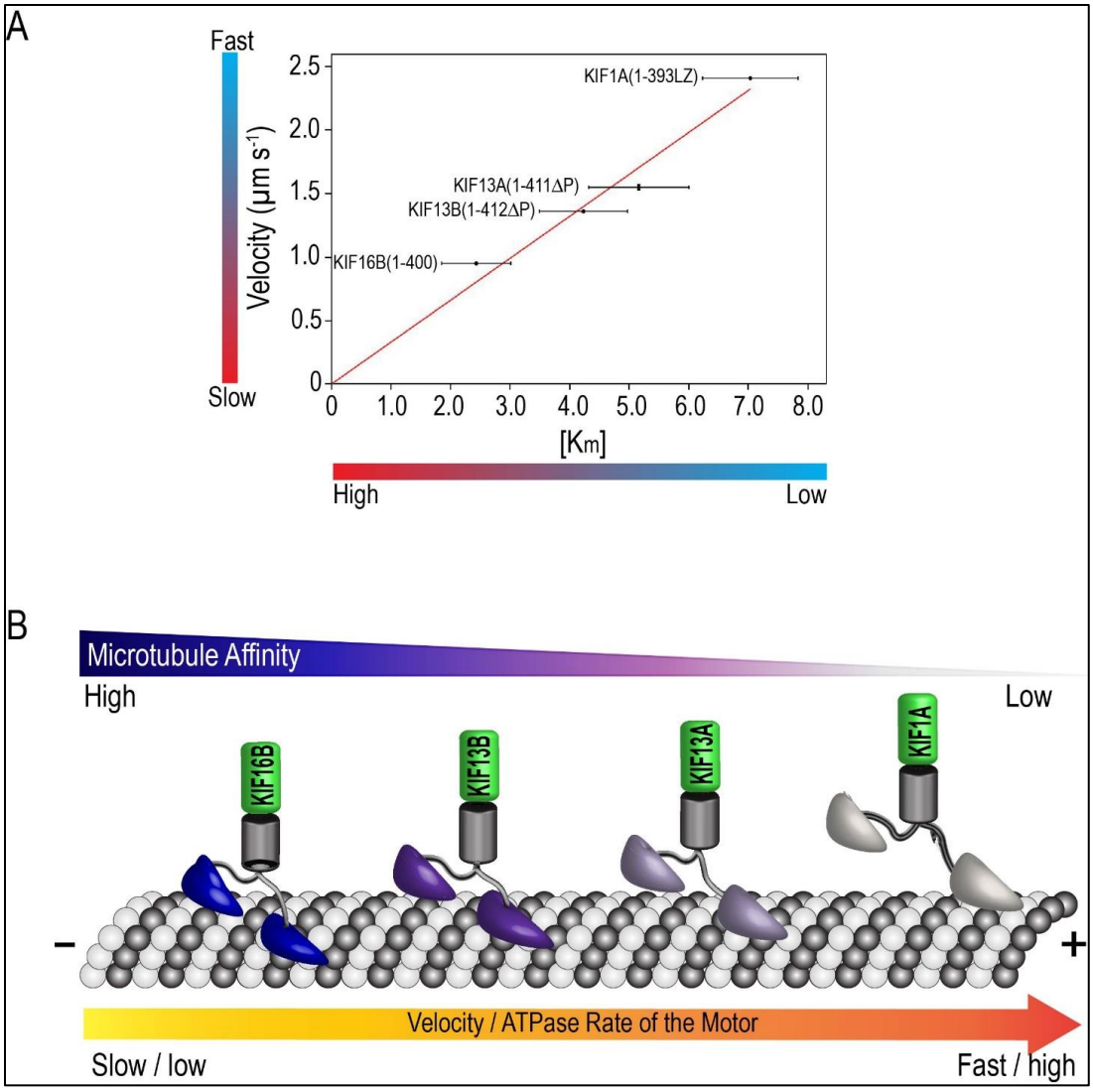

Figure 4.9. Kinesin-3 motor velocity inversely correlates with microtubule affinity. (A) The measured velocity of kinesin-1 and kinesin-3 motors in single-molecule motility assays was found to be inversely proportional to the microtubule binding affinity obtained from ATPase analysis. (B) Cartoon diagram showing kinesin-3 family (KIF1A, KIF13A, KIF13B and KIF16B) motors are robust ATPases, complementing with their measured velocities. These velocities inversely correlate with their differential microtubule-binding affinity.

Recent molecular-dynamics simulations and binding energetic calculations reveal that the loop8 region establishes multiple engagements with the negatively charged H12 segment of β-tubulin and possibly provides extended microtubule affinity for kinesin-3 motors (Scarabelli et al., 2015; Uchimura et al., 2010). Specifically, the measured higher

microtubule binding affinity for KIF13A and KIF13B motors are possibly due to arginine residue at R167 and R168, respectively, rather than a conserved lysine residue (K163 in KIF1A) **(Figure 5.1A)**. Similarly, for KIF16B, the determined high microtubule binding affinity, presumably due to additional arginine (R165 and R166) and lysine (K181) residues in loop8 **(Figure 5.1A)**. Arginine and lysine are largely exposed to the protein surface and play critical roles in protein stability and affinity through electrostatic interactions. Most importantly, arginine residue enables multiple stable electrostatic interactions compared to lysine owing to its guanidinium group. Additionally, arginine residue generates more stable interactions due to its higher aqueous pKa (13.8) than lysine (10.53) residue (Armstrong et al., 2016; Fitch et al., 2015).

To test this, we mutated one of the arginine residues (R167C) in loop8 of KIF1A, which is critical for establishing stable interaction with negatively charged Glutamate residue (E420) at the C-terminal tail region of tubulin subunits **(Figure 5.0)** while generating processive motility (Kikkawa et al., 2001; Lee et al., 2015; Nitta et al., 2004). R167C is a heterozygous missense mutation found in patients suffering from Spastic Paraparesis (Lee et al., 2015). Relative to the wild-type motor, COS-7 cells expressing mutant motors showed peripheral accumulation, albeit with less efficiency **(Figure 5.1B)**.

To further quantify its ability to take processive steps along the microtubule, we performed a CAD cell processivity assay (Soppina et al., 2014). Whereas differentiated CAD cells expressing wild-type motors showed substantial accumulation to the neurite tip, cells expressing mutant (R167C) motors showed significantly reduced tip accumulation **(Figure 5.1 C and D)**. To substantiate, we performed *in vitro* motility assays to measure their motility properties at the single-molecule level. Wild-type motors showed uniform superprocessive motility along the microtubule surface **(Figure 5.1 E and F)**. However, mutant motors exhibited one-dimensional back-and-forth motion along the microtubules **(Figure 5.1 E and F)** and a significant decrease in the number of motors landing on the microtubules, compared to wild-type motors **(Figure 5.1G).**

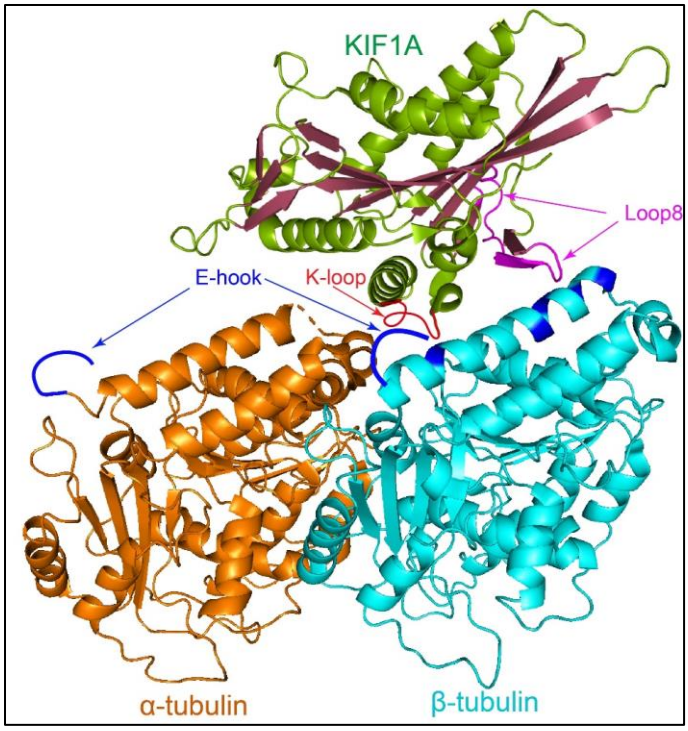

Figure 5.0. Ribbon diagram of KIF1A motor domain interacting with tubulin subunits. Cartoon diagram showing the position of the conserved K-loop (red) and loop8 (magenta) of KIF1A (PDB 2HXF) interacting with the negatively charged residues in the E-hooks (blue) at the C-terminal tail regions of tubulin dimers.

To determine the direct effect of mutation R167C on KIF1A microtubule affinity, we measured the enzyme kinetics using purified motors. Consistent with the motility data (Figure 5.1), the mutant exhibited a significant decrease in the rate of ATP hydrolysis (~33%) and microtubule affinity (~1.5 times), compared to wild-type motors **(Figure 5.1 H and I)** (Aguilera et al., 2021). The residue R167 establishes multiple stable interactions with microtubule in ATP and ADP states (Li and Zheng, 2011). Therefore, mutation R167C significantly affects motor microtubule interaction, thereby affecting KIF1A motion along the microtubule. Additionally, the equivalent mutations (R167C) in other members of the kinesin-3 family, KIF13B (K172A) and KIF16B (R173A), resulted in a similar decrease in the rate of ATP hydrolysis and microtubule affinity **(Figure 5.1 H and I)**. Together, these results suggest that akin to R167 (KIF1A), its equivalent residues in other kinesin-3 motors make hydrogen bonding with negatively charged E420 at the tubulin tail region and contribute to the microtubule affinity and processive motility.

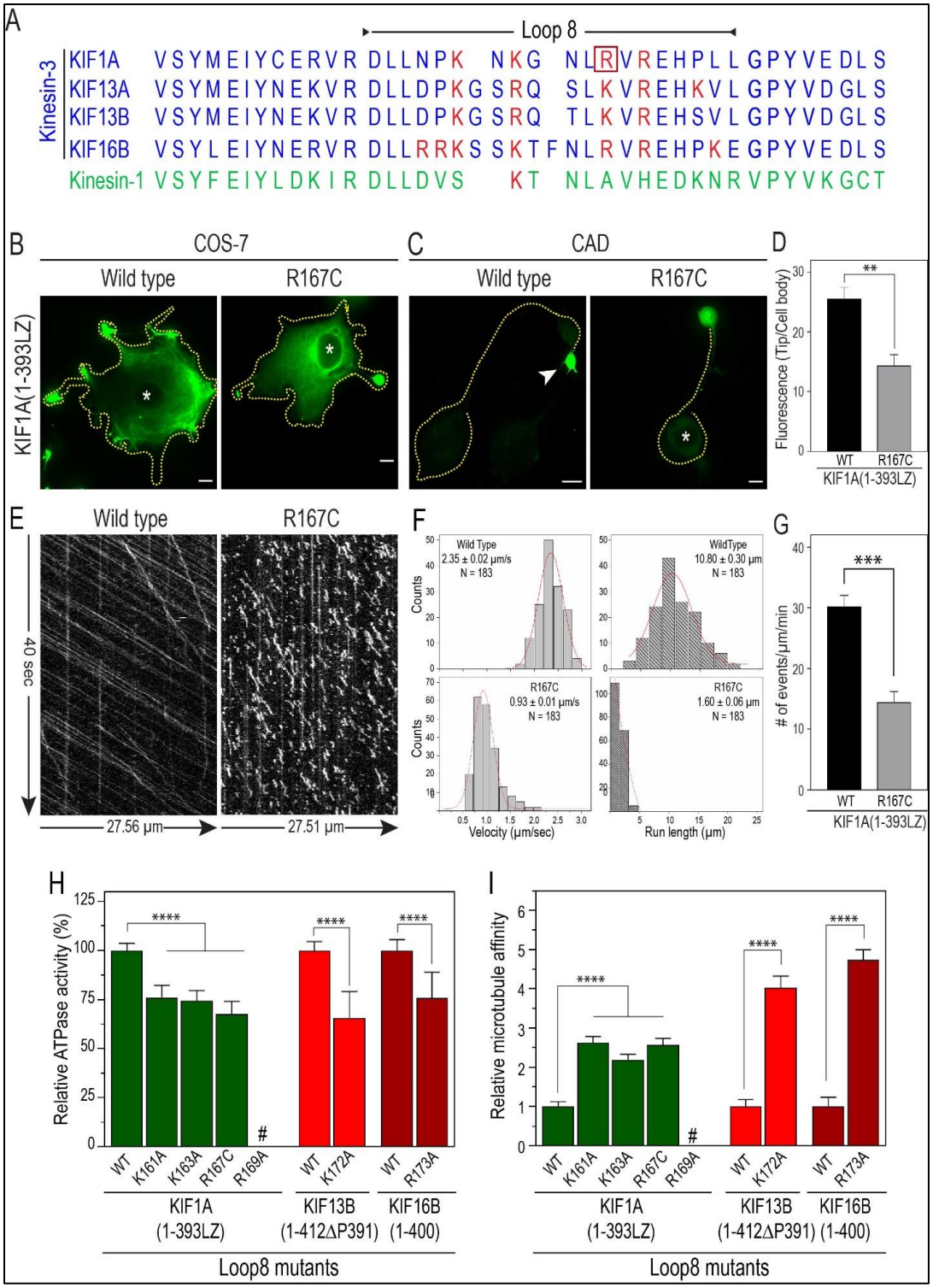

Figure 5.1. Loop8 contributes to the strong microtubule-binding affinity for kinesin-3 motors. (A) Amino acid sequence alignment of the loop8 region of mammalian kinesin-3 family motors (blue text) and kinesin-1 (green text). Clusters of

positively charged residues are (red text). COS-7 (B) and CAD (C) cells expressing KIF1A(1-393LZ) wild-type and a loop8 mutant (R167C). (D) Quantification of motor accumulation at the neurite tip. The mean ± SEM for wild type and mutant motors were plotted as the ratio of average fluorescence intensity in the neurite tip to that in the cell body. (E-F) Single-molecule motility assays of KIF1A (1-393LZ) wild-type and R167 mutant motors. The C-terminal 3xmCit tagged wild type and mutant motors were expressed in COS-7 cells and their lysates were used to measure the single-molecule motility properties. (E) Representative kymographs of wild type or mutant single kinesin motors processively walking (white diagonal lines) along the microtubule. Distance is on x-axis (horizontal arrow) and time is on y-axis (vertical arrow). (F) Velocity (left panel) and run length (right panel) histograms of KIF1A (1-393LZ) wild type and R167C mutant motors fit to a single Gaussian. Average velocity and run length of the corresponding population of motors (N) are indicated on top-right or left-corner as mean ± SEM. Data presented from three independent experiments. (G) Quantification of the microtubule landing rates for the indicated wild type and a loop 8 mutant (R167C). Yellow dotted line indicates the cell boundary, arrowhead indicates neurite tip and asterisk indicates the nucleus. Scale bars, 10 μm. Statistical difference calculated using Student's t-test (***p<0.0005). (H-I) Relative ATP hydrolysis rate (H) and microtubule affinity (I) of wild type and kinesin-3 loop8 mutants. #, could not measure the ATPase activity due to protein expression problems. The ATPase activity of wild-type motor is considered as 100% and the relative activity of the loop8 mutants was then calculated. Values from three independent experiments.

We further assessed the contribution of positively charged residues in the loop8 to the differential microtubule-binding by mutating other positively charged residues (K161A, K163A and R169A) in KIF1A and measuring their ATPase kinetics using purified motors. Similar to R167C, the ATPase analysis of K161A and K163A mutants also showed a significant decrease in the ATP hydrolysis rates and affinity for the microtubules **(Figure 5.1 H and I)**, consistent with the previous work that conversion of all the positively charged residues in loop8 to Alanine (K161A/R167A/R169A/K183A) strongly affected microtubule binding affinity (Aguilera et al., 2021; Lee et al., 2015; Nitta et al., 2004). We did not measure the ATPase activity of the R169A mutant because the motor showed very low expression levels even after two days in mammalian cells

and failed to express in Sf9 cells despite several attempts. Collectively, these results suggest that individual positively charged residues in the loop8 contribute substantially to the differential microtubule-binding affinity for the kinesin 3 motors, which is critical for establishing an inverse correlation between the rate of ATP hydrolysis and microtubule affinity.

Together, we hypothesize that although kinesin family motors share a highly conserved motor domain, a fine balance between the rate of ATP hydrolysis and its affinity for the microtubule is critical for generating family-specific motility outputs. Indeed, previous studies on kinesin and myosin motors have suggested that the rate of ATP hydrolysis and nature of interaction with the microtubule directly regulates family-specific mechanical outputs (Barany, 1967; Friel and Howard, 2012). The best example that illustrates such a correlation would be the studies done on sprinters of the land, cheetah (Hudson et al., 2012). Analogies between kinesin-3 unique mechanical outputs and a sprinting cheetah: powerful muscle strength (high ATPase activity), firm traction (K-loop and loop8) and decreased ground contact time (lower microtubule affinity). However, detailed kinetics of ATP turnover cycle is needed to understand quantitative differences in the transition rates of ATPase cycle. Collectively, we demonstrate that a fine balance between the rate of ATP hydrolysis and microtubule-binding affinity enables kinesin 3 motors with novel mechanical outputs.

4.5. Kinesin-3 motors influence microtubule bending *in vitro.*

In vitro single-molecule motility properties correspond with measured biochemical properties of kinesin motors. Next, we wanted to investigate the collective behavior of kinesin-3 motors, which can be studied *in vitro* by microtubule gliding assay (Bohm et al., 2000; Porter et al., 1987; Tao and Scholey, 2010). In the gliding assay, constitutively active kinesin-1 or kinesin-3 motors, purified from Sf9 cells, were immobilized on the glass surface inside the motility flow chamber **(Figure 5.2A)**. As our purified motors contain a C-terminal mCit (mCitrine)-tag, we used GFP nanobodies (Sommese et al., 2016) to attach motors to the glass surface. Rhodamine-labeled microtubules were polymerized and sheared with a syringe before infusing into the motility flow chamber.

The gliding motion of microtubules was recorded under TIRF illumination. The landing of microtubules on the glass surface coated with motor proteins showed smooth microtubule sliding. We also observed efficient microtubules crossover without any noticeable hindrance in their gliding velocities (Kerssemakers et al., 2009; Liu et al., 2011). We manually tracked multiple gliding microtubules for each kinesin motor and plotted them as histograms to determine their average velocities **(Figure 5.2B-G)**.

For kinesin-1, KHC (1-560) motor displayed smooth translocation of microtubules over long distances with an average speed of 0.46± 0.06 μm s^{-1} **(Figure 5.2B, Figure 5.3A; Table 3 and Video 1)**, as shown previously (Bieling et al., 2008; Kaneko et al., 2020; Tomishige et al., 2002; Vale et al., 1985). Akin to kinesin-1, members of kinesin-3 motors purified from Sf9 cells showed smooth microtubule sliding, albeit with higher velocities. KIF1A (1-393LZ) showed robust microtubules sliding with an average speed of 1.16 ± 0.14 μm s^{-1}**(Figure 5.2C, Figure 5.3B; Table 3 and Video 2)**, which is ~ 2.5-fold higher than the average velocity determined for kinesin-1. The fast velocity observed for KIF1A is comparable to previously reported gliding velocity of 0.91±0.09 μm s^{-1} measured using protein expressed in mammalian cells (Kaur et al., 2020). However, similar studies using motors purified from bacterial expression system showed velocities ranging from 0.05–0.35 μm s^{-1} (Esmaeeli Nieh et al., 2015; Mitra et al., 2019; Oriola et al., 2015), presumably due to lack of specific chaperon system or premature termination of protein synthesis leading to misfolded or truncated proteins (Korten et al., 2016). Surprisingly, we noticed that microtubules propelled by KIF1A (1-393LZ) motors induced frequent microtubule bending. Quantitative analysis revealed that ~90% of microtubules showed bending in the range of 45^{o} to 135^{o}, significantly higher than kinesin-1, which ranges from 90^{o} to 180^{o} **(Figure 5.4A-B)**.

Microtubule gliding analysis of constitutively active KIF13 family members, KIF13A (1-411ΔP) and KIF13B (1-412ΔP), displayed vigorous microtubule sliding with intermittent bending. The average velocity of sliding microtubules was determined to be 0.58±0.05 μm s^{-1} and 0.60±0.06 μm s^{-1} for KIF13A (1-411ΔP) and KIF13B (1-412ΔP), respectively **(Figure 5.2D-E, Figure 5.3 C-D; Table 3 and Video 3-4)**, as shown

previously (Horiguchi et al., 2006; Nakagawa et al., 2000; Zhou et al., 2013). Similar to KIF1A, quantitative analysis showed ~90% of microtubules bending in the range of 45^{o} to 135^{o} for both KIF13A (1-411ΔP) and KIF13B (1-412ΔP) motors **(Figure 5.4A-B)**. Lastly, analysis of KIF16B (1-400) also showed uniform microtubule gliding, with occasional microtubule bending. The tracking analysis yielded an average velocity of 0.48±0.08μm s^{-1} **(Figure 5.2F, Figure 5.3E; Table 3 and Video 5)** (Hoepfner et al., 2005), which is much slower than other kinesin-3 members but still comparable to the velocity determined for kinesin-1. Unlike other kinesin-3 motors, KIF16B showed ~70% microtubule bending between 90^{o} – 135^{o} **(Figure 5.4A-B)**.

Together, the data suggest that our low-density microtubule (~ 0.5 microtubules/μm^2) gliding assays using purified constitutively active kinesin-3 family motors influence microtubule bending without affecting their gliding velocities. Interestingly, the observed microtubule bending does not require pinning of the leading end or any other physical barrier as reported previously (Amos and Amos, 1991; Kent et al., 2016; VanDelinder et al., 2016). Therefore, understanding the mechanism that influences microtubule bending requires further characterization.

4.6. Kinesin-3 motors influence microtubule bending *in vivo.*

To investigate the underlying mechanism of microtubule bending at the cellular level, we performed live-cell imaging in cells expressing kinesin-3 or kinesin-1 motors. We imaged microtubule architecture in COS-7 cells expressing mCherry-α-tubulin under TIRF illumination. Cells coexpressing constitutively active wild-type kinesin-3 or kinesin-1 motors with mCherry-tubulin displayed varying microtubule decoration and architecture **(Figure 5.5)**. For kinesin 1, KHC(1-560) motor, a significant population (~95%) of cells showed a characteristic radial array of microtubules with shallow microtubule decoration. Only a small (5%) population of cells showed microtubule bending **(Figure 5.6A)**. In contrast, the majority (50% - 60%) of the cell population expressing constitutively active kinesin-3 motors showed strong microtubule decoration and microtubule bending **(Figure 5.6A)**. microtubule bending analysis of cells expressing kinesin-3 motors revealed ~95% of bending between 45^{o} to 135^{o}, which is

significantly higher than kinesin-1, ranging from 90° to 180° **(Figure 5.6B)**. The extent of microtubule decoration agrees with the previously observed significant difference in microtubule landing and binding affinities *in vitro* (Soppina and Verhey, 2014). Together these results suggest that kinesin-3 motors influence microtubule bending *in vivo*.

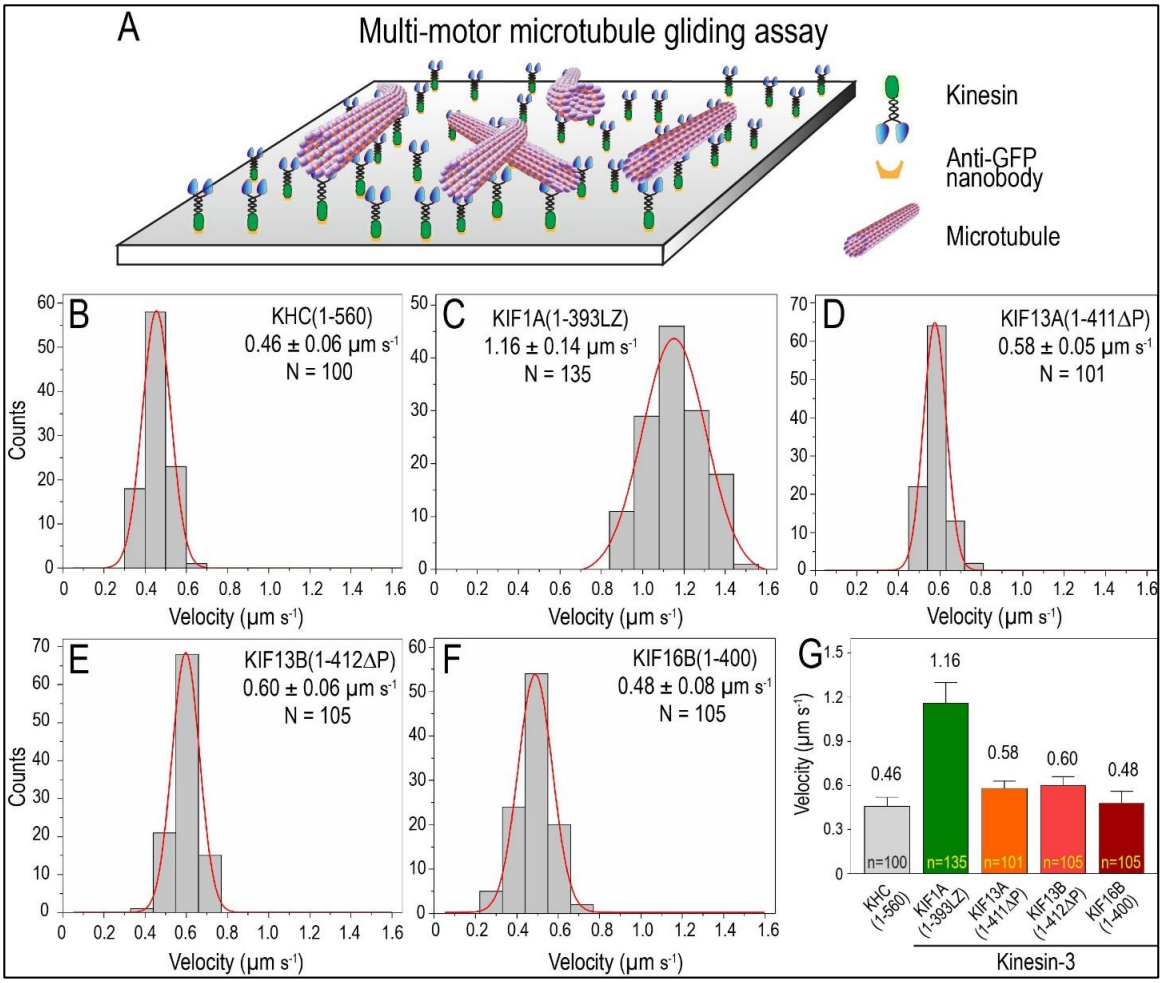

Figure 5.2. Kinesin-3 motors glide microtubules faster. Collective motor properties of kinesin-3 motors in microtubule gliding assays. (A) Schematic representation of microtubule gliding assay. C-terminal mCitrine-tagged truncated constitutively active kinesin-3 motors were attached to a glass surface coated with GFP-nanobodies. Subsequently, fluorescently labeled microtubules were introduced into the flow chamber. (B-F) Histograms showing velocity of microtubule sliding by kinesin-1 motor (B) KHC (1-560) and kinesin-3 motors (C) KIF1A(1-393LZ), (D) KIF13A(1-411ΔP), (E)

KIF13B(1-412ΔP) and (F) KIF16B(1-400) were plotted and fit to Gaussian distribution. Average gliding velocities are indicated as mean ± SEM on top right or left corner. N, number of motility events analyzed across three independent experiments. (G) Gliding velocities for kinesin-1 and kinesin-3 motors were plotted as mean ± SEM.

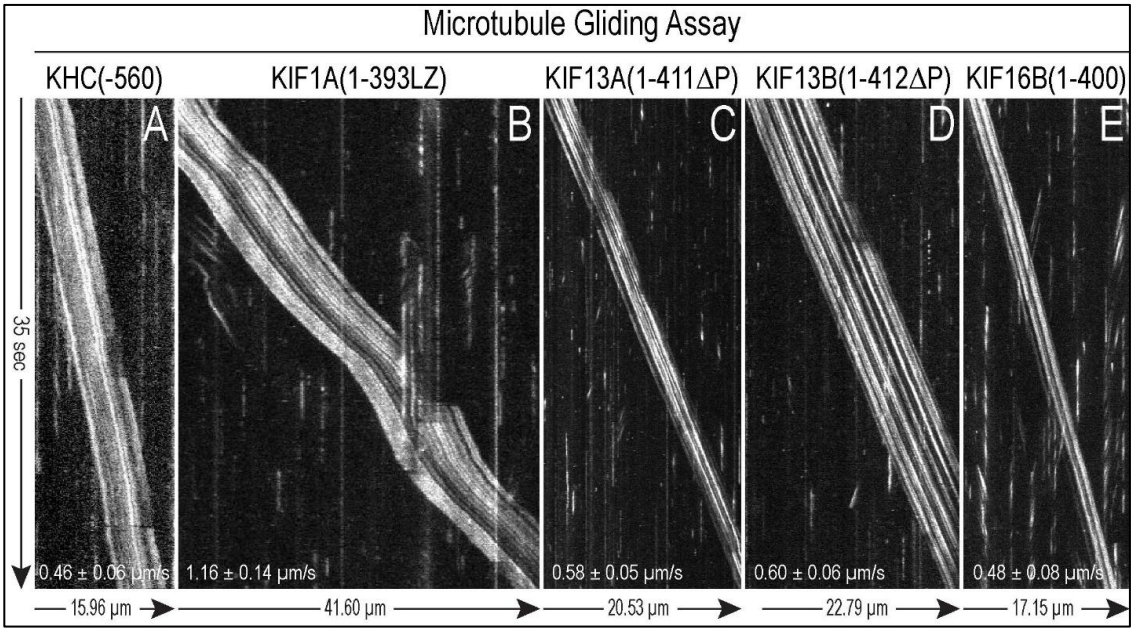

Figure 5.3. Multi-motor microtubule gliding analysis of kinesin-3 motors. (A-E) Representative kymographs show microtubule gliding driven by the indicated motors (A) KHC (1-560), (B) KIF1A(1-393LZ), (C) KIF13A(1-411ΔP), (D) KIF13B(1-412ΔP) and (E) KIF16B(1-400) moving with uniform velocity. Time on the y-axis and distance on the x-axis. Microtubule gliding velocities are described as mean ± SEM on bottom-left corner.

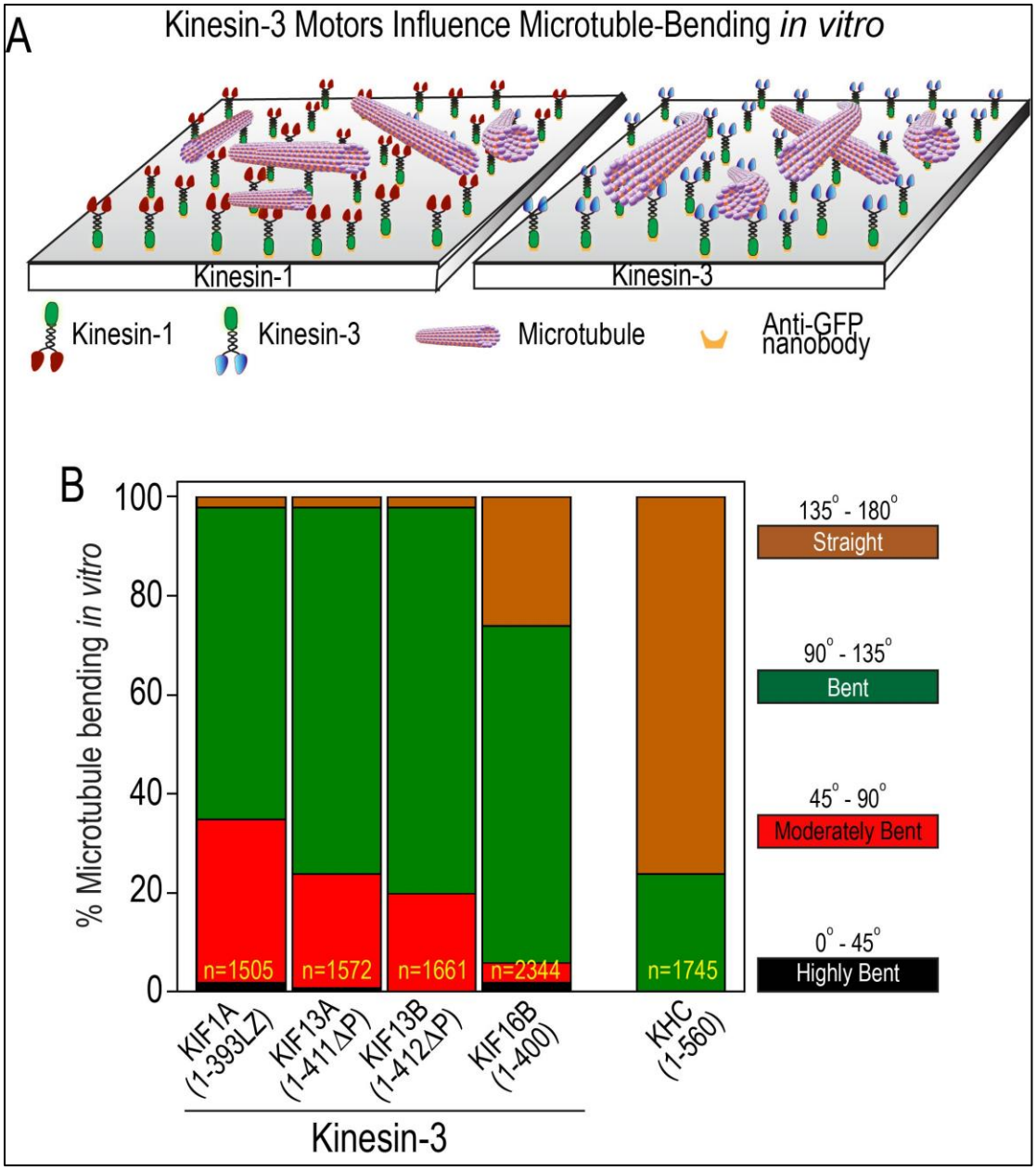

Figure 5.4. Kinesin-3 motors induce frequent microtubule bending in multi-motor gliding assay. (A) Cartoon representation of constitutively active kinesin-3 motors influence significant microtubule bending in multi-motor gliding assay in vitro compared to kinesin-1 motor. (B) Bar graph indicating the percent microtubule bending in multi-motor gliding assay with constitutively active kinesin-3 and kinesin-1 motors. Microtubules ≤ 20 µm were considered for bending analysis. n values represent number of bending events analyzed for angle measurement. Values from three independent experiments.

4.7. The K-loop influences microtubule bending *in vivo*.

The K-loop, a conserved, hallmark insert in loop 12 of kinesin-3 motor domain, contains several positively charged lysine residues **(Figure 5.7A)** that play essential roles in motor microtubule interaction in the ADP state (Nitta et al., 2004; Okada and Hirokawa, 1999, 2000). The detailed biochemical and biophysical analysis has demonstrated that the K-loop influences motors affinity for the microtubule, landing rate, and diffusion through an electrostatic interaction with negatively charged E-hook at the C-terminal tubulin dimers (Cooper and Wordeman, 2009; Kikkawa et al., 2000; Okada and Hirokawa, 1999, 2000; Soppina and Verhey, 2014). However, the influence of K-loop in microtubule bending in kinesin-3 motors has never been explored. Thus, we examined its role in microtubule bending using constitutively active dimeric kinesin-3 wild-type and its K-loop mutants, KIF1A(1-393LZ), KIF13A(1-411ΔP), KIF13B(1-412ΔP), and KIF16B(1-400) (Soppina et al., 2014; Soppina and Verhey, 2014). As a control, we used KHC(1-560), a well-characterized constitutively active dimeric kinesin-1 motor (Soppina et al., 2014; Soppina and Verhey, 2014).

To dissect the contribution of the K-loop in microtubule bending at a molecular level, we expressed K-loop mutants (All-ala), in which all lysine residues in the K-loop of each motor mutated to alanine residues **(Figure 5.7B)** (Soppina and Verhey, 2014). Consistent with previous findings that mutation of lysine-to-alanine residues in the K-loop, all the kinesin-3 motors significantly lost their ability to bind microtubules and remained largely cytoplasmic. In addition, these cells showed no significant microtubule bending; instead showed radial microtubule arrays extending towards the cell periphery, with occasional bending similar to cells expressing kinesin-1 **(Figure 5.8A-D, Figure 5.6B)**. However, the conversion of a single lysine residue to alanine in the K-loop of kinesin-1 showed no change in its ability to interact with microtubules **(Figure 5.8E, Figure 5.6B)**. Together, these results suggest that positively charged lysine residues in the K-loop influence kinesin-3 driven microtubule bending in cells.

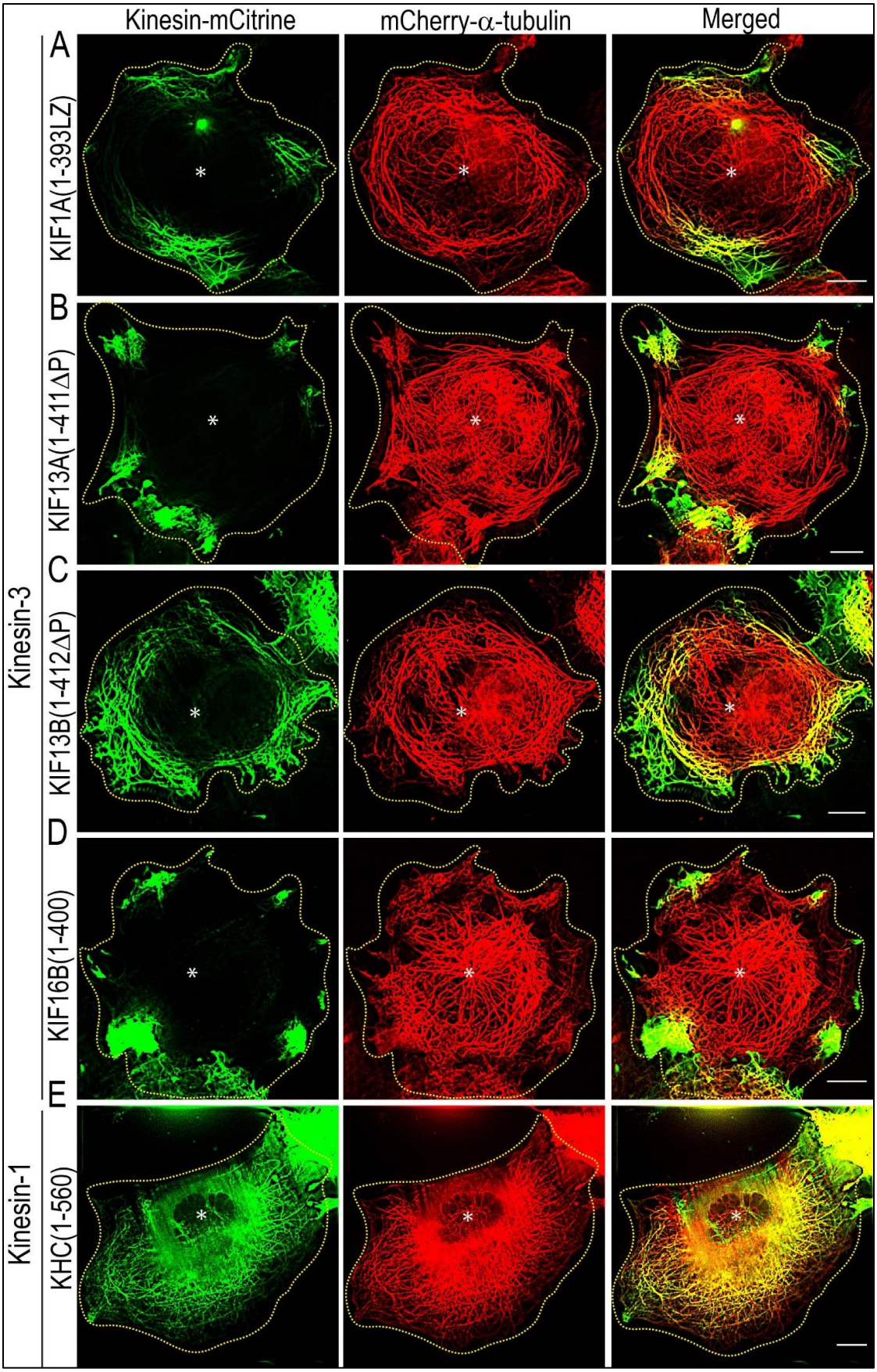
Kinesin-mCitrine
mCherry-α-tubulin
Merged
A
KIF1A(1-393LZ)
B
KIF13A(1-411ΔP)
C
KIF13B(1-412ΔP)
D
KIF16B(1-400)
E
KHC(1-560)
Kinesin-3
Kinesin-1

Figure 5.5. Kinesin-3 motors induce microtubule bending in cells. COS-7 cells were cotransfected with plasmids coding for mCherry-α-tubulin and individual members of constitutively active wild-type kinesin-3 A) KIF1A(1-393LZ), B) KIF13A(1-411ΔP), C) KIF13B(1-412ΔP) and D) KIF16B(1-400), and kinesn-1 E) KHC(1-560) motors. Yellow dotted line indicates the cell boundary, and asterisk indicates the nucleus. Scale bars, 10 µm.

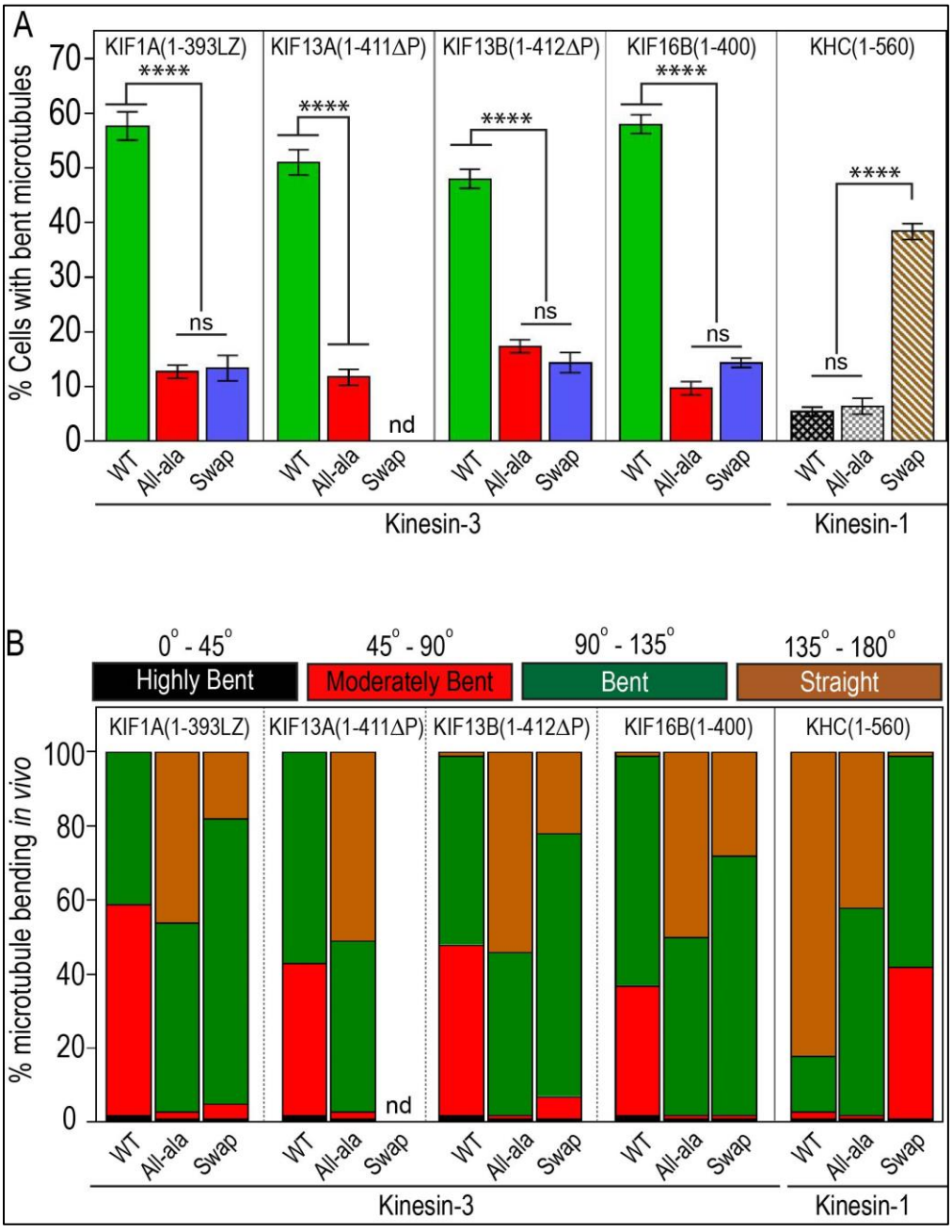

Figure 5.6. Kinesin-3 motors influence microtubule bending *in vivo*. (A) Quantification of cotransfected cells exhibiting curved MTs for wild type or K-loop mutants; alanine (All-ala) or Swap (K-loop swap) mutants. n = 110–130 cells each. Statistical difference calculated using Student's t-test (****p<0.0001), ns (non-significant), The values and error bars represent mean ± SEM (B) Quantification percent cotransfected cells exhibiting microtubule-bending angle for wild-type or K-loop mutants; alanine (All-ala) or Swap (K-loop swap) mutants. n = 30-35 cells each.. nd (not determined). Values from three independent experiments.

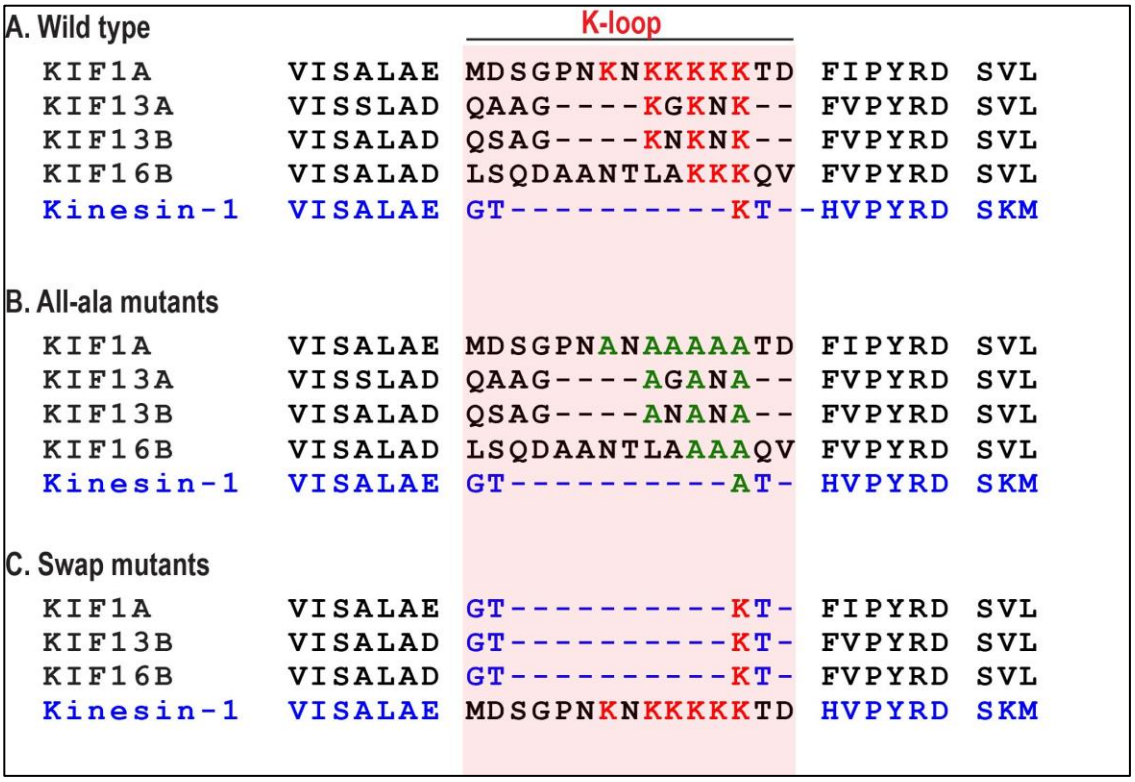

Figure 5.7. Amino acid sequence alignment of kinesin-3 and kinesin-1 K-loop and their mutants. (A) Wild-type kinesin-3 (black text) and kinesin-1 (blue text). (B)All-Alanine mutants, in which all the positively charged lysine residues are mutated to alanine in the kinesin-3 and kinesin-1 K-loop regions. (C) Swap mutants, replacement of kinesin-3 K-loop with that of kinesin 1 and the replacement of kinesin-1 K-loop with that of KIF1A.

To further explore the specificity of K-loop in microtubule bending, we expressed swap mutants, in which the K-loop sequence of each kinesin-3 motor is replaced with that of kinesin 1 **(Figure 5.7C)** (Soppina and Verhey, 2014). KIF13A and KIF13B are homologs and share ~62% amino acid identity (Venkateswarlu et al., 2004). Their constitutively active dimeric versions showed identical motility properties and regulation mechanisms; we only included the analysis for the KIF13B motor for the sake of simplicity. The cells expressing kinesin 3 swap mutants not only significantly lost their ability to decorate microtubules but also considerably lost microtubule bending ability **(Figure 5.9A-C)**. The extent of microtubule bending was similar to kinesin-3 All-ala and wild-type kinesin 1 motors **(Figure 5.6B)**. Paradoxically, the generation of kinesin-1 swap mutant by substituting the corresponding loop 12 of kinesin-1 with that of KIF1A showed a marked increase in microtubule decoration and bending **(Figure 5.9D, Figure 5.6B)**, which is comparable to wild-type kinesin-3 motors.

4.8. The K-loop influences microtubule bending *in vitro.*

As kinesin-3 all-alanine and swap mutants failed to exhibit microtubule-bending and kinesin-1 swap mutant showed significant microtubule bending *in vivo*, we decided to test these results in a purified system using in vitro microtubule gliding assays. Assays with kinesin-3 All-ala mutants exhibited very few loosely bound microtubules on the surface, resulting in no microtubule gliding events **(Figure 5.10 A-B)**. Microtubule gliding assay with KIF1A All-ala mutant is provided as a representative video **(Video 6)**. These results agree with our previous single-molecule motility assays of kinesin 3 All-ala mutants that failed to show processive motion along the microtubule surface (Soppina and Verhey, 2014). However, gliding analysis with kinesin-3 Swap mutant exhibited smooth and uniform microtubule motion at an average speed between 0.49 μm s^{-1} to 0.58 μm s^{-1} with occasional microtubule-bending (~10%) similar to wild-type kinesin-1 **(Figure 5.10 A-B)**. Microtubule gliding assay with KIF1A Swap mutant is provided as a representative video **(Video 7)**. In contrast, experiments with kinesin-1 Swap mutant displayed uniform and smooth microtubule gliding at an average velocity of 0.63±0.01 μm s^{-1} with significant microtubule-bending (~90%), which is comparable to KIF1A wild-type motor (90%) **(Figure 5.10 and Video 8)**. Together, these results demonstrate

that the K-loop not only increases affinity for the microtubule but also influences microtubule bending.

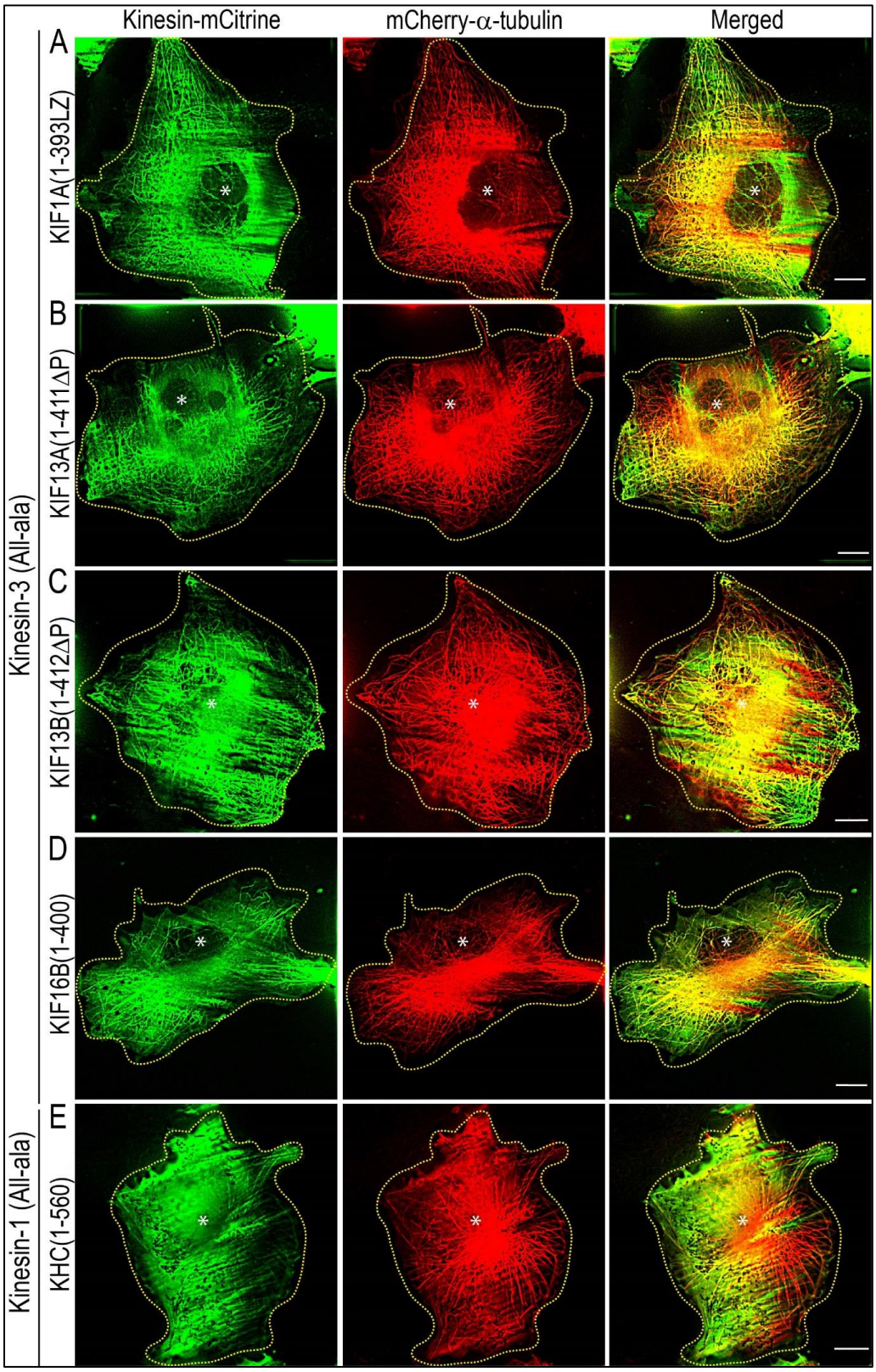

Figure 5.8. Positively charged lysine resides in the K-loop influence microtubule bending in cells. COS 7 cells were cotransfected with plasmids coding for mCherry-α-tubulin and individual members of constitutively active alanine (All-ala) mutants of kinesin-3 A) KIF1A(1-393LZ), B) KIF13A(1-411ΔP), C) KIF13B(1-412ΔP) and D) KIF16B(1-400), and kinesn-1 E) KHC(1-560), in which positively charged lysine residues in the K-loop were mutated to alanine as described previously [17]. Yellow dotted line indicates the cell boundary, and asterisk indicates the nucleus. Scale bars, 10 μm.

Microtubules are long cylindrical rigid structures that can withstand compressive loads to resist and balance the tensional forces in cells and their network supports a myriad of biological processes (Brangwynne et al., 2007). Microtubules exhibit divergent behavior in various cellular processes ranging from mechanical support to intracellular transport to cellular signaling. Particularly, microtubule bending has been shown to alter growing plus-end dynamics, localization, and its role in targeting and biochemical signaling (Howard and Hyman, 2003; Kaverina et al., 1999; Prosser et al., 2011). Microtubule bending on both short and long length scales is ubiquitous in mammalian and fungal cells due to large forces generated by the action of molecular motors (Bicek et al., 2009; Brangwynne et al., 2006; Brangwynne et al., 2007; Luria et al., 2011; Odde et al., 1999; Straube et al., 2006). Microtubule bending has also been observed in cell-free and obstacle-free systems through an unknown mechanism (Shekhar et al., 2013). Despite microtubule architecture playing prime biological roles, the mechanism of microtubule bending and it's *in vivo* significance remains poorly studied. More recently, detyrosination of α-tubulin has been shown to regulate the microtubule bending and stiffness in beating cardiomyocytes. Interestingly, increased detyrosination prompted microtubule bending, stiffened the myocyte, and implicated cardiac and muscular dystrophy (Robison et al., 2016). However, understanding the physiological significance of this interesting phenomenon requires detailed biophysical and structural characterization, which may further provide important insights on microtubule bending observed in nerve cells undergoing degeneration (Sanchez-Soriano et al., 2009; Voelzmann et al., 2016; Voelzmann et al., 2017).

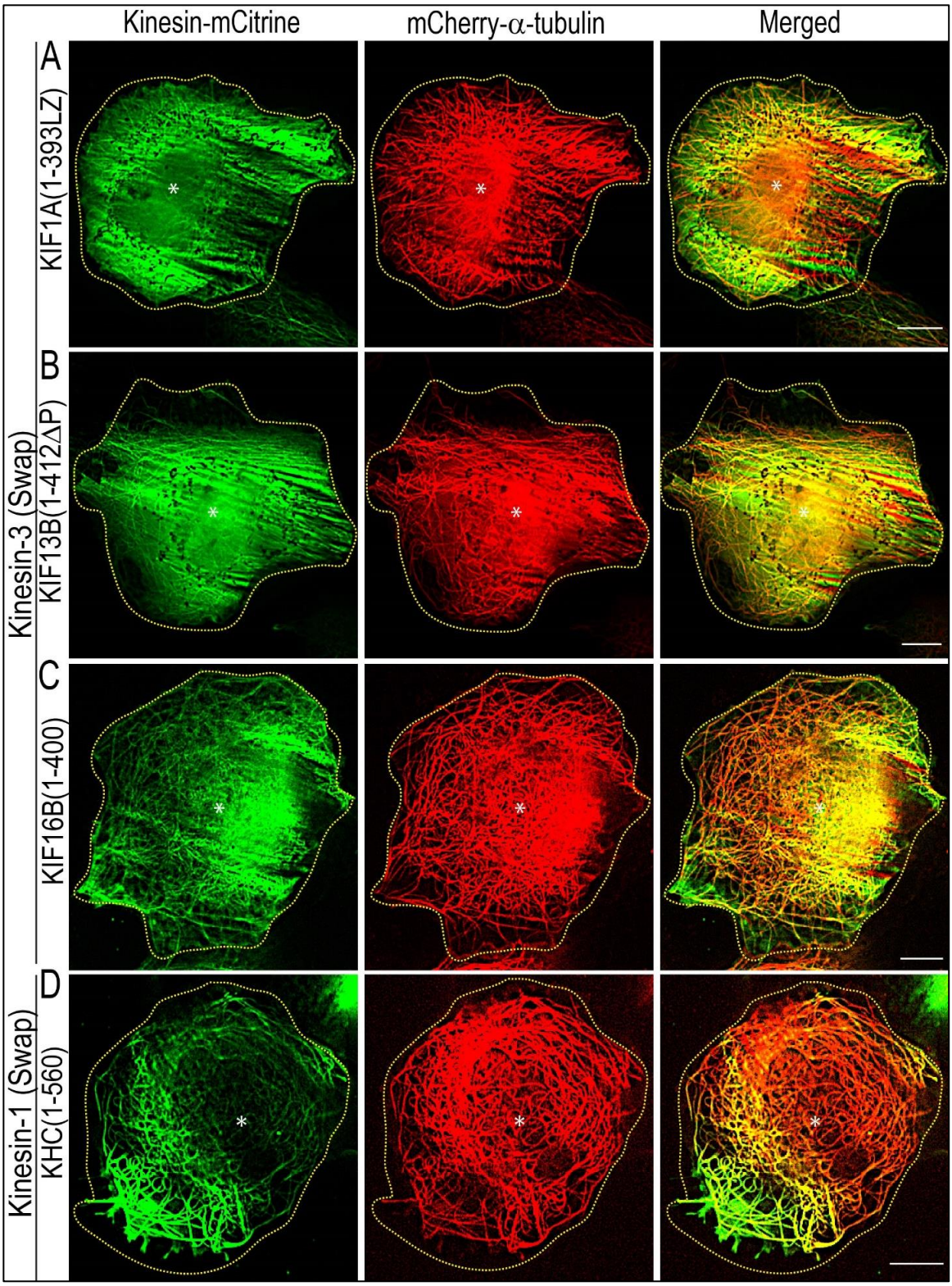
Kinesin-mCitrine
mCherry-α-tubulin
Merged
A
KIF1A(1-393LZ)
B
KIF13B(1-412ΔP)
C
KIF16B(1-400)
D
KHC(1-560)
Kinesin-3 (Swap)
Kinesin-1 (Swap)

Figure 5.9. Positively charged lysine resides in the K-loop influence microtubule bending in cells. COS 7 cells were cotransfected with plasmids coding for mCherry-α-tubulin and individual members of constitutively active swap mutants in which the K-loop of each kinesin-3 motors (A) KIF1A(1-393LZ), (B) KIF13B(1-412ΔP) and (C) KIF16B(1-400) were replaced with that of kinesin-1 and (D) the K-loop of kinesin-1 was replaced with that of KIF1A. Yellow dotted line indicates the cell boundary, and asterisk indicates the nucleus. Scale bars, 10 μm.

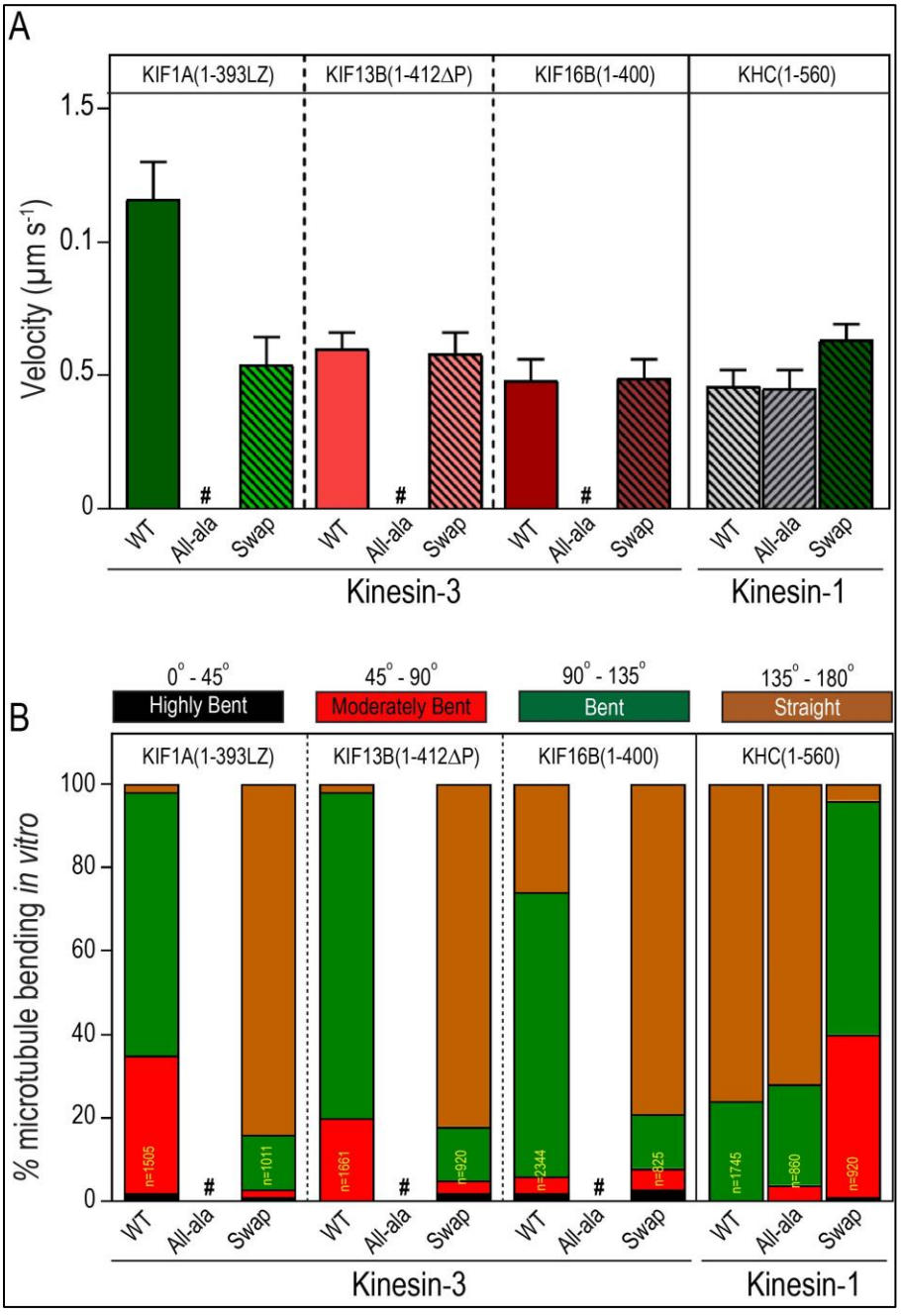

Figure 5.10. K-loop, a family specific insert in the loop12 of Kinesin-3 motor domain, influence microtubule bending. (A) Microtubule gliding velocities for wild-type and K-loop mutants (All-ala and Swap) of kinesin-3 (KIF1A, KIF13B and KIF16B) and kinesin-1 (KHC) motors were plotted as mean ± SD. (B) Microtubule-bending analysis of wild-type and K-loop mutants (All-ala and Swap) of kinesin-3 (KIF1A, KIF13B and KIF16B) and kinesin-1 (KHC) motors in multi-motor microtubule gliding assay.

Chapter 5

Conclusions

An immensely crowded cell environment poses many challenges in sorting destined proteins and molecules. This intense workload of organization and spatiotemporal distribution of molecules within the cytoplasm is facilitated by molecular motors and cytoskeletal tracks. Molecular motors are mechanochemical enzymes that hydrolyze energy currencies such as ATP and utilize that energy during motion and force generation (Vale, 2003). Kinesin and dynein class of molecular motors mainly carries out long-distance intracellular cargo transport. These motors use microtubules as tracks to transport cargoes in anterograde (plus-end of microtubules) and retrograde directions (minus-end of microtubules), respectively. Based on the amino acid sequence similarity, kinesins are grouped into 14 families. Despite high similarity, each motor contributes uniquely to the functioning of a cell. Kinesin-3 family motors constitute one of the largest, comprising five subfamilies (KIF1, KIF13, KIF14, KIF16, and KIF28) (Miki et al., 2005), associated with diverse cellular and physiological functions, including vesicle transport, signaling, mitosis, nuclear migration, and development (Hirokawa et al., 2010; Hirokawa and Takemura, 2005; Patel et al., 2021). Impairment in kinesin-3 transport function implicates in many neurodegenerative disorders, developmental defects, and cancer diseases (Franker and Hoogenraad, 2013; Gunawardena et al., 2014; Rath and Kozielski, 2012).

Recent work has demonstrated that kinesin-3 motors are monomers but undergo cargo-induced dimerization and result in fast and superprocessive motility compared to conventional kinesin (Guo et al., 2019; Scarabelli et al., 2015; Soppina et al., 2014; Soppina and Verhey, 2014). Their biochemical and biophysical characterization needs a large quantity of purified, active proteins. However, their production in the prokaryotic expression system resulted in inactive or aggregated motors, presumably due to incompatible protein synthesis, folding and modification machinery (Korten et al., 2016; Kurland and Gallant, 1996; Schmidt, 2004; Tao and Scholey, 2010). To circumvent such

limitations and increase the yield, here we have established a robust Sf9-baculovirus expression system to express and purify these motors.

The baculovirus expression system utilizes Sf9 insect cell lines as a host system for high-throughput eukaryotic recombinant protein expression (Felberbaum, 2015; Kost et al., 2005). Baculovirus possesses a strong polyhedrin promoter that assists in heterologous gene expression and the production of soluble recombinant proteins (Kurland and Gallant, 1996). Due to its cost-effectiveness, safe to handle and high amount of active protein expression, it has become a powerful tool (Kumar et al., 2018). A key step in expressing a protein of interest in Sf9 cells is generating a recombinant bacmid. As commercially available bacmid generating kits are expensive and will be working with several samples, we developed an in-house protocol for both large and small inserts of kinesin-3 motors into bacmids. Sf9-purified kinesin-3 motors were used to characterize in vitro single-molecule and multi-motor microtubule gliding properties using total internal reflection fluorescence (TIRF) microscopy. Motors are C-terminally tagged with 3-tandem fluorescent molecules to provide enhanced signal and decreased photobleaching. Due to its increased signal-to-noise ratio, less phototoxicity, and selective imaging of a very small area close to the coverslip, TIRF imaging has been widely used to visualize protein dynamics at the single-molecule level *in vivo* and *in vitro*.

In summary, we successfully purified recombinant full-length and constitutively active kinesin-3 family motors using Sf9-baculovirus expression system. To check the homogeneity and proper folding of purified protein we performed size-exclusion-high performance liquid chromatography (SEC-HPLC) and circular dichroism (CD) respectively. Single-molecule motility assay using purified motors demonstrated that the motility properties are comparable to the mammalian lysates shown previously. The results also suggest that the high velocity and superprocessivity of kinesin 3 motors is inherent to their motor domains. Hence, we believe that the Sf9-baculovirus system can be adapted to express and purify any motor protein of interest.

Biochemical studies using Sf9 purified kinesin-3 motors display high ATP turnover rate compared to well-characterized motor, kinein-1 that is almost 3-fold difference. This also suggest Sf9 purified motors are active and of high purity. For the first time we have shown that ATP hydrolysis rate matches with the stepping rate of kinesin-3 motors and both chemical and mechanical properties are tightly coupled. Interestingly, velocity rate of these motors showed an inverse correlation with their microtubule binding affinities. Hence, further detailed study revealed that positively charged amino acid residues clustered in the loop8 of kinesin-3 motor domain largely contribute to the determined differential microtubule-binding affinities.

Furthermore, to understand the collective behavior of kinesin-3 motors, we performed multi motor microtubule gliding analysis using Sf9 purified motors. Interestingly, these motors displayed uniform microtubule sliding and smooth crossing over with significant microtubule bending than kinesin-1 motor without affecting their gliding velocities. Live-cell imaging studies suggested that this microtubule bending is largely influenced by K-loop, a family-specific insert in the loop-12 of kinesin-3 motor domain.

To our knowledge, this is the first comprehensive demonstration of kinesin-3 family motors with diverse mechanical outputs. Thus, we propose that kinesin-3 motors are fine-tuned at the molecular level to endow diverse mechanical outputs critical for myriad cellular processes.

Movie legends (Movies provided as separate file)

Movie 1. Microtubule gliding assay of constitutively active kinesin-1 motor, KHC(1-560). TIRF imaging of MT gliding by KHC(1-560), kinesin-1 motor purified from Sf9-baculovirus system. Movie was acquired at 100 msec exposure and shown at 60 frames/sec. Scale bar, 10 μm. Selected bending events are marked by arrow.

Movie 2. Microtubule gliding assay of constitutively active kinesin-3 motor, KIF1A(1-393LZ). TIRF imaging of MT gliding by KIF1A(1-393LZ), kinesin-3 motor purified from Sf9-baculovirus system. Movie was acquired at 100 msec exposure and shown at 60 frames/sec. Scale bar, 10 μm. Selected bending events are marked by arrow.

Movie 3. Microtubule gliding assay of constitutively active kinesin-3 motor, KIF13A(1-411ΔP). TIRF imaging of MT by KIF13A(1-411ΔP), kinesin-3 motor purified from Sf9-baculovirus system. Movie was acquired at 100 msec exposure and shown at 60 frames/sec. Scale bar, 10 μm. Selected bending events are marked by arrow.

Movie 4. Microtubule gliding assay of constitutively active kinesin-3 motor, KIF13B(1-412ΔP). TIRF imaging of MT gliding by KIF13B(1-412ΔP), kinesin-3 motor purified from Sf9-baculovirus system. Movie was acquired at 100 msec exposure and shown at 60 frames/sec. Scale bar, 10 μm. Selected bending events are marked by arrow.

Movie 5. Microtubule gliding assay of constitutively active kinesin-3 motor, KIF16B(1-400). TIRF imaging of MT gliding by KIF16B(1-400), kinesin-3 motor purified from Sf9-baculovirus system. Movie was acquired at 100 msec exposure and shown at 60 frames/sec. Scale bar, 10 μm. Selected bending events are marked by arrow.

Movie 6. Microtubule gliding assay of KIF1A(1-393LZ) All-alanine mutant. TIRF imaging of MT gliding by KIF1A(1-393LZ) All-alanine mutant, in which the lysine residues in the K-loop were mutated to Alanine, purified from Sf9-baculovirus system. Movie was acquired at 100 msec exposure and shown at 60 frames/sec. Scale bar, 10 μm. Selected bending events are marked by arrow.

Movie 7. Microtubule gliding assay of KIF1A(1-393LZ) Swap mutant. TIRF imaging of MT gliding by KIF1A(1-393LZ) Swap mutant, in which the K-loop of KIF1A motor is swapped with that of kinesin-1, purified from Sf9-baculovirus system. Movie was acquired at 100 msec exposure and shown at 60 frames/sec. Scale bar, 10 μm. Selected bending events are marked by arrow.

Movie 8. Microtubule gliding assay of KHC(1-560) Swap mutant. TIRF imaging of MT gliding by KHC(1-560) Swap mutant, in which the K-loop of kinesin-1 motor is swapped with that of KIF1A, purified from Sf9-baculovirus system. Movie was acquired at 100 msec exposure and shown at 60 frames/sec. Scale bar, 10 μm. Selected bending events are marked by arrow.

Bibliography

Aguilera, C., Hummer, S., Masanas, M., Gabau, E., Guitart, M., Jeyaprakash, A.A., Segura, M.F., Santamaria, A., and Ruiz, A. (2021). The Novel KIF1A Missense Variant (R169T) Strongly Reduces Microtubule Stimulated ATPase Activity and Is Associated With NESCAV Syndrome. Front Neurosci *15*, 618098.

Ahmed, S.M., Theriault, B.L., Uppalapati, M., Chiu, C.W., Gallie, B.L., Sidhu, S.S., and Angers, S. (2012). KIF14 negatively regulates Rap1a-Radil signaling during breast cancer progression. J Cell Biol *199*, 951-967.

Al-Bassam, J., Cui, Y., Klopfenstein, D., Carragher, B.O., Vale, R.D., and Milligan, R.A. (2003). Distinct conformations of the kinesin Unc104 neck regulate a monomer to dimer motor transition. J Cell Biol *163*, 743-753.

Al-Bassam, J., and Nithianantham, S. (2018). Malleable folding of coiled-coils regulates kinesin-3 dimerization. Proc Natl Acad Sci U S A *115*, 12845-12847.

Allan, V.J. (2011). Cytoplasmic dynein. Biochem Soc Trans *39*, 1169-1178.

Amos, L.A., and Amos, W.B. (1991). The bending of sliding microtubules imaged by confocal light microscopy and negative stain electron microscopy. J Cell Sci Suppl *14*, 95-101.

Anderson, E.N., White, J.A.I., and Gunawardena, S. (2013). Axonal transport and neurodegenerative disease: vesicle-motor complex formation and their regulation. Degernative Neurological and Neuromuscular Disease *4*, 29-47.

Aoki, T., Tomishige, M., and Ariga, T. (2013). Single molecule FRET observation of kinesin-1's head-tail interaction on microtubule. Biophysics (Nagoya-shi) *9*, 149-159.

Armstrong, C.T., Mason, P.E., Anderson, J.L., and Dempsey, C.E. (2016). Arginine side chain interactions and the role of arginine as a gating charge carrier in voltage sensitive ion channels. Sci Rep *6*, 21759.

Arora, K., Talje, L., Asenjo, A.B., Andersen, P., Atchia, K., Joshi, M., Sosa, H., Allingham, J.S., and Kwok, B.H. (2014). KIF14 binds tightly to microtubules and adopts a rigor-like conformation. J Mol Biol *426*, 2997-3015.

Asaba, N., Hanada, T., Takeuchi, A., and Chishti, A.H. (2003). Direct interaction with a kinesin-related motor mediates transport of mammalian discs large tumor suppressor homologue in epithelial cells. J Biol Chem *278*, 8395-8400.

Atherton, J., Farabella, I., Yu, I.M., Rosenfeld, S.S., Houdusse, A., Topf, M., and Moores, C.A. (2014). Conserved mechanisms of microtubule-stimulated ADP release, ATP binding, and force generation in transport kinesins. Elife *3*, e03680.

Barany, M. (1967). ATPase activity of myosin correlated with speed of muscle shortening. J Gen Physiol *50*, Suppl:197-218.

Barkus, R.V., Klyachko, O., Horiuchi, D., Dickson, B.J., and Saxton, W.M. (2008). Identification of an axonal kinesin-3 motor for fast anterograde vesicle transport that facilitates retrograde transport of neuropeptides. Mol Biol Cell *19*, 274-283.

Belyy, V., Schlager, M.A., Foster, H., Reimer, A.E., Carter, A.P., and Yildiz, A. (2016). The mammalian dynein-dynactin complex is a strong opponent to kinesin in a tug-of-war competition. Nat Cell Biol *18*, 1018-1024.

Bicek, A.D., Tuzel, E., Demtchouk, A., Uppalapati, M., Hancock, W.O., Kroll, D.M., and Odde, D.J. (2009). Anterograde microtubule transport drives microtubule bending in LLC-PK1 epithelial cells. Mol Biol Cell *20*, 2943-2953.

Bieling, P., Telley, I.A., Piehler, J., and Surrey, T. (2008). Processive kinesins require loose mechanical coupling for efficient collective motility. EMBO Rep *9*, 1121-1127.

Bloom, G.S. (2001). The UNC-104/KIF1 family of kinesins. Curr Opin Cell Biol *13*, 36-40.

Bohm, K.J., Stracke, R., Baum, M., Zieren, M., and Unger, E. (2000). Effect of temperature on kinesin-driven microtubule gliding and kinesin ATPase activity. FEBS Lett *466*, 59-62.

Brangwynne, C.P., MacKintosh, F.C., Kumar, S., Geisse, N.A., Talbot, J., Mahadevan, L., Parker, K.K., Ingber, D.E., and Weitz, D.A. (2006). Microtubules can bear enhanced compressive loads in living cells because of lateral reinforcement. J Cell Biol *173*, 733-741.

Brangwynne, C.P., MacKintosh, F.C., and Weitz, D.A. (2007). Force fluctuations and polymerization dynamics of intracellular microtubules. Proc Natl Acad Sci U S A *104*, 16128-16133.

Budaitis, B.G., Jariwala, S., Rao, L., Yue, Y., Sept, D., Verhey, K.J., and Gennerich, A. (2021). Pathogenic mutations in the kinesin-3 motor KIF1A diminish force generation and movement through allosteric mechanisms. J Cell Biol *220*.

Cai, D., Verhey, K.J., and Meyhofer, E. (2007). Tracking single Kinesin molecules in the cytoplasm of mammalian cells. Biophys J *92*, 4137-4144.

Case, R.B., Pierce, D.W., Hom-Booher, N., Hart, C.L., and Vale, R.D. (1997). The directional preference of kinesin motors is specified by an element outside of the motor catalytic domain. Cell *90*, 959-966.

Castoldi, M., and Popov, A.V. (2003). Purification of brain tubulin through two cycles of polymerization-depolymerization in a high-molarity buffer. Protein Expr Purif *32*, 83-88.

Chen, X.J., Xu, H., Cooper, H.M., and Liu, Y. (2014). Cytoplasmic dynein: a key player in neurodegenerative and neurodevelopmental diseases. Sci China Life Sci *57*, 372-377.

Cheon, C.K., Lim, S.H., Kim, Y.M., Kim, D., Lee, N.Y., Yoon, T.S., Kim, N.S., Kim, E., and Lee, J.R. (2017). Autosomal dominant transmission of complicated hereditary

spastic paraplegia due to a dominant negative mutation of KIF1A, SPG30 gene. Sci Rep *7*, 12527.

Clancy, B.E., Behnke-Parks, W.M., Andreasson, J.O., Rosenfeld, S.S., and Block, S.M. (2011). A universal pathway for kinesin stepping. Nat Struct Mol Biol *18*, 1020-1027.

Cooper, J.R., and Wordeman, L. (2009). The diffusive interaction of microtubule binding proteins. Curr Opin Cell Biol *21*, 68-73.

Coy, D.L., Hancock, W.O., Wagenbach, M., and Howard, J. (1999). Kinesin's tail domain is an inhibitory regulator of the motor domain. Nat Cell Biol *1*, 288-292.

Cross, R.A. (1997). Molecular motors: the natural economy of kinesin. Curr Biol *7*, R631-633.

Cross, R.A. (2016). Review: Mechanochemistry of the kinesin-1 ATPase. Biopolymers *105*, 476-482.

De Vos, K.J., Grierson, A.J., Ackerley, S., and Miller, C.C. (2008). Role of axonal transport in neurodegenerative diseases. Annu Rev Neurosci *31*, 151-173.

Drerup, C.M., Lusk, S., and Nechiporuk, A. (2016). Kif1B Interacts with KBP to Promote Axon Elongation by Localizing a Microtubule Regulator to Growth Cones. J Neurosci *36*, 7014-7026.

Duncan, J.E., and Goldstein, L.S. (2006). The genetics of axonal transport and axonal transport disorders. PLoS Genet *2*, e124.

Esmaeeli Nieh, S., Madou, M.R., Sirajuddin, M., Fregeau, B., McKnight, D., Lexa, K., Strober, J., Spaeth, C., Hallinan, B.E., Smaoui, N., *et al.* (2015). De novo mutations in KIF1A cause progressive encephalopathy and brain atrophy. Ann Clin Transl Neurol *2*, 623-635.

Fehling, S.K., Noda, T., Maisner, A., Lamp, B., Conzelmann, K.K., Kawaoka, Y., Klenk, H.D., Garten, W., and Strecker, T. (2013). The microtubule motor protein

KIF13A is involved in intracellular trafficking of the Lassa virus matrix protein Z. Cell Microbiol *15*, 315-334.

Felberbaum, R.S. (2015). The baculovirus expression vector system: A commercial manufacturing platform for viral vaccines and gene therapy vectors. Biotechnol J *10*, 702-714.

Fitch, C.A., Platzer, G., Okon, M., Garcia-Moreno, B.E., and McIntosh, L.P. (2015). Arginine: Its pKa value revisited. Protein Sci *24*, 752-761.

Franker, M.A., and Hoogenraad, C.C. (2013). Microtubule-based transport - basic mechanisms, traffic rules and role in neurological pathogenesis. J Cell Sci *126*, 2319-2329.

Friedman, D.S., and Vale, R.D. (1999). Single-molecule analysis of kinesin motility reveals regulation by the cargo-binding tail domain. Nat Cell Biol *1*, 293-297.

Friel, C.T., Bagshaw, C.R., and Howard, J. (2011). Analysing the ATP turnover cycle of microtubule motors. Methods Mol Biol *777*, 177-192.

Friel, C.T., and Howard, J. (2012). Coupling of kinesin ATP turnover to translocation and microtubule regulation: one engine, many machines. J Muscle Res Cell Motil *33*, 377-383.

Gennerich, A., Carter, A.P., Reck-Peterson, S.L., and Vale, R.D. (2007). Force-induced bidirectional stepping of cytoplasmic dynein. Cell *131*, 952-965.

Goodson, H.V., and Jonasson, E.M. (2018). Microtubules and Microtubule-Associated Proteins. Cold Spring Harb Perspect Biol *10*.

Gunawardena, S., Anderson, E.N., and White, J. (2014). Axonal transport and neurodegenerative disease: vesicle-motor complex formation and their regulation. Degernative Neurological and Neuromuscular Disease *4*, 29-47.

Guo, S.K., Shi, X.X., Wang, P.Y., and Xie, P. (2019). Run length distribution of dimerized kinesin-3 molecular motors: comparison with dimeric kinesin-1. Sci Rep *9*, 16973.

Hackney, D.D. (1988). Kinesin ATPase: rate-limiting ADP release. Proc Natl Acad Sci U S A *85*, 6314-6318.

Hackney, D.D. (1994). Evidence for alternating head catalysis by kinesin during microtubule-stimulated ATP hydrolysis. Proc Natl Acad Sci U S A *91*, 6865-6869.

Hackney, D.D., and Stock, M.F. (2000). Kinesin's IAK tail domain inhibits initial microtubule-stimulated ADP release. Nat Cell Biol *2*, 257-260.

Hackney, D.D., and Stock, M.F. (2008). Kinesin tail domains and Mg2+ directly inhibit release of ADP from head domains in the absence of microtubules. Biochemistry *47*, 7770-7778.

Hall, D.H., and Hedgecock, E.M. (1991). Kinesin-related gene unc-104 is required for axonal transport of synaptic vesicles in C. elegans. Cell *65*, 837-847.

Hammond, J.W., Cai, D., Blasius, T.L., Li, Z., Jiang, Y., Jih, G.T., Meyhofer, E., and Verhey, K.J. (2009). Mammalian Kinesin-3 motors are dimeric in vivo and move by processive motility upon release of autoinhibition. PLoS Biol *7*, e72.

Hammond, J.W., Huang, C.F., Kaech, S., Jacobson, C., Banker, G., and Verhey, K.J. (2010). Posttranslational modifications of tubulin and the polarized transport of kinesin-1 in neurons. Mol Biol Cell *21*, 572-583.

Hirokawa, N., Niwa, S., and Tanaka, Y. (2010). Molecular motors in neurons: transport mechanisms and roles in brain function, development, and disease. Neuron *68*, 610-638.

Hirokawa, N., and Takemura, R. (2005). Molecular motors and mechanisms of directional transport in neurons. Nat Rev Neurosci *6*, 201-214.

Hirokawa, N., and Tanaka, Y. (2015). Kinesin superfamily proteins (KIFs): Various functions and their relevance for important phenomena in life and diseases. Exp Cell Res *334*, 16-25.

Hoepfner, S., Severin, F., Cabezas, A., Habermann, B., Runge, A., Gillooly, D., Stenmark, H., and Zerial, M. (2005). Modulation of receptor recycling and degradation by the endosomal kinesin KIF16B. Cell *121*, 437-450.

Hook, P., and Vallee, R.B. (2006). The dynein family at a glance. J Cell Sci *119*, 4369-4371.

Horiguchi, K., Hanada, T., Fukui, Y., and Chishti, A.H. (2006). Transport of PIP3 by GAKIN, a kinesin-3 family protein, regulates neuronal cell polarity. J Cell Biol *174*, 425-436.

Hou, Y., and Witman, G.B. (2015). Dynein and intraflagellar transport. Exp Cell Res *334*, 26-34.

Howard, J., and Hyman, A.A. (2003). Dynamics and mechanics of the microtubule plus end. Nature *422*, 753-758.

Huckaba, T.M., Gennerich, A., Wilhelm, J.E., Chishti, A.H., and Vale, R.D. (2011). Kinesin-73 is a processive motor that localizes to Rab5-containing organelles. J Biol Chem *286*, 7457-7467.

Hudson, P.E., Corr, S.A., and Wilson, A.M. (2012). High speed galloping in the cheetah (Acinonyx jubatus) and the racing greyhound (Canis familiaris): spatio-temporal and kinetic characteristics. J Exp Biol *215*, 2425-2434.

Hung, C.O., and Coleman, M.P. (2016). KIF1A mediates axonal transport of BACE1 and identification of independently moving cargoes in living SCG neurons. Traffic *17*, 1155-1167.

Huo, L., Yue, Y., Ren, J., Yu, J., Liu, J., Yu, Y., Ye, F., Xu, T., Zhang, M., and Feng, W. (2012). The CC1-FHA tandem as a central hub for controlling the dimerization and activation of kinesin-3 KIF1A. Structure *20*, 1550-1561.

Hyman, A., Drechsel, D., Kellogg, D., Salser, S., Sawin, K., Steffen, P., Wordeman, L., and Mitchison, T. (1991). Preparation of modified tubulins. Methods Enzymol *196*, 478-485.

Kaan, H.Y., Hackney, D.D., and Kozielski, F. (2011). The structure of the kinesin-1 motor-tail complex reveals the mechanism of autoinhibition. Science *333*, 883-885.

Kalantari, S., and Filges, I. (2020). 'Kinesinopathies': emerging role of the kinesin family member genes in birth defects. J Med Genet *57*, 797-807.

Kaneko, T., Furuta, K., Oiwa, K., Shintaku, H., Kotera, H., and Yokokawa, R. (2020). Different motilities of microtubules driven by kinesin-1 and kinesin-14 motors patterned on nanopillars. Sci Adv *6*, eaax7413.

Kapitein, L.C., and Hoogenraad, C.C. (2011). Which way to go? Cytoskeletal organization and polarized transport in neurons. Mol Cell Neurosci *46*, 9-20.

Kaur, S., Van Bergen, N.J., Verhey, K.J., Nowell, C.J., Budaitis, B., Yue, Y., Ellaway, C., Brunetti-Pierri, N., Cappuccio, G., Bruno, I., *et al.* (2020). Expansion of the phenotypic spectrum of de novo missense variants in kinesin family member 1A (KIF1A). Hum Mutat.

Kaverina, I., Krylyshkina, O., and Small, J.V. (1999). Microtubule targeting of substrate contacts promotes their relaxation and dissociation. J Cell Biol *146*, 1033-1044.

Kent, I.A., Rane, P.S., Dickinson, R.B., Ladd, A.J., and Lele, T.P. (2016). Transient Pinning and Pulling: A Mechanism for Bending Microtubules. PLoS One *11*, e0151322.

Kerssemakers, J., Ionov, L., Queitsch, U., Luna, S., Hess, H., and Diez, S. (2009). 3D nanometer tracking of motile microtubules on reflective surfaces. Small *5*, 1732-1737.

Kikkawa, M., Okada, Y., and Hirokawa, N. (2000). 15 A resolution model of the monomeric kinesin motor, KIF1A. Cell *100*, 241-252.

Kikkawa, M., Sablin, E.P., Okada, Y., Yajima, H., Fletterick, R.J., and Hirokawa, N. (2001). Switch-based mechanism of kinesin motors. Nature *411*, 439-445.

Klopfenstein, D.R., Holleran, E.A., and Vale, R.D. (2002). Kinesin motors and microtubule-based organelle transport in Dictyostelium discoideum. J Muscle Res Cell Motil *23*, 631-638.

Korten, T., Chaudhuri, S., Tavkin, E., Braun, M., and Diez, S. (2016). Kinesin-1 Expressed in Insect Cells Improves Microtubule in Vitro Gliding Performance, Long-Term Stability and Guiding Efficiency in Nanostructures. IEEE Trans Nanobioscience *15*, 62-69.

Kost, T.A., Condreay, J.P., and Jarvis, D.L. (2005). Baculovirus as versatile vectors for protein expression in insect and mammalian cells. Nat Biotechnol *23*, 567-575.

Kumar, N., Pandey, D., and Halder, A. (2017). Preventive, Diagnostic and Therapeutic Applications of Baculovirus Expression Vector System. Trends in Insect Molecular Biology and Biotechnology *16*.

Kurland, C., and Gallant, J. (1996). Errors of heterologous protein expression. Curr Opin Biotechnol *7*, 489-493.

Kuznetsov, S.A., and Gelfand, V.I. (1986). Bovine brain kinesin is a microtubule-activated ATPase. Proc Natl Acad Sci U S A *83*, 8530-8534.

Langlois, S., Tarailo-Graovac, M., Sayson, B., Drogemoller, B., Swenerton, A., Ross, C.J., Wasserman, W.W., and van Karnebeek, C.D. (2016). De novo dominant variants affecting the motor domain of KIF1A are a cause of PEHO syndrome. Eur J Hum Genet *24*, 949-953.

Lee, J.R., Shin, H., Choi, J., Ko, J., Kim, S., Lee, H.W., Kim, K., Rho, S.H., Lee, J.H., Song, H.E., *et al.* (2004). An intramolecular interaction between the FHA domain and a coiled coil negatively regulates the kinesin motor KIF1A. EMBO J *23*, 1506-1515.

Lee, J.R., Shin, H., Ko, J., Choi, J., Lee, H., and Kim, E. (2003). Characterization of the movement of the kinesin motor KIF1A in living cultured neurons. J Biol Chem *278*, 2624-2629.

Lee, J.R., Srour, M., Kim, D., Hamdan, F.F., Lim, S.H., Brunel-Guitton, C., Decarie, J.C., Rossignol, E., Mitchell, G.A., Schreiber, A., *et al.* (2015). De novo mutations in the motor domain of KIF1A cause cognitive impairment, spastic paraparesis, axonal neuropathy, and cerebellar atrophy. Hum Mutat *36*, 69-78.

Lessard, D.V., Zinder, O.J., Hotta, T., Verhey, K.J., Ohi, R., and Berger, C.L. (2019). Polyglutamylation of tubulin's C-terminal tail controls pausing and motility of kinesin-3 family member KIF1A. J Biol Chem *294*, 6353-6363.

Li, J., Lee, G.I., Van Doren, S.R., and Walker, J.C. (2000). The FHA domain mediates phosphoprotein interactions. J Cell Sci *113 Pt 23*, 4143-4149.

Li, M., and Zheng, W. (2011). Probing the structural and energetic basis of kinesin-microtubule binding using computational alanine-scanning mutagenesis. Biochemistry *50*, 8645-8655.

Liu, L., Tuzel, E., and Ross, J.L. (2011). Loop formation of microtubules during gliding at high density. J Phys Condens Matter *23*, 374104.

Lo, K.Y., Kuzmin, A., Unger, S.M., Petersen, J.D., and Silverman, M.A. (2011). KIF1A is the primary anterograde motor protein required for the axonal transport of dense-core vesicles in cultured hippocampal neurons. Neurosci Lett *491*, 168-173.

Luria, I., Crenshaw, J., Downs, M., Agarwal, A., Seshadri, S., Gonzales, J., Idan, O., Kamcev, J., Katira, P., Pandey, S., *et al.* (2011). Microtubule nanospool formation by active self-assembly is not initiated by thermal activation. Soft Matter *7*, 3108-3115.

Mallik, R., Carter, B.C., Lex, S.A., King, S.J., and Gross, S.P. (2004). Cytoplasmic dynein functions as a gear in response to load. Nature *427*, 649-652.

Mallik, R., and Gross, S.P. (2004). Molecular motors: strategies to get along. Curr Biol *14*, R971-982.

Mandelkow, E., and Mandelkow, E.M. (1995). Microtubules and microtubule-associated proteins. Curr Opin Cell Biol *7*, 72-81.

Marx, A., Hoenger, A., and Mandelkow, E. (2009). Structures of kinesin motor proteins. Cell Motil Cytoskeleton *66*, 958-966.

Matsushita, M., Tanaka, S., Nakamura, N., Inoue, H., and Kanazawa, H. (2004). A novel kinesin-like protein, KIF1Bbeta3 is involved in the movement of lysosomes to the cell periphery in non-neuronal cells. Traffic *5*, 140-151.

Matthews, R.E.F. (1982). Classification and nomenclature of viruses. Fourth report of the International Committee on Taxonomy of Viruses. Intervirology *17*, 3.

Micsonai, A., Wien, F., Bulyaki, E., Kun, J., Moussong, E., Lee, Y.H., Goto, Y., Refregiers, M., and Kardos, J. (2018). BeStSel: a web server for accurate protein secondary structure prediction and fold recognition from the circular dichroism spectra. Nucleic Acids Res *46*, W315-W322.

Micsonai, A., Wien, F., Kernya, L., Lee, Y.H., Goto, Y., Refregiers, M., and Kardos, J. (2015). Accurate secondary structure prediction and fold recognition for circular dichroism spectroscopy. Proc Natl Acad Sci U S A *112*, E3095-3103.

Miki, H., Okada, Y., and Hirokawa, N. (2005). Analysis of the kinesin superfamily: insights into structure and function. Trends Cell Biol *15*, 467-476.

Mitra, A., Sune, M., Diez, S., Sancho, J.M., Oriola, D., and Casademunt, J. (2019). A Brownian Ratchet Model Explains the Biased Sidestepping of Single-Headed Kinesin-3 KIF1A. Biophys J *116*, 2266-2274.

Mukherjee, R., Soppina, P., Patel, N.M., Soppina, V., and Rane, K. (2022). Effect of Binding-Affinity and ATPase Activity on the Velocities of Kinesins Using Ratchet Models. Cell Biochem Biophys *80*, 31-38.

Muyldermans, S. (2013). Nanobodies: natural single-domain antibodies. Annu Rev Biochem *82*, 775-797.

Nakagawa, T., Setou, M., Seog, D., Ogasawara, K., Dohmae, N., Takio, K., and Hirokawa, N. (2000). A novel motor, KIF13A, transports mannose-6-phosphate receptor to plasma membrane through direct interaction with AP-1 complex. Cell *103*, 569-581.

Nangaku, M., Sato-Yoshitake, R., Okada, Y., Noda, Y., Takemura, R., Yamazaki, H., and Hirokawa, N. (1994). KIF1B, a novel microtubule plus end-directed monomeric motor protein for transport of mitochondria. Cell *79*, 1209-1220.

Nitta, R., Kikkawa, M., Okada, Y., and Hirokawa, N. (2004). KIF1A alternately uses two loops to bind microtubules. Science *305*, 678-683.

Nogales, E. (2000). Structural insights into microtubule function. Annu Rev Biochem *69*, 277-302.

Odde, D.J., Ma, L., Briggs, A.H., DeMarco, A., and Kirschner, M.W. (1999). Microtubule bending and breaking in living fibroblast cells. J Cell Sci *112 (Pt 19)*, 3283-3288.

Okada, Y., Higuchi, H., and Hirokawa, N. (2003). Processivity of the single-headed kinesin KIF1A through biased binding to tubulin. Nature *424*, 574-577.

Okada, Y., and Hirokawa, N. (1999). A processive single-headed motor: kinesin superfamily protein KIF1A. Science *283*, 1152-1157.

Okada, Y., and Hirokawa, N. (2000). Mechanism of the single-headed processivity: diffusional anchoring between the K-loop of kinesin and the C terminus of tubulin. Proc Natl Acad Sci U S A *97*, 640-645.

Okada, Y., Yamazaki, H., Sekine-Aizawa, Y., and Hirokawa, N. (1995). The neuron-specific kinesin superfamily protein KIF1A is a unique monomeric motor for anterograde axonal transport of synaptic vesicle precursors. Cell *81*, 769-780.

Okamoto, N., Miya, F., Tsunoda, T., Yanagihara, K., Kato, M., Saitoh, S., Yamasaki, M., Kanemura, Y., and Kosaki, K. (2014). KIF1A mutation in a patient with progressive neurodegeneration. J Hum Genet *59*, 639-641.

Olmsted, Z.T., Colliver, A.G., and Paluh, J.L. (2015). The kinesin–tubulin complex: considerations in structural and functional complexity. Cell Health and Cytoskeleton *7*.

Oriola, D., Roth, S., Dogterom, M., and Casademunt, J. (2015). Formation of helical membrane tubes around microtubules by single-headed kinesin KIF1A. Nat Commun *6*, 8025.

Patel, N.M., Siva, M.S.A., Kumari, R., Shewale, D.J., Rai, A., Ritt, M., Sharma, P., Setty, S.R.G., Sivaramakrishnan, S., and Soppina, V. (2021). KIF13A motors are regulated by Rab22A to function as weak dimers inside the cell. Sci Adv *7*, eabd2054.

Pierce, D.W., Hom-Booher, N., Otsuka, A.J., and Vale, R.D. (1999). Single-molecule behavior of monomeric and heteromeric kinesins. Biochemistry *38*, 5412-5421.

Porter, M.E., Scholey, J.M., Stemple, D.L., Vigers, G.P., Vale, R.D., Sheetz, M.P., and McIntosh, J.R. (1987). Characterization of the microtubule movement produced by sea urchin egg kinesin. J Biol Chem *262*, 2794-2802.

Prosser, B.L., Ward, C.W., and Lederer, W.J. (2011). X-ROS signaling: rapid mechano-chemo transduction in heart. Science *333*, 1440-1445.

Qi, Y., Wang, J.K., McMillian, M., and Chikaraishi, D.M. (1997). Characterization of a CNS cell line, CAD, in which morphological differentiation is initiated by serum deprivation. J Neurosci *17*, 1217-1225.

Rath, O., and Kozielski, F. (2012). Kinesins and cancer. Nat Rev Cancer *12*, 527-539.

Reck-Peterson, S.L., Yildiz, A., Carter, A.P., Gennerich, A., Zhang, N., and Vale, R.D. (2006). Single-molecule analysis of dynein processivity and stepping behavior. Cell *126*, 335-348.

Ren, J., Huo, L., Wang, W., Zhang, Y., Li, W., Lou, J., Xu, T., and Feng, W. (2016). Structural Correlation of the Neck Coil with the Coiled-coil (CC1)-Forkhead-associated (FHA) Tandem for Active Kinesin-3 KIF13A. J Biol Chem *291*, 3581-3594.

Ren, J., Wang, S., Chen, H., Wang, W., Huo, L., and Feng, W. (2018). Coiled-coil 1-mediated fastening of the neck and motor domains for kinesin-3 autoinhibition. Proc Natl Acad Sci U S A *115*, E11933-E11942.

Rice, S., Lin, A.W., Safer, D., Hart, C.L., Naber, N., Carragher, B.O., Cain, S.M., Pechatnikova, E., Wilson-Kubalek, E.M., Whittaker, M., *et al.* (1999). A structural change in the kinesin motor protein that drives motility. Nature *402*, 778-784.

Robison, P., Caporizzo, M.A., Ahmadzadeh, H., Bogush, A.I., Chen, C.Y., Margulies, K.B., Shenoy, V.B., and Prosser, B.L. (2016). Detyrosinated microtubules buckle and bear load in contracting cardiomyocytes. Science *352*, aaf0659.

Sagona, A.P., Nezis, I.P., Pedersen, N.M., Liestol, K., Poulton, J., Rusten, T.E., Skotheim, R.I., Raiborg, C., and Stenmark, H. (2010). PtdIns(3)P controls cytokinesis through KIF13A-mediated recruitment of FYVE-CENT to the midbody. Nat Cell Biol *12*, 362-371.

Sanchez-Soriano, N., Travis, M., Dajas-Bailador, F., Goncalves-Pimentel, C., Whitmarsh, A.J., and Prokop, A. (2009). Mouse ACF7 and drosophila short stop modulate filopodia formation and microtubule organisation during neuronal growth. J Cell Sci *122*, 2534-2542.

Scarabelli, G., Soppina, V., Yao, X.Q., Atherton, J., Moores, C.A., Verhey, K.J., and Grant, B.J. (2015). Mapping the Processivity Determinants of the Kinesin-3 Motor Domain. Biophys J *109*, 1537-1540.

Schmidt, F.R. (2004). Recombinant expression systems in the pharmaceutical industry. Appl Microbiol Biotechnol *65*, 363-372.

Schnitzer, M.J., and Block, S.M. (1997). Kinesin hydrolyses one ATP per 8-nm step. Nature *388*, 386-390.

Seitz, A., and Surrey, T. (2006). Processive movement of single kinesins on crowded microtubules visualized using quantum dots. EMBO J *25*, 267-277.

Shekhar, N., Neelam, S., Wu, J., Ladd, A.J., Dickinson, R.B., and Lele, T.P. (2013). Fluctuating Motor Forces Bend Growing Microtubules. Cell Mol Bioeng *6*, 120-129.

Shin, H., Wyszynski, M., Huh, K.H., Valtschanoff, J.G., Lee, J.R., Ko, J., Streuli, M., Weinberg, R.J., Sheng, M., and Kim, E. (2003). Association of the kinesin motor KIF1A with the multimodular protein liprin-alpha. J Biol Chem *278*, 11393-11401.

Siddiqui, N., and Straube, A. (2017). Intracellular Cargo Transport by Kinesin-3 Motors. Biochemistry (Mosc) *82*, 803-815.

Sommese, R.F., Hariadi, R.F., Kim, K., Liu, M., Tyska, M.J., and Sivaramakrishnan, S. (2016). Patterning protein complexes on DNA nanostructures using a GFP nanobody. Protein Sci *25*, 2089-2094.

Soppina, V., Norris, S.R., Dizaji, A.S., Kortus, M., Veatch, S., Peckham, M., and Verhey, K.J. (2014). Dimerization of mammalian kinesin-3 motors results in superprocessive motion. Proc Natl Acad Sci U S A *111*, 5562-5567.

Soppina, V., Rai, A.K., Ramaiya, A.J., Barak, P., and Mallik, R. (2009). Tug-of-war between dissimilar teams of microtubule motors regulates transport and fission of endosomes. Proc Natl Acad Sci U S A *106*, 19381-19386.

Soppina, V., and Verhey, K.J. (2014). The family-specific K-loop influences the microtubule on-rate but not the superprocessivity of kinesin-3 motors. Mol Biol Cell *25*, 2161-2170.

Steinmetz, M.O., and Akhmanova, A. (2008). Capturing protein tails by CAP-Gly domains. Trends Biochem Sci *33*, 535-545.

Straube, A., Hause, G., Fink, G., and Steinberg, G. (2006). Conventional kinesin mediates microtubule-microtubule interactions in vivo. Mol Biol Cell *17*, 907-916.

Sudhakar, S., Abdosamadi, M.K., Jachowski, T.J., Bugiel, M., Jannasch, A., and Schaffer, E. (2021). Germanium nanospheres for ultraresolution picotensiometry of kinesin motors. Science *371*.

Svoboda, K., Schmidt, C.F., Schnapp, B.J., and Block, S.M. (1993). Direct observation of kinesin stepping by optical trapping interferometry. Nature *365*, 721-727.

Tanaka, Y., Niwa, S., Dong, M., Farkhondeh, A., Wang, L., Zhou, R., and Hirokawa, N. (2016). The Molecular Motor KIF1A Transports the TrkA Neurotrophin Receptor and Is Essential for Sensory Neuron Survival and Function. Neuron *90*, 1215-1229.

Tao, L., and Scholey, J.M. (2010). Purification and assay of mitotic motors. Methods *51*, 233-241.

Theisen, U., Straube, E., and Straube, A. (2012). Directional persistence of migrating cells requires Kif1C-mediated stabilization of trailing adhesions. Dev Cell *23*, 1153-1166.

Tirumala, N.A., and Ananthanarayanan, V. (2020). Role of Dynactin in the Intracellular Localization and Activation of Cytoplasmic Dynein. Biochemistry *59*, 156-162.

Tomishige, M., Klopfenstein, D.R., and Vale, R.D. (2002). Conversion of Unc104/KIF1A kinesin into a processive motor after dimerization. Science *297*, 2263-2267.

Tomishige, M., and Vale, R.D. (2000). Controlling kinesin by reversible disulfide cross-linking. Identifying the motility-producing conformational change. J Cell Biol *151*, 1081-1092.

Trybus, K.M. (2000). Biochemical studies of myosin. Methods *22*, 327-335.

Uchimura, S., Oguchi, Y., Hachikubo, Y., Ishiwata, S., and Muto, E. (2010). Key residues on microtubule responsible for activation of kinesin ATPase. EMBO J *29*, 1167-1175.

Ueno, H., Huang, X., Tanaka, Y., and Hirokawa, N. (2011). KIF16B/Rab14 molecular motor complex is critical for early embryonic development by transporting FGF receptor. Dev Cell *20*, 60-71.

Vale, R.D. (2003). The molecular motor toolbox for intracellular transport. Cell *112*, 467-480.

Vale, R.D., and Milligan, R.A. (2000). The way things move: looking under the hood of molecular motor proteins. Science *288*, 88-95.

Vale, R.D., Reese, T.S., and Sheetz, M.P. (1985). Identification of a novel force-generating protein, kinesin, involved in microtubule-based motility. Cell *42*, 39-50.

VanDelinder, V., Adams, P.G., and Bachand, G.D. (2016). Mechanical splitting of microtubules into protofilament bundles by surface-bound kinesin-1. Sci Rep *6*, 39408.

Venkateswarlu, K., Brandom, K.G., and Lawrence, J.L. (2004). Centaurin-alpha1 is an in vivo phosphatidylinositol 3,4,5-trisphosphate-dependent GTPase-activating protein for ARF6 that is involved in actin cytoskeleton organization. J Biol Chem *279*, 6205-6208.

Verhey, K.J., Dishinger, J., and Kee, H.L. (2011a). Kinesin motors and primary cilia. Biochem Soc Trans *39*, 1120-1125.

Verhey, K.J., and Gaertig, J. (2007). The tubulin code. Cell Cycle *6*, 2152-2160.

Verhey, K.J., and Hammond, J.W. (2009). Traffic control: regulation of kinesin motors. Nat Rev Mol Cell Biol *10*, 765-777.

Verhey, K.J., Kaul, N., and Soppina, V. (2011b). Kinesin assembly and movement in cells. Annu Rev Biophys *40*, 267-288.

Voelzmann, A., Hahn, I., Pearce, S.P., Sanchez-Soriano, N., and Prokop, A. (2016). A conceptual view at microtubule plus end dynamics in neuronal axons. Brain Res Bull *126*, 226-237.

Voelzmann, A., Liew, Y.T., Qu, Y., Hahn, I., Melero, C., Sanchez-Soriano, N., and Prokop, A. (2017). Drosophila Short stop as a paradigm for the role and regulation of spectraplakins. Semin Cell Dev Biol *69*, 40-57.

Wang, W., Cao, L., Wang, C., Gigant, B., and Knossow, M. (2015). Kinesin, 30 years later: Recent insights from structural studies. Protein Sci *24*, 1047-1056.

Westerholm-Parvinen, A., Vernos, I., and Serrano, L. (2000). Kinesin subfamily UNC104 contains a FHA domain: boundaries and physicochemical characterization. FEBS Lett *486*, 285-290.

Wickstead, B., and Gull, K. (2011). The evolution of the cytoskeleton. J Cell Biol *194*, 513-525.

Wloga, D., and Gaertig, J. (2010). Post-translational modifications of microtubules. J Cell Sci *123*, 3447-3455.

Woehlke, G., Ruby, A.K., Hart, C.L., Ly, B., Hom-Booher, N., and Vale, R.D. (1997). Microtubule interaction site of the kinesin motor. Cell *90*, 207-216.

Woehlke, G., and Schliwa, M. (2000). Walking on two heads: the many talents of kinesin. Nat Rev Mol Cell Biol *1*, 50-58.

Wojtovich, A.P., and Foster, T.H. (2014). Optogenetic control of ROS production. Redox Biol *2*, 368-376.

Xing, B.M., Yang, Y.R., Du, J.X., Chen, H.J., Qi, C., Huang, Z.H., Zhang, Y., and Wang, Y. (2012). Cyclin-dependent kinase 5 controls TRPV1 membrane trafficking and the heat sensitivity of nociceptors through KIF13B. J Neurosci *32*, 14709-14721.

Yamada, K.H., Hanada, T., and Chishti, A.H. (2007). The effector domain of human Dlg tumor suppressor acts as a switch that relieves autoinhibition of kinesin-3 motor GAKIN/KIF13B. Biochemistry *46*, 10039-10045.

Yamada, K.H., Nakajima, Y., Geyer, M., Wary, K.K., Ushio-Fukai, M., Komarova, Y., and Malik, A.B. (2014). KIF13B regulates angiogenesis through Golgi to plasma membrane trafficking of VEGFR2. J Cell Sci *127*, 4518-4530.

Yildiz, A., Tomishige, M., Vale, R.D., and Selvin, P.R. (2004). Kinesin walks hand-over-hand. Science *303*, 676-678.

Zaniewski, T.M., Gicking, A.M., Fricks, J., and Hancock, W.O. (2020). A kinetic dissection of the fast and superprocessive kinesin-3 KIF1A reveals a predominate one-head-bound state during its chemomechanical cycle. J Biol Chem.

Zhai, Y., Zhang, D., Yu, L., Sun, F., and Sun, F. (2019). SmartBac, a new baculovirus system for large protein complex production. J Struct Biol X *1*, 100003.

Zhao, C., Takita, J., Tanaka, Y., Setou, M., Nakagawa, T., Takeda, S., Yang, H.W., Terada, S., Nakata, T., Takei, Y., *et al.* (2001). Charcot-Marie-Tooth disease type 2A caused by mutation in a microtubule motor KIF1Bbeta. Cell *105*, 587-597.

Zheng, Q., Jockusch, S., Zhou, Z., and Blanchard, S.C. (2014). The contribution of reactive oxygen species to the photobleaching of organic fluorophores. Photochem Photobiol *90*, 448-454.

Zhou, H.M., Brust-Mascher, I., and Scholey, J.M. (2001). Direct visualization of the movement of the monomeric axonal transport motor UNC-104 along neuronal processes in living Caenorhabditis elegans. J Neurosci *21*, 3749-3755.

Zhou, R., Niwa, S., Guillaud, L., Tong, Y., and Hirokawa, N. (2013). A molecular motor, KIF13A, controls anxiety by transporting the serotonin type 1A receptor. Cell Rep *3*, 509-519.

List of Publications

1. **Pushpanjali Soppina**, Nishaben M. Patel, Dipeshwari J. Shewale, Ashim Rai, Sivaraj Sivaramakrishnan, Pradeep Kumar Naik and Virupakshi Soppina* (2022) Kinesin-3 Motors are Fine-Tuned at the Molecular Level to Endow Distinct Mechanical Outputs. ***BMC Biology, 20, 177 (2022)***.

2. **Pushpanjali Soppina**, Dipeshwari J. Shewale, Pradeep Kumar Naik and Virupakshi Soppina* (2022) Single molecule analysis of Sf-9 purified superprocessive Kinesin-3 family motors. ***The Journal of Visualized Experiments, (185), e63837.***

3. Roopsha Mukherjee, **Pushpanjali Soppina**, Nishaben M. Patel, Virupakshi Soppina and Kaustubh Rane (2022) Effect of binding-affinity and ATPase activity on the velocities of kinesins using ratchet models. ***Cell Biochemistry and Biophysics,*** **80(1): 31–38.**

4. Deepmala Singh, **Pushpanjali Soppina**, Virupakshi Soppina* and Sriram Kanvah* (2022) Imaging of Lipid Droplets using Coumarin Fluorophores in Live Cells and C.elegans. ***Journal of Photochemistry and Photobiology B: Biology***, **237: 112589.**

5. Prateek Goyal[#], **Pushpanjali Soppina**[#], Superb K. Misra, Eva-Valsami Jones, Virupakshi Soppina* and Swaroop Chakraborty* (2022) Rhodamine labelled ZIF-8 MOF nanoprobes for in vivo nanoparticles tracing. ***Frontiers in Toxicology,*** **4:917749.**

6. Pravalika Butreddy, Swaroop Chakraborty, **Pushpanjali Soppina**, Virupakshi Soppina and Superb K. Misra (2021) Rhodamine B tagged ^{65}CuO nanoparticles: A dual labeled stable isotope enriched fluorescent nanoprobe for efficient *in vivo* toxicity assessment. ***Chemosphere,*** **286(2): 131698.**

7. Ching-On Wonga, Nicholas E. Karagas, Jewon Jung, Qiaochu Wang, Morgan A. Rousseau, Yufang Chao , Ryan Insolera, **Pushpanjali Soppina**, Catherine A. Collins, Yong Zhoua, John F. Hancock, Michael X. Zhu and Kartik Venkatachalam (2021) Regulation of longevity by depolarization-induced activation of PLC-β-IP $_3$ R signaling in neurons. ***Proceedings of the National Academy of Sciences, USA***, **118(16), e2004253118.**

Manuscripts under preparation/submitted:

1. Dipeshwari J. Shewale, **Pushpanjali Soppina**, Surabhi R. Sharma, Nishaben M. Patel and Virupakshi Soppina ***** (2022) Rab10 regulates KIF13B dimerization and motility essential for RE tubulation and cargo recycling. (***In preparation***)

2. Dipeshwari J. Shewale**#**, **Pushpanjali Soppina**# and Virupakshi Soppina* (2022) KIF1A-mediated neurodegenerative mutations largely affect the mechanochemical properties of motor domain. **(*Submitted*)**

3. Deepmala Singh, Regar Ramprasad**, Pushpanjali Soppina**, Virupakshi Soppina***** & Sriram Kanvah* (2022) Mitochondria targeted fluorescent probe for imaging based photodynamic therapy with mtDNA release in cytosol of live cells. (***Submitted***)

Soppina *et al. BMC Biology* (2022) 20:177
https://doi.org/10.1186/s12915-022-01370-8

BMC Biology

RESEARCH ARTICLE

Open Access

Kinesin-3 motors are fine-tuned at the molecular level to endow distinct mechanical outputs

Pushpanjali Soppina[1,2], Nishaben Patel[1,3], Dipeshwari J. Shewale[1], Ashim Rai[3], Sivaraj Sivaramakrishnan[3], Pradeep K. Naik[2] and Virupakshi Soppina[1*]

Abstract

Background: Kinesin-3 family motors drive diverse cellular processes and have significant clinical importance. The ATPase cycle is integral to the processive motility of kinesin motors to drive long-distance intracellular transport. Our previous work has demonstrated that kinesin-3 motors are fast and superprocessive with high microtubule affinity. However, chemomechanics of these motors remain poorly understood.

Results: We purified kinesin-3 motors using the Sf9-baculovirus expression system and demonstrated that their motility properties are on par with the motors expressed in mammalian cells. Using biochemical analysis, we show for the first time that kinesin-3 motors exhibited high ATP turnover rates, which is 1.3- to threefold higher compared to the well-studied kinesin-1 motor. Remarkably, these ATPase rates correlate to their stepping rate, suggesting a tight coupling between chemical and mechanical cycles. Intriguingly, kinesin-3 velocities (KIF1A > KIF13A > KIF13B > KIF16B) show an inverse correlation with their microtubule-binding affinities (KIF1A < KIF13A < KIF13B < KIF16B). We demonstrate that this differential microtubule-binding affinity is largely contributed by the positively charged residues in loop8 of the kinesin-3 motor domain. Furthermore, microtubule gliding and cellular expression studies displayed significant microtubule bending that is influenced by the positively charged insert in the motor domain, K-loop, a hallmark of kinesin-3 family.

Conclusions: Together, we propose that a fine balance between the rate of ATP hydrolysis and microtubule affinity endows kinesin-3 motors with distinct mechanical outputs. The K-loop, a positively charged insert in the loop12 of the kinesin-3 motor domain promotes microtubule bending, an interesting phenomenon often observed in cells, which requires further investigation to understand its cellular and physiological significance.

Keywords: Chemomechanical, Kinesin-3, Microtubule bending, Baculovirus, Superprocessive, ATPases

Background

Kinesin motors are ATPases that convert the chemical energy of adenosine triphosphate (ATP) into mechanical work, which enables their movement on microtubules (MTs) to carry out multiple cellular processes, such as intracellular transport and cell division [1–3]. Kinesins contain a highly conserved ~ 350 amino acid catalytic motor domain responsible for MT binding and ATP hydrolysis. Although the kinesin motor domains exhibit a high degree of sequence conservation (50% identity) between different subfamilies, their cellular functions have remarkable diversity [4]. Our current understanding of kinesins' mechanical and biophysical properties is derived mainly from the studies on kinesin-1, the

*Correspondence: vsoppina@gmail.com; vsoppina@iitgn.ac.in

[1] Discipline of Biological Engineering, Indian Institute of Technology Gandhinagar, Gandhinagar, Gujarat 382355, India
Full list of author information is available at the end of the article

jove

Single-Molecule Analysis of Sf9 Purified Superprocessive Kinesin-3 Family Motors

Pushpanjali Soppina[1,2], **Dipeshwari J. Shewale**[1], **Pradeep K. Naik**[2], **Virupakshi Soppina**[1]

[1] Discipline of Biological Engineering, Indian Institute of Technology Gandhinagar [2] Department of Biotechnology and Bioinformatics, Sambalpur University

Corresponding Authors

Virupakshi Soppina
vsoppina@gmail.com

Pradeep K. Naik
pknaik1973@gmail.com

Citation

Soppina, P., Shewale, D.J., Naik, P.K., Soppina, V. Single-Molecule Analysis of Sf9 Purified Superprocessive Kinesin-3 Family Motors. *J. Vis. Exp.* (), e63837, doi:10.3791/63837 (2022).

Date Published

July 27, 2022

DOI

10.3791/63837

URL

jove.com/t/63837

Abstract

A complex cellular environment poses challenges for single-molecule motility analysis. However, advancement in imaging techniques have improved single-molecule studies and has gained immense popularity in detecting and understanding the dynamic behavior of fluorescent-tagged molecules. Here, we describe a detailed method for *in vitro* single-molecule studies of kinesin-3 family motors using Total Internal Reflection Fluorescence (TIRF) microscopy. Kinesin-3 is a large family that plays critical roles in cellular and physiological functions ranging from intracellular cargo transport to cell division to development. We have shown previously that constitutively active dimeric kinesin-3 motors exhibit fast and superprocessive motility with high microtubule affinity at the single-molecule level using cell lysates prepared by expressing motor in mammalian cells. Our lab studies kinesin-3 motors and their regulatory mechanisms using cellular, biochemical and biophysical approaches, and such studies demand purified proteins at a large scale. Expression and purification of these motors using mammalian cells would be expensive and time-consuming, whereas expression in a prokaryotic expression system resulted in significantly aggregated and inactive protein. To overcome the limitations posed by bacterial purification systems and mammalian cell lysate, we have established a robust Sf9-baculovirus expression system to express and purify these motors. The kinesin-3 motors are C-terminally tagged with 3-tandem fluorescent proteins (3xmCitirine or 3xmCit) that provide enhanced signals and decreased photobleaching. *In vitro* single-molecule and multi-motor gliding analysis of Sf9 purified proteins demonstrate that kinesin-3 motors are fast and superprocessive akin to our previous studies using mammalian cell lysates. Other applications using these assays include detailed knowledge of oligomer conditions of motors, specific binding partners paralleling biochemical studies, and their kinetic state.

Cell Biochemistry and Biophysics (2022) 80:31–38
https://doi.org/10.1007/s12013-021-01057-x

ORIGINAL PAPER

Effect of Binding-Affinity and ATPase Activity on the Velocities of Kinesins Using Ratchet Models

Rupsha Mukherjee[1] · Pushpanjali Soppina[2,3] · Nishaben M. Patel[2] · Virupakshi Soppina[2] · Kaustubh Rane[1]

Received: 1 April 2021 / Accepted: 20 December 2021 / Published online: 28 January 2022

Abstract

We use two-state ratchet models containing single and coupled Brownian motors to understand the role of motor-microtubule binding, ATPase reaction rate and dimerisation on the translational velocities of Kinesin motors. We use model parameters derived from the experimental measurements on KIF1A, KIF13A, KIF13B, and KIF16B motors to compute velocities in μm/s. We observe that both the models show the same trend in velocities (KIF1A > KIF13A > KIF13B > KIF16B) as the experimental results. However, the models significantly underpredict the velocities when compared with the experiments. The predictions of the coupled-motor model are closer to the experiments than those of the single-motor model. Our results indicate that the variation of ATPase reaction rate governs the trend in velocities for the above four motors. The variation of motor-microtubule binding affinity and the coupling strength between the motor domains may only have a secondary effect. More rigorous models that incorporate the power-stroke mechanism are necessary for better quantitative compliance with the experiments.

Introduction

Kinesins are microtubule-based motor proteins involved in the transportation of chemical constituents within the cell by using the chemical energy stored in the Adenosine triphosphate (ATP) molecules to translate along the microtubule. The translational motion of the kinesin is typically studied via experimental observables like velocity, processivity, and stall force [1, 2]. An extensive study of these experimental observables was previously performed to monitor the malfunctioning in kinesin that may lead to neurodegenerative diseases such as Alzheimer's disease [3, 4] and Hereditary spastic paraplegia [5, 6]. These diseases are mainly caused due to the defect in the Kinesin-3. Kinesin-3 is the largest superfamily of Kinesin motors and has five sub-families named as KIF1, KIF13, KIF14, KIF16 and KIF28 [7]. Kinesin-3 motors are known to be superprocessive [8] and are reported to have robust motility properties [9].

In this paper, we use two-state ratchet models to understand the effect of the following factors on the translational velocities of motors: (1) Binding between motor domain and microtubule, (2) Rate of ATPase activity, and (3) the association between the two monomers. We use two models: (1) A two-state ratchet model containing two Brownian motors that are coupled via a spring of suitable spring constant and equilibrium length, and (2) a two-state ratchet model containing a single Brownian motor. The parameters used in the model are estimated from the experimental observables of KIF1A, KIF13A, KIF13B and KIF16B motors. For the unknown parameters, we scan a suitable range of values to consider the effect of their variation. Several stochastic models have been introduced that idealise biomolecular motors as Brownian motors [2, 10–12]. The motor domain is considered as a point particle moving along the microtubule under overdamped conditions. The motion is subjected to the thermal noise creating a non-equilibrium mechanical motion mediated by the chemical reaction. The mechano-chemical coupling of the motor-microtubule system is modelled via two asymmetric periodic potentials. Each potential corresponds to a motor domain in a particular chemical state and the chemical reaction is modelled by switching between the above potentials. The two chemical

✉ Kaustubh Rane
kaustubhrane@iitgn.ac.in

[1] Chemical Engineering, Indian Institute of Technology Gandhinagar, Gandhinagar, Gujarat 382355, India

[2] Biological Engineering, Indian Institute of Technology Gandhinagar, Gandhinagar, Gujarat 382355, India

[3] Department of Biotechnology and Bioinformatics, Sambalpur University, Sambalpur, Orissa 768019, India